May 2018

Environmental Impact Predictions for Disposal of Emerging Energy Technologies in Solid Waste Landfills: Application to Lithium Ion Batteries and Photovoltaic Modules

Mary Kayla Kilgo
Clemson University, mkc081@gmail.com

ENVIRONMENTAL IMPACT PREDICTIONS FOR DISPOSAL OF EMERGING ENERGY TECHNOLOGIES IN SOLID WASTE LANDFILLS: APPLICATION TO LITHIUM ION BATTERIES AND PHOTOVOLTAIC MODULES

A Dissertation
Presented to
the Graduate School of
Clemson University

In Partial Fulfillment
of the Requirements for the Degree
Doctor of Philosophy
Environmental Engineering and Science

---

by
Mary Kayla Kilgo
May 2018

Accepted by:
Brian Powell, Committee Chair
Annick Anctil, Committee Co-chair
Cindy Lee
Marian Kennedy

Abstract

As the use of photovoltaic (PV) modules and batteries rapidly increases to meet the growing worldwide energy demand, so does the waste stream of these products at end-of-life (EOL). In locations without sufficient recycling laws or take-back programs, these products could be landfilled with municipal solid waste (MSW). To determine the potential effects from landfill disposal of these products, metal leaching from PV modules and two types of batteries (Li-ion and nickel metal hydride (NiMH)) was studied using the regulatory Toxicity Characteristic Leaching Procedure (TCLP) as well as batch leaching and outdoor column testing. The data from the leaching tests were used to build waste scenarios utilizing life cycle assessment (LCA) software.

The experimental data collected from the batch leaching tests and outdoor columns in Chapters 4, 5, and 7 demonstrate the complexity of characterizing PV and battery e-waste and developing EOL regulations and procedures that are applicable to each type of e-waste. In Chapter 4, the TCLP, the California Waste Extraction Test, and modified versions of both were performed on a multi-crystalline silicon module and cells and a copper indium gallium diselenide (CIGS) module. Metal leachate concentrations varied with changes in testing parameters, which raises doubt if regulatory methods can adequately characterize PV modules. In Chapter 5, the TCLP, microwave digestions, and batch leaching tests in two simulated leachates sampled over a period of 100 days were conducted for seven types of Li-ion batteries, one type of NiMH battery, and two types of PV modules. Additionally, one product of each type (Li-ion battery, NiMH battery, and PV module) was mixed with MSW components and a simulated landfill leachate to compare leaching in a more realistic waste matrix to the batch leaching tests. Results from the TCLP showed that one of the two PV modules and three of the eight batteries would be classified as hazardous waste in the US. For the batch tests with e-waste mixed with MSW, both lower (Pb

and Hg) and higher (Co and Ni) metal leachate concentrations were observed than for the batch tests without MSW. Chapter 6 describes the design and build of the lysimeter test bed, which is utilized for column experiments in Chapter 7. Three columns were built to simulate the conditions within a bioreactor solid waste landfill and were subjected to outdoor temperature fluctuations. For the column with the c-Si module pieces, Pb was not detected in the leachate even though Pb was observed in the previous tests for this product described in Chapter 5. For the column with the NiMH power tool battery, Co, Cu, and Ni were measured in the leachate, but As, Hg, Pb, and Zn were not detected in the column leachate samples even though they were observed in the previous tests. For the column with the Li-ion laptop battery, Co, Cu, and Ni were measured in the leachate samples and were also found in the previous batch tests. Although As, Hg, and Pb were not found in the leachate samples, the other soluble and potentially mobile metals, including Co, Cu, and Ni, found in the leachate could be of concern in an improperly managed landfill and could cause contamination of soils and aquifers.

In Chapter 8, the data gathered from the leaching tests were used to build EOL scenarios for metal emissions to groundwater using LCA software and characterization methods to determine potential human and eco-toxicity effects. Additionally, composition data from disassembly and digestions were used to build assemblies of the PV module and Li-ion and NiMH batteries. The results showed that the worst-case EOL scenario effects exceeded those of the assemblies of each product, and with notable effects for the other scenarios, the inclusion of the potential for EOL metal leaching is merited in LCAs of these products. Appropriate characterization tools and techniques to ensure adequate protection of the environment are necessary to avoid a growing e-waste problem while simultaneously promoting renewable energy sources.

Acknowledgments

First, I would like to thank my advisors, Drs. Brian Powell and Annick Anctil, for their continued support and unwavering optimism throughout my PhD experience. My committee members, Drs. Cindy Lee and Molly Kennedy, also deserve recognition for their much valued input, feedback, and guidance. Without these four people, this dissertation would not have been possible. I would like to thank the Department of Environmental Engineering and Earth Sciences for assistantship support and the General Engineering Program for the opportunity to teach. I would also like to thank three undergraduate students, Macey Bosley, Andrew Shealy, and Alan Martuch, for their assistance with this work. I am thankful for my fellow graduate students, including past and present Powell group members, for their support and friendship throughout my graduate school experience. Without the inspiration, motivation, and dedication instilled in me by my parents, Doug and Teresa Collins, I likely would not have persisted in graduate school. Thanks are due to my husband, Paul Kilgo, for being understanding and accommodating throughout this process but more importantly, for pushing me pursue my goals and encouraging me at every step. I would also like to thank Marley for being the best kind of friend.

I would like to thank Clemson University for the Transformative Initiative for Generating Extramural Research (TIGER) grant, which funded the work with Li-ion batteries, and NSF for the Research Experience for Undergraduates grant (1460863), which supported Macey Bosley. Additionally, funding for the production of the lysimeter test bed and assistantship support was provided by the US Department of Energy Office of Science, Office of Basic Energy Sciences, and Office of Biological and Environmental Research under Award Number DE-SC-00012530.

Table of Contents

Table of Contents (continued)

List of Tables

List of Tables (continued)

List of Figures

List of Figures (continued)

Page

List of Figures (continued)

Page

Chapter 1: Introduction

One of the greatest challenges of modern society is to meet the growing energy demand while minimizing long-term environmental effects from both the production and storage of energy. Renewable energy resources, including solar energy, represent the most sustainable way to meet the growing energy requirements (Sanaeepur et al., 2013). Because emerging energy technologies, including photovoltaic (PV) modules and lithium ion (Li-ion) batteries, are increasing rapidly to meet the growing worldwide energy demand, investigating their entire life cycles is important to ensure impacts from all life cycle stages are included. There is a limited understanding of the end-of-life phase of PV modules and Li-ion batteries and the associated risks to human and environmental health (Hawkins et al., 2012; Kang et al., 2013). Many of the studies of Li-ion batteries and PV modules at end-of-life focus on recycling, and few consider landfill disposal, which necessitates the investigation of the appropriateness of hazardous waste regulatory methods to characterize the toxicity and appropriate disposal at end-of-life (Collins and Anctil, 2015). Li-ion battery manufacturing has been the subject of recent research, but the risks from toxic metal emissions from disposal have not been quantified (Gaustad et al., 2012). Disposing of Li-ion batteries in landfills could present environmental risks from leaching of organic electrolytes, toxic metals, lithium salts, and carbonaceous material (Richa et al., 2014). Similarly, PV modules are not subject to regulations mandating manufacturer take-back programs or recycling in the United States (US), and their environmental impacts from disposal at end-of-life have not been quantified. ***By investigating the end-of-life phase for emerging energy technologies, my research contributes to the development of end-of-life strategies that ensure the growing energy demand can be met without unintentional risks to human and environmental health.***

1.1 References

Collins, M. K.; Anctil, A. Implications for Current Regulatory Waste Toxicity Characterisation Methods from Analysing Metal and Metalloid Leaching from Photovoltaic Modules. *Int. J. Sustain. Energy* **2015**, 1–14.

Gaustad, G.; Ganter, M.; Wang, X.; Bailey, C.; Babbitt, C.; Landi, B. Economic and Environmental Trade Offs for Li-Based Battery Recycling. In *Energy Technology 2012: Carbon Dioxide Management and Other Technologies*; **2012;** pp 219–226.

Hawkins, T.; Gausen, O.; Stromman, A. Environmental Impacts of Hybrid and Electric Vehicles—A Review. *Int. J. Life Cycle Assess.* **2012**, *17* (8), 997–1014.

Kang, D.; Chen, M.; Ogunseitan, O. Potential Environmental and Human Health Impacts of Rechargeable Lithium Batteries in Electronic Waste. *Environ. Sci. Technol.* **2013**, *47* (10), 5495–5503.

Richa, K.; Babbitt, C.; Gaustad, G.; Wang, X. A Future Perspective on Lithium-Ion Battery Waste Flows from Electric Vehicles. *Resour. Conserv. Recycl.* **2014**, *83*, 63–76.

Sanaeepur, S.; Sanaeepur, H.; Kargari, A.; Habibi, M. H. Renewable Energies: Climate-Change Mitigation and International Climate Policy. *Int. J. Sustain. Energy* **2013**, *33* (1), 203–212.

Chapter 2: Background

2.1 Growth in the PV and Li-ion Battery Markets

Solar photovoltaic (PV) installation is increasing in the US and is forecasted to continue to rise due to the increased number of renewable portfolio standards and policies by government entities that require certain percentages of energy from renewable sources (Dinçer, 2011; Solangi et al., 2011; Timilsina et al., 2012) (Figure 2.1a). Current trends in solar installation show that the market for PV technologies is expanding in the US with a total of 42.9 gigawatts installed as of 2016 and a moderate outlook of 112 gigawatts installed by 2021 (SolarPower Europe, 2017). Additionally, costs for residential and commercial PV systems declined on average by 6-7% per year from 1998 to 2013 but more rapidly in 2012 and 2013 reaching a decline in price of 12-15% (Feldman et al., 2014), therefore suggesting the number of PV installations are likely to increase faster in the upcoming years.

The increase in solar PV installation will result in an increase in energy storage to be able to use the energy produced at any time of day, and Li-ion batteries are a viable option for energy storage (Chen et al., 2009). With decreasing prices, Li-ion batteries are becoming economically viable for home energy storage systems for electricity produced by PV modules (Naumann et al., 2015). As an example. the Telsa Powerwall Li-ion battery is installed in homes to store energy from PV modules, which allows the home to be independent of the elecricity grid (Tesla Motors, 2016). Likewise at the utility scale, energy storage is needed when production exceeds demand for renewable sources, and Li-ion batteries are becoming one of the preferred technologies (Scott and Simon, 2015) with 15 deployments of greater than one megawatt capacity in the US (USDOE, 2013). In addition to solar related applications, Li-ion batteries are increasing in use in consumer electronics and electric vehicles, with the global lithium battery market increasing from

$11 billion to nearly $13.4 billion over the next five years (Lithium Batteries: Markets and Materials, 2013) and automotive Li-ion batteries increasing to $30 billion by 2018 (USEPA, 2013) (Figure 2.1b).

The increase in solar PV installation will lead to an enormous waste stream in the future (McDonald and Pearce, 2010), but the timing of the waste stream will depend not only on the lifetime of the modules installed but also on their reliability and failure rates, meaning the waste stream could grow faster than anticipated. The diversity of the technologies installed will lead to a diverse electronic waste stream with varying chemical composition which can impede recycling processes. Worldwide, approximately 85% of production is wafer-based silicon modules, but thin-film technologies, including amorphous silicon (a-Si), cadmium telluride (CdTe), and copper indium gallium diselenide (CIGS) modules, are emerging and represented 10% of the market share in 2007 (Jäger-Waldau, 2012).

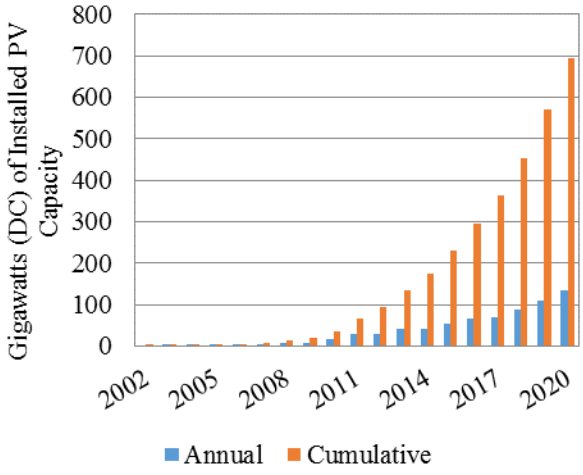

(a)

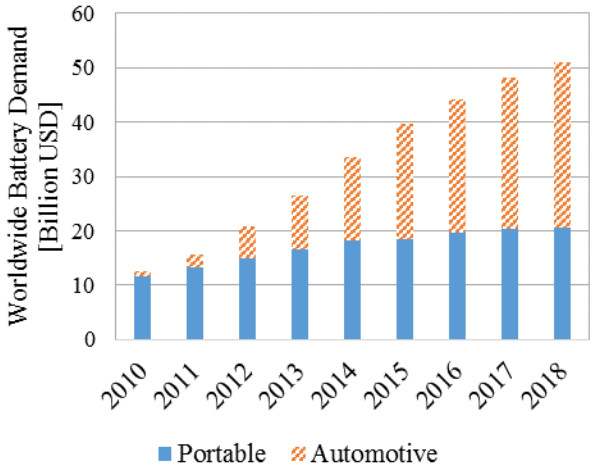

(b)

Figure 2.1: (a) Annual and cumulative worldwide PV demand through 2020 (GTM Research, 2018) and (b) Worldwide portable and automotive Li-ion battery demand (USEPA, 2013)

Similar to PV, the battery waste stream is predicted to grow in proportion to the global lithium battery market. The waste stream from automotive Li-ion batteries is expected to reach 750,000 batteries by 2030 (Commission for Environmental Cooperation, 2015). Differing from batteries in portable consumer products, automotive batteries are more likely to have infrastructure and policies in place to ensure their collection and recycling at end-of-life (Commission for Environmental Cooperation, 2015). Li-ion batteries can be repurposed when their charge capacity decreases, such as from automotive to stationary applications, delaying the time to enter the waste stream for disposal or recycling. However for batteries in portable devices, consumers currently only return 20-40% of spent batteries for recycling in the US (BU-705: How to Recycle Batteries, 2015) with most of the batteries that would be available for recycling either sequestered in homes and businesses or entering the municipal solid waste stream (Goonan, 2012).

2.2 Landfill Regulations and Recycling of PV and Li-ion Batteries in the United States

The balance between the recycling and landfill disposal rates of batteries and PV modules is determined by many factors, including the profitability of recycling, the existence of government regulations (Richa et al., 2014) and the availability of recycling facilities. The profitability of recycling can incentivize companies to recycle. For example, the company Retriev Technologies located in Anaheim, California, recovers the cobalt, copper, and aluminum from Li-ion batteries (Retriev Technologies: Lithium Ion, 2015), and First Solar at their Perrysburg, Ohio, location recovers cadmium and tellurium from CdTe PV modules (First Solar, 2015). Small changes in composition, such as the replacement of cobalt in Li-ion battery cathodes with manganese compounds or the use of earth abundant and less expensive materials in PV modules, can reduce

the incentive to recycle due to the decrease in profitability of recovering relatively low value materials when the costs for recovery are relatively high (Wang et al., 2014b).

If profitability does not drive recycling efforts, government regulation might. The Mercury-Containing and Rechargeable Battery Act requires that batteries be easily removable from consumer products to facilitate recycling and to include the battery chemistry on packaging (USEPA, 2015). However, this federal act does not require recycling, and the recycling of e-waste (which includes batteries) varies between states. While electronic recycling laws have been passed in 25 states, these laws vary substantially regarding the types of electronics collected for recycling (National Center for Electronics Recycling (NCER): Laws, 2015). Currently only three states have an outright ban on the landfill disposal of Li-ion batteries: New York, California, and Minnesota (Household battery recycling and disposal; Wang et al., 2014a). These three states comprise approximately 5% of the US population (US Census Bureau, 2011), and if Li-ion battery usage per person is assumed not to vary across states, then only up to 5% of the Li-ion batteries in the US are currently banned from landfills, which does not consider the transfer of waste across states for disposal. As an example, 2.5% of the total solid waste disposed of in South Carolina landfills in 2015 was "imported" waste from New York (DHEC, 2015). In South Carolina, computers, computer monitors, printers and televisions cannot be discarded into waste streams destined for solid waste landfills, but the disposal of Li-ion batteries is not regulated (SCDHEC, 2018). Likewise, PV modules are not specifically regulated in the United States. However in the European Union member states the Waste Electrical and Electronic Equipment (WEEE) Directive as of 2012 requires PV modules to be collected for recycling and no longer discarded as waste (European Parliament and Council of the European Union). The potential of PV modules to be classified as hazardous waste in the US could lead to adopting take-back programs and recycling even if they are currently economically and logistically infeasible in the

United States. Temporal and spatial boundaries should be considered when implementing take-back and recycling programs, and mathematical models which include varying material prices, transportation, and external costs have been developed to aid in maximizing profits for recycling PV modules (Choi and Fthenakis, 2010, 2014).

Another factor affecting recycling is ensuring the availability of recycling facilities. A small number of dedicated battery recycling facilities exist in North America; eight companies currently recycle Li-ion batteries with recovering cobalt as the economic driving force for recycling (Commission for Environmental Cooperation, 2015). With over 34,000 collection sites in the US and Canada, Call2recycle is the largest battery collection and recycling firm currently in operation, collecting batteries at no direct cost to municipalities and businesses (Call2Recycle, 2018). Also, the US Department of Energy in 2009 helped subsidize the construction of the first US facility for recycling Li-ion vehicle batteries (Jaskula, 2011). Despite these efforts to adjust government regulations and increase the number of dedicated Li-ion battery recycling firms, the volume of Li-ion batteries in landfills will significantly increase with their increased use and diminished end-of-life value. Similarly, recycling technologies are being developed and implemented for thin-film PV technologies (Marwede et al., 2013) and silicon cells (Klugmann-Radziemska et al., 2010), but collection programs will need to be implemented to ensure all PV modules are recycled. Nevertheless, the growing number of consumer products with PV cells, such as solar yard lights, will contribute to an increased volume of PV materials sent to landfills at the end of their useful life.

2.3 Limitations to Regulatory Toxicity Characterization Methods

US Environmental Protection Agency (EPA) regulations and some individual state standards are used to determine the toxicity of potentially hazardous e-waste. EPA Method 1311 (USEPA,

1992), which outlines the Toxicity Characteristic Leaching Procedure (TCLP) is widely used to categorize the toxicity of light-emitting diodes (Lim et al., 2011), personal computer components (Li et al., 2009a; Komilis et al., 2013), mobile phones (Yadav and Yadav, 2014), and other household e-waste (Musson et al., 2006). However, the use of these current regulatory leaching methods to assess the toxicity of different e-wastes may be less than accurate (Poon and Lio, 1997; Kosson et al., 2002; Ghosh et al., 2004; Karamalidis and Voudrias, 2007). Specifically, the TCLP may be inadequate due to evaluating and regulating wastes using a single, worst-case test condition leading to both over-regulation and inadequate protection of the environment (Kosson et al., 2002). The TCLP does not account for a range of pH values, which is known to affect the leaching of metals and anions (Karamalidis and Voudrias, 2007). Additionally, the TCLP is ill-suited to truly assess the Li-ion leaching potential because of the acid neutralizing capacity of other landfill wastes, in addition to the assessment of long-term leaching after the acid neutralizing capacity diminishes (Poon and Lio, 1997). Drastic differences in lead concentrations have been found by changing the minimum particle size and the contact time, which are not specified by the TCLP (Janusa et al., 1998). Finally, the regulatory limits were set to account for the likely dilution and attenuation that will occur in subsurface transport by multiplying the drinking water standards of 1986, authorized by the Safe Drinking Water Act, by a factor of 100 (USEPA, 1995). Although the drinking water standards have changed since 1986 (USEPA, 2018), the regulatory limits for the TCLP have not. Additionally, the regulatory limits assume that the potential exposure at concentrations below the defined levels are not hazardous and that the defined concentrations are predictive of human and eco-toxicity effects. Thus, comparing TCLP results with results from laboratory scale landfill leachate experiments and intermediate-scale landfill experiments is needed, and the ability of these methods to properly characterize disposal of e-waste, particularly Li-ion batteries and PV modules, can be assessed.

2.4 Prior Leaching and Landfill Degradation Studies

Waste-filled columns, or lysimeters, constructed and operated to simulate the landfill processes have been used to understand the degradation of household e-waste within municipal solid waste (MSW). These lysimeters have been used to identify metal ions leaching from e-waste (Karnchanawong and Limpiteeprakan, 2009; Li et al., 2009b; Visvanthan et al., 2010) and also from spent zinc-carbon, alkaline, nickel-cadmium, and nickel-metal hydride batteries (Karnchanawong and Limpiteeprakan, 2009; Komilis et al., 2011). Such procedures are useful in landfill simulations because either simulated or excavated MSW can be used within the columns, and it is possible to either add or develop a synthetic leachate. Initial studies have shown that metal ions from e-waste are not significantly mobile and appear at low concentrations within leachate. In a two-year landfill study, researchers noted the absence of Pb in the leachate circulating through columns containing personal computers and cathode ray tubes within a two-year time frame (Li et al., 2009b). However, it was hypothesized that Pb might possibly migrate into the leachate solution because of increased levels of Pb within the material beneath the e-waste (Li et al., 2009b). In one study, lysimeters containing e-waste scraps from mostly computer parts mixed with MSW were studied for 280 days. Fe and Zn concentrations from the lysimeters were comparable to TCLP test concentrations, however the Pb concentration was much lower than the TCLP concentration (Visvanthan et al., 2010). In another study, broken and intact e-waste was added to outdoor columns filled with MSW and then exposed to rain. Although sampling showed a slow, continuous leaching of Al, Ba, Be, Cd, Co, Cr, Cu, Ni, Pb, Sb and V, the concentrations of these metals were far below TCLP regulatory limits but in some cases exceeded limits for drinking water (Kiddee et al., 2013). In a similar study using synthetic and excavated MSW, lead concentrations within columns containing electronics did not significantly differ from control columns over a monitoring period of 440 days (Spalvins et al., 2008). These

studies show that the proper management of e-waste in landfills can prevent inorganic pollutants from contaminating soils and aquifers. However, improperly operated landfills can cause environmental contamination of soils and aquifers from these pollutants (Komilis et al., 1999).

2.5 Life Cycle Assessment (LCA) of Li-ion Batteries and PV Modules

LCA quantifies ecological and human health impacts of a product from "cradle-to-grave"; e.g. from raw material extraction (cradle) to the ultimate disposal of end products to the earth (grave). Used by both manufacturers and external evaluators, LCA studies serve as best practices for designing products that pose a limited risk to both human and environmental health, and to help policy makers make informed decisions regarding their management. An inventory of inputs (energy and materials) and outputs (emissions) throughout the product's life cycle is compiled, and an impact assessment based on environmental indicators is performed (Owens, 1997). The four components to conducting a LCA include (1) defining the goal and scope, (2) compiling the inventory, (3) conducting an impact assessment, and (4) interpretation and improvement assessment (Owens, 1997). The process is iterative with each component informing other components.

Although recent LCA models have been used to analyze the manufacturing, use and disposal stages of Li-ion batteries, there is wide variation in the assumptions, and the quality of the incorporated data within these studies. For example, in several Li-ion LCAs, material inventory was used from either Li-ion battery manufacturing process or identified during battery disassembly (i.e. in all cases, it was assumed that the battery material remained unaltered during battery lifetime and upon disposal) (Gaustad et al., 2012). Although global warming potential, cumulative energy demand, and abiotic depletion potential were calculated, unfortunately, there were little data on disposal in a LCA of lithium manganese oxide batteries (Notter et al., 2010). In

another LCA, batteries were assumed to be dismantled and cryogenically shattered at end-of-life, but specific information about the process was not provided (Hawkins et al., 2013). Also it is overly optimistic to assume that the current rate of Li-ion battery recycling even exceeds 20%, despite several LCA studies indicating as such (Olofsson and Romare, 2013; USEPA, 2013). Elucidating the entire Li-ion battery life cycle requires determining and characterizing the metal emissions at the end-of-life phase to ensure an accuracy of results (Gaustad et al., 2012). However, little is currently known about the fate and potential risks of those Li-ion battery emissions caused by leaching during landfill disposal (Hawkins et al., 2012). Although some limited data are available regarding of the leaching of Li-ion cell phone batteries, it was incomplete for determining the occurrence of Li-ion battery leaching in landfills (Kang et al., 2013). In addition, there is a large diversity in the composition of Li-ion batteries and Kang et al. (2013) do not discuss possible variations in leaching due to these changes. Nonetheless, when the Li-ion cell phone battery leaching data were included in an LCA, cobalt, copper, nickel, thallium and silver leaching did exhibit potential freshwater and terrestrial eco-toxicities, possible abiotic resource depletion, and human toxicity (Kang et al., 2013). The study validated the necessity of identifying these leaching mechanisms, the fate of metal emissions during disposal, and the end of life morphology of those batteries upon disposal, data that current lithium-ion battery LCAs do not incorporate.

While PV installations are considered clean energy because they are non-polluting during their use phase, impacts occur from their production, transportation, and recycling or disposal. Life cycle inventories for a small sampling of PV modules have been assembled from manufacturing data (Fthenakis et al., 2011), but these studies exclude minority materials and usually do not consider disposal at end of life. A literature review of LCAs of PV systems published in 2014 noted only three studies which consider end-of-life in the analysis (Gerbinet et

al., 2014). One of these studies is of a PV plant located in Italy for which the authors included three decommissioning scenarios: landfilling, recycling only glass and aluminum, and recycling all components; however, only the impact categories from the complete recycling scenario were presented in the results (Desideri et al., 2012). In another LCA of PV plants with and without axis tracking, which allows the modules to rotate to produce more energy from direct sunlight as the position of the sun changes, an end-of-life scenario was discussed, but no specific end-of-life results were presented (Bayod-Rújula et al., 2011). In a study comparing a polycrystalline PV module and wind turbine, landfill disposal of all components and recycling of glass, plastic, and metal components were compared (Zhong et al., 2011). For the landfilling scenario, 51.2% of the impacts were found to be from the plastic components, and the PV cells were assumed to be inert waste (Zhong et al., 2011). One LCA of the balance of system components (all necessary components not including the PV panels) for a power plant PV installation included disposal of the plant components at end-of-life and assumed a transportation distance of 160 km (Mason et al., 2006), but the study did not consider the actual PV materials and their fate at end-of-life. Another study of a roof installation in Rome, Italy, recognized that impacts from system disposal at end of life need to be considered, however disposal was assumed to have a negligible impact (Battisti and Corrado, 2005), most likely due to a lack of data. Similarly, a LCA study of crystalline and thin film technologies installed in Europe recognized that recycling and disposal of PV modules needs be included in LCA studies, but they were not included or discussed as part of the hazardous emissions results (Alsema et al., 2006). A study of four commercially available PV systems showed very promising results for reducing greenhouse gas emissions by producing modules using PV solar energy sources, but limited their scope to cradle to gate (raw materials to manufacturing) and considered heavy metal emissions from direct sources (losses during manufacturing or disposal) to be minute compared to the indirect emissions from electricity and

fuel use in manufacturing (Fthenakis et al., 2008). These studies highlight the knowledge gap in potential emissions from disposal or recycling which needs to be studied further.

2.6 References

Alsema, E. A.; de Wild-Scholten, M. J.; Fthenakis, V. M. Environmental Impacts of PV Electricity Generation-a Critical Comparison of Energy Supply Options. In *21st European Photovoltaic Solar Energy Conference, Dresden, Germany*; **2006**; Vol. 3201.

Battisti, R.; Corrado, A. Evaluation of Technical Improvements of Photovoltaic Systems through Life Cycle Assessment Methodology. *Energy* **2005**, *30* (7), 952–967.

Bayod-Rújula, Á. A.; Lorente-Lafuente, A. M.; Cirez-Oto, F. Environmental Assessment of Grid Connected Photovoltaic Plants with 2-Axis Tracking versus Fixed Modules Systems. *Energy* **2011**, *36* (5), 3148–3158.

BU-705: How to Recycle Batteries http://batteryuniversity.com/learn/article/recycling_batteries (accessed Sep 23, 2015).

Call2Recycle http://www.call2recycle.org (accessed April 16, 2018).

Chen, H.; Cong, T. N.; Yang, W.; Tan, C.; Li, Y.; Ding, Y. Progress in Electrical Energy Storage System: A Critical Review. *Prog. Nat. Sci.* **2009**, *19* (3), 291–312.

Choi, J.-K.; Fthenakis, V. Economic Feasibility of Recycling Photovoltaic Modules. *J. Ind. Ecol.* **2010**, *14* (6), 947–964.

Choi, J.-K.; Fthenakis, V. Crystalline Silicon Photovoltaic Recycling Planning: Macro and Micro Perspectives. *J. Clean. Prod.* **2014**, *66*, 443–449.

Commission for Environmental Cooperation. *Environmentally Sound Management of End-of-Life Batteries from Electric-Drive Vehicles in North America*; **2015**.

Desideri, U.; Proietti, S.; Zepparelli, F.; Sdringola, P.; Bini, S. Life Cycle Assessment of a Ground-Mounted 1778kW P Photovoltaic Plant and Comparison with Traditional Energy Production Systems. *Appl. Energy* **2012**, *97*, 930–943.

DHEC. *S.C. Solid Waste Management Annual Report for Fiscal Year 2015*; **2015**.

Dinçer, F. The Analysis on Photovoltaic Electricity Generation Status, Potential and Policies of the Leading Countries in Solar Energy. *Renew. Sustain. Energy Rev.* **2011**, *15* (1), 713–720.

European Parliament and Council of the European Union. Official Journal of the European Union. *55* (L197), 1–71.

Feldman, D.; Barbose, G.; Margolis, R.; James, T.; Weaver, S.; Darghouth, N.; Fu, R.; Davidson, C.; Booth, S.; Wiser, R. *Photovoltaic System Pricing Trends: Historical, Recent, and Near-Term Projections. 2014 Edition (Presentation). Sunshot, U.S. Department of Energy (DOE).*; **2014**.

First Solar. The Recycling Advantage http://www.firstsolar.com/en/Technologies-and-Capabilities/Recycling-Services.aspx (accessed Oct 5, 2015).

Fthenakis, V.; Kim, H. C.; Frischknecht, R.; Raugei, M.; Sinha, P.; Stucki, M. *Life Cycle Inventories and Life Cycle Assessment of Photovoltaic Systems*; International Energy Agency, **2011**; Vol. T12–02:201.

Fthenakis, V. M.; Kim, H. C.; Alsema, E. Emissions from Photovoltaic Life Cycles. *Environ. Sci. Technol.* **2008**, *42* (6), 2168–2174.

Gaustad, G.; Ganter, M.; Wang, X.; Bailey, C.; Babbitt, C.; Landi, B. Economic and Environmental Trade Offs for Li-Based Battery Recycling. In *Energy Technology 2012: Carbon Dioxide Management and Other Technologies*; **2012**; pp 219–226.

Gerbinet, S.; Belboom, S.; Léonard, A. Life Cycle Analysis (LCA) of Photovoltaic Panels: A Review. *Renew. Sustain. Energy Rev.* **2014**, *38*, 747–753.

Ghosh, A.; Mukiibi, M.; Ela, W. TCLP Underestimates Leaching of Arsenic from Solid Residuals under Landfill Conditions. *Environ. Sci. Technol.* **2004**, *38* (17), 4677–4682.

Goonan, T. G. *Lithium Use in Batteries Circular 1371*; US Department of the Interior, US Geological Survey, **2012**.

GTM Research. Global PV Demand Outlook 2015-2020: Exploring Risk in Downstream Solar Markets https://www.greentechmedia.com/research/report/global-pv-demand-outlook-2015-2020 (accessed April 16, 2018).

Hawkins, T.; Gausen, O.; Stromman, A. Environmental Impacts of Hybrid and Electric vehicles—A Review. *Int. J. Life Cycle Assess.* **2012**, *17* (8), 997–1014.

Hawkins, T.; Singh, B.; Majeau-Bettez, G.; Strømman, A. Comparative Environmental Life Cycle Assessment of Conventional and Electric Vehicles. *J. Ind. Ecol.* **2013**, *17* (1), 53–64.

Household battery recycling and disposal https://www.pca.state.mn.us/sites/default/files/w-hhw4-12.pdf (accessed May 24, 2016).

Jäger-Waldau, A. *PV Status Report 2012*; European Commission, **2012**.

Janusa, M. A.; Bourgeois, J. C.; Heard, G. E.; Kliebert, N. M.; Landry, A. A. Effects of Particle Size and Contact Time on the Reliability of Toxicity Characteristic Leaching Procedure for Solidified/Stabilized Waste. *Microchem. J.* **1998**, *59* (2), 326–332.

Jaskula, B. W. *2009 Minerals Yearbook*; **2011**.

Kang, D.; Chen, M.; Ogunseitan, O. Potential Environmental and Human Health Impacts of Rechargeable Lithium Batteries in Electronic Waste. *Environ. Sci. Technol.* **2013**, *47* (10), 5495–5503.

Karamalidis, A. K.; Voudrias, E. A. Release of Zn, Ni, Cu, SO4(2-) and CrO4(2-) as a Function of pH from Cement-Based Stabilized/solidified Refinery Oily Sludge and Ash from Incineration of Oily Sludge. *J. Hazard. Mater.* **2007**, *141* (3), 591–606.

Karnchanawong, S.; Limpiteeprakan, P. Evaluation of Heavy Metal Leaching from Spent Household Batteries Disposed in Municipal Solid Waste. *Waste Manag.* **2009**, *29* (2), 550–558.

Kiddee, P.; Naidu, R.; Wong, M. H. Metals and Polybrominated Diphenyl Ethers Leaching from Electronic Waste in Simulated Landfills. *J. Hazard. Mater.* **2013**, *252–253*, 243–249.

Klugmann-Radziemska, E.; Ostrowski, P.; Drabczyk, K.; Panek, P.; Szkodo, M. Experimental Validation of Crystalline Silicon Solar Cells Recycling by Thermal and Chemical Methods. *Sol. Energy Mater. Sol. Cells* **2010**, *94* (12), 2275–2282.

Komilis, D.; Bandi, D.; Kakaronis, G.; Zouppouris, G. The Influence of Spent Household Batteries to the Organic Fraction of Municipal Solid Wastes during Composting. *Sci. Total Environ.* **2011**, *409* (13), 2555–2566.

Komilis, D.; Tataki, V.; Tsakmakis, T. Leaching of Heavy Metals from Personal Computer Components: Comparison of TCLP with a European Leaching Test. *J. Environ. Eng.* **2013**, *139* (11), 1375–1381.

Komilis, D. P.; Ham, R. K.; Stegmann, R. The Effect of Landfill Design and Operation Practices on Waste Degradation Behavior: A Review. *Waste Manag. Res.* **1999**, *17* (1), 20–26.

Kosson, D. S.; van der Sloot, H. A.; Sanchez, F.; Garrabrants, A. C. An Integrated Framework for Evaluating Leaching in Waste Management and Utilization of Secondary Materials. *Environ. Eng. Sci.* **2002**, *19* (3), 159–204.

Li, Y.; Richardson, J. B.; Niu, X.; Jackson, O. J.; Laster, J. D.; Walker, A. K. Dynamic Leaching Test of Personal Computer Components. *J. Hazard. Mater.* **2009a**, *171* (1–3), 1058–1065.

Li, Y.; Richardson, J. B.; Bricka, R. M.; Niu, X.; Yang, H.; Li, L.; Jimenez, A. Leaching of Heavy Metals from E-Waste in Simulated Landfill Columns. *Waste Manag.* **2009b**, *29* (7), 2147–2150.

Lim, S.-R.; Kang, D.; Ogunseitan, O. A.; Schoenung, J. M. Potential Environmental Impacts of Light-Emitting Diodes (LEDs): Metallic Resources, Toxicity, and Hazardous Waste Classification. *Environ. Sci. Technol.* **2011**, *45* (1), 320–327.

Lithium Batteries: Markets and Materials http://www.bccresearch.com/market-research/fuel-cell-and-battery-technologies/batteries-lithium-fcb028f.html (accessed Sep 23, 2015).

Marwede, M.; Berger, W.; Schlummer, M.; Mäurer, A.; Reller, A. Recycling Paths for Thin-Film Chalcogenide Photovoltaic Waste – Current Feasible Processes. *Renew. Energy* **2013**, *55* (0), 220–229.

Mason, J. E.; Fthenakis, V. M.; Hansen, T.; Kim, H. C. Energy Payback and Life-Cycle CO2 Emissions of the BOS in an Optimized 3· 5 MW PV Installation. *Prog. Photovoltaics Res. Appl.* **2006**, *14* (2), 179–190.

McDonald, N. C.; Pearce, J. M. Producer Responsibility and Recycling Solar Photovoltaic Modules. *Energy Policy* **2010**, *38* (11), 7041–7047.

Musson, S. E.; Vann, K. N.; Jang, Y.-C.; Mutha, S.; Jordan, A.; Pearson, B.; Townsend, T. G. RCRA Toxicity Characterization of Discarded Electronic Devices. *Environ. Sci. Technol.* **2006**, *40* (8), 2721–2726.

National Center for Electronics Recycling (NCER): Laws http://www.electronicsrecycling.org/?page_id=39 (accessed Sep 23, 2015).

Naumann, M.; Karl, R. C.; Truong, C. N.; Jossen, A.; Hesse, H. C. Lithium-Ion Battery Cost Analysis in PV-Household Application. *Energy Procedia* **2015**, *73*, 37–47.

Notter, D.; Gauch, M.; Widmer, R.; Wager, P.; Stamp, A.; Zah, R.; Althaus, H. Contribution of Li-Ion Batteries to the Environmental Impact of Electric Vehicles. *Environ. Sci. Technol.* **2010**, *44* (17), 6550–6556.

Olofsson, Y.; Romare, M. Life Cycle Assessment of Lithium-Ion Batteries from Plug-in Hybrid Buses, Chalmers University of Technology, **2013**.

Owens, J. W. Life-Cycle Assessment: Constraints on Moving from Inventory to Impact Assessment. *J. Ind. Ecol.* **1997**, *1* (1), 37–49.

Poon, C. S.; Lio, K. W. The Limitation of the Toxicity Characteristic Leaching Procedure for Evaluating Cement-Based Stabilised/solidified Waste Forms. *Waste Manag.* **1997**, *17* (1), 15–23.

Retriev Technologies: Lithium Ion http://www.retrievtech.com/recycling/lithium-ion (accessed Oct 5, 2015).

Richa, K.; Babbitt, C.; Gaustad, G.; Wang, X. A Future Perspective on Lithium-Ion Battery Waste Flows from Electric Vehicles. *Resour. Conserv. Recycl.* **2014**, *83*, 63–76.

SCDHEC. Electronics Recycling Overview http://www.scdhec.gov/HomeAndEnvironment/Recycling/Electronics/OverviewEcycling/ (accessed April 16, 2018).

Scott, P.; Simon, M. *Utility Scale Energy Storage: Grid-Saver Fast Energy Storage System*; **2015**.

Solangi, K. H.; Islam, M. R.; Saidur, R.; Rahim, N. A.; Fayaz, H. A Review on Global Solar Energy Policy. *Renew. Sustain. Energy Rev.* **2011**, *15* (4), 2149–2163.

SolarPower Europe. *Global Market Outlook for Solar Power 2017-2021*; **2017**.

Spalvins, E.; Dubey, B.; Townsend, T. Impact of Electronic Waste Disposal on Lead Concentrations in Landfill Leachate. *Environ. Sci. Technol.* **2008**, *42* (19), 7452–7458.

Tesla Motors. Energy Storage for a Sustainable Home https://www.teslamotors.com/powerwall (accessed Jan 6, 2016).

Timilsina, G. R.; Kurdgelashvili, L.; Narbel, P. A. Solar Energy: Markets, Economics and Policies. *Renew. Sustain. Energy Rev.* **2012**, *16* (1), 449–465.

US Census Bureau. *2010 Census Data*; **2011**.

USDOE. *Grid Energy Storage*; **2013**.

USEPA. Method 1311 Toxicity Characteristic Leaching Procedure.

USEPA. *Applicability of the Toxicity Characteristic Leaching Procedure to Mineral Processing Wastes*; **1995**.

USEPA. *Application of Life-Cycle Assessment to Nanoscale Technology: Lithium-Ion Batteries from Electric Vehicles EPA 744-R-12-001*; **2013**.

USEPA. National Primary Drinking Water Regulations http://water.epa.gov/drink/contaminants/#List (accessed April 16, 2018).

USEPA. Wastes - Resource Conservation - Common Wastes & Materials http://www.epa.gov/wastes/conserve/materials/battery.htm (accessed Sep 23, 2015).

Visvanthan, C.; Yin, N. H.; Karthikeyan, O. P. Co-Disposal of Electronic Waste with Municipal Solid Waste in Bioreactor Landfills. *Waste Manag.* **2010**, *30* (12), 2608–2614.

Wang, X.; Gaustad, G.; Babbitt, C.; Bailey, C.; Ganter, M.; Landi, B. Economic and Environmental Characterization of an Evolving Li-Ion Battery Waste Stream. *J. Environ. Manage.* **2014a**, *135*, 126–134.

Wang, X.; Gaustad, G.; Babbitt, C.; Richa, K. Economies of Scale for Future Lithium-Ion Battery Recycling Infrastructure. *Resour. Conserv. Recycl.* **2014b**, *83*, 53–62.

Yadav, S.; Yadav, S. Investigations of Metal Leaching from Mobile Phone Parts Using TCLP and WET Methods. *J. Environ. Manage.* **2014**, *144*, 101–107.

Zhong, Z. W.; Song, B.; Loh, P. E. LCAs of a Polycrystalline Photovoltaic Module and a Wind Turbine. *Renew. Energy* **2011**, *36* (8), 2227–2237.

Chapter 3: Motivation and Research Objectives

The motivation of my research lies in addressing gaps in knowledge for emerging energy technologies at the end of their useful lives when they are disposed of in landfills. Will their disposal pose a risk to human and environmental health? How does this compare to other end-of-life options such as recycling? With the increased quantity of both PV installations and Li-ion batteries, current trends suggest large waste streams will result in the not so distant future, adding to the e-waste problem. Without policies or infrastructure in place to capture these waste streams, increased quantities will enter into landfills where their effects are largely unstudied. My research addresses these unknowns by studying the chemical and physical degradation under landfill conditions, which is applied to improve current life cycle assessments of these technologies. Although metals are not the only contaminant of concern, my work focuses on metals because of the quantities and concentrations in which they are present in PV modules and Li-ion batteries and the likelihood of being released under landfill conditions. Moreover, metals leached from PV modules and Li-ion batteries are the most likely contaminants to cause these technologies to be labeled as hazardous waste under current regulatory methods.

I hypothesize that degradation of Li-ion batteries and PV modules followed by metal ion release is facilitated by acidic leachate in the early lifetime of a municipal solid waste landfill and that the metal ions released could be at concentrations of concern in landfill leachate. In the later stages of landfill exposure, the metal ion release is dominated by organic ligands, which varies in rate and extent from early landfill exposure. Information gained from the field and laboratory studies can be useful for informing landfill policies and filling knowledge gaps in current LCAs of PV modules and batteries. The hypotheses and related research objectives are organized into four tasks, which are described in Table 3.1.

Table 3.1: Summary of the research approach including experimental tasks and descriptions.

Task	Description	Chapters
1. Lab-scale Degradation of Lithium Ion Batteries and PV Modules	• Quantify metal ion dissolution from Li-ion batteries and PV modules in simulated landfill leachates and waste representing worst-case disposal scenarios and simulating the acid phase of landfills. • Characterize chemical and physical changes in Li-ion battery anodes and cathodes from exposure to landfill leachate. • Conduct regulatory methods for comparison with other leachates and leaching data from Task 3.	4,5
2. Lysimeter Test Bed Design and Implementation	• Document the design and build of the DOE EPSCoR lysimeter test bed for dynamic monitoring of transport under environmental conditions, which is utilized in Task 3.	6
3. Simulated Bioreactor Landfill Conditions Utilizing the Lysimeter Test Bed Facility	• Construct columns to simulate conditions in bioreactor landfills containing municipal solid waste components, Li-ion and nickel metal hydride batteries and PV module samples, and landfill leachate. • Monitor metal ion concentrations, pH, redox potential, temperature, moisture content, and bulk electrical conductivity over time in outdoor conditions. • Characterize the physical and chemical decomposition of Li-ion batteries and PV modules in municipal solid waste landfill conditions.	7
4. Improving LCAs of Lithium Ion and Nickel Metal Hydride Batteries and PV Modules	• Compare the life cycle inventory from disassembly and digestions of Li-ion and nickel metal hydride batteries and a c-Si PV module to the inventories in the ecoinvent database. • Build waste scenarios to update current LCA models of these products to include potential metal leaching from landfill disposal during the end-of-life phase and calculate the impact assessment.	8

Chapter 4: Implications for Current Regulatory Waste Toxicity Characterization Methods from Analyzing Metal and Metalloid Leaching from Photovoltaic Modules*

Abstract

The appropriateness of regulatory methods to characterize the toxicity of photovoltaic modules was investigated to quantify potential environmental impacts for modules disposed of in landfills. Because solar energy is perceived as a green technology, it is important to ensure that end-of-life issues will not be detrimental to solar energy's success. EPA Method 1311, California WET, and modified versions of both were performed on a multi-crystalline silicon module and cells and a copper indium gallium diselenide (CIGS) module. Variations in metal leachate concentrations were found with changes in testing parameters. Lead concentrations from the multi-crystalline module ranged from 16.2 to 50.2 mg/L. Cadmium concentrations from the CIGS module ranged from 0.1 to 3.52 mg/L. This raises doubt that regulatory methods can adequately characterize PV modules. The results are useful for developing end-of-life procedures, which is a positive step towards avoiding an e-waste problem and continuing trends of increasing installation and cost reduction in the PV market.

---

*Chapter 4 is reproduced from: Collins, M. K.; Anctil, A. Implications for Current Regulatory Waste Toxicity Characterisation Methods from Analysing Metal and Metalloid Leaching from Photovoltaic Modules. *Int. J. Sustain. Energy* **2015**;36(6)531-44.

4.1 Introduction

Renewable energy resources, including solar energy, represent the most sustainable way to meet growing energy requirements (Sanaeepur et al., 2013). Solar photovoltaic (PV) installation is increasing in the United States and is forecasted to continue to rise due to the increased number of renewable portfolio standards and policies (Dinçer, 2011; Solangi et al., 2011; Timilsina et al., 2012). Current trends in solar installation show that the market for PV technologies is expanding in the United States with a total of 4.4 gigawatts installed as of 2011 and a moderate outlook of 30.5 gigawatts installed by 2016 (EPIA, 2012). PV systems prices for residential and commercial systems have declined on average by 6-7% per year from 1998 to 2013 but more rapidly in 2012-2013 to reach 12-15% (Feldman et al., 2014), therefore suggesting that the number of PV installations are likely to increase even faster in the upcoming years.

The increase in installation will lead to an enormous waste stream in the future (McDonald and Pearce, 2010), but the timing of this waste stream will depend not only on the lifetime of the modules installed but also on their reliability and failure rates – meaning this waste stream could grow faster than anticipated. The diversity of the technologies installed will lead to a diverse electronic waste stream with varying chemical composition which can impede recycling processes. Worldwide, approximately 85% of production is wafer-based silicon modules, but thin-film technologies, including amorphous silicon (a-Si), cadmium telluride (CdTe), and copper indium gallium diselenide (CIGS) modules, are emerging and represented 10% of the market share in 2007 (Jäger-Waldau, 2012).

4.1.1 Objective

The size and diversity of this waste stream brings urgency to be proactive and develop feasible end-of-life procedures to ensure a dire electronic waste problem does not occur in the near future. The fate of this waste stream will be dependent on several factors including the recyclability of

the different technologies, the possible classification of the waste stream as hazardous waste due to the leaching of metals and metalloids from the modules, economical issues considering the value of the materials used in modules, and social concerns involving policies and the availability of take-back programs.

The objective of this study is to investigate the appropriateness of the current regulatory methods for accessing the toxicity of PV modules by applying the methods and variations of the methods to a small sampling of modules currently available to consumers to acquire preliminary leaching test results.

In a previous study, natural waters were used to benchmark metal and metalloid leaching from copper indium gallium selenide (CIGS) and organic PV cells with an aim to derive predicted environmental concentrations for scenarios of roof-top acidic rain, marine and surface water environments (Zimmermann et al., 2013). This previous study did not consider the applicability of current regulatory methods to PV waste as considered in this study.

Previous work has considered life cycle inventories of CdTe and mono- and multi-crystalline modules using manufacturing data available in the literature, but these estimates were based on a small sampling of modules and possibly excluded minority materials (Fthenakis et al., 2011). PV modules differ in composition from typical electronic waste which has environmental concerns for lead, antimony, mercury, cadmium, and nickel (Robinson, 2009). PV modules can contain tellurium, indium, germanium, and gallium which are limited in supply (Anctil and Fthenakis, 2013) in addition to cadmium, selenium, molybdenum, tin, zinc, and silicon (Goe and Gaustad, 2014). A lack of knowledge exists of the complete composition of many PV modules, and therefore the potential toxicity of the PV modules being installed needs to be examined.

4.1.2 Toxicity Methods

In this study, two methods, EPA Method 1311, the Toxicity Characteristic Leaching Procedure (TCLP) (USEPA, 1992), and California Waste Extraction Test (WET) (DTSC, 2005) and variations of each were used to investigate the toxicity potential of PV modules and cells. Each of these methods was developed to classify a waste as either hazardous or non-hazardous based on replicating the co-disposal of the waste with municipal solid waste following a prescribed laboratory procedure. These methods were developed to simulate contaminant release in this specific environmental scenario, in which the waste is co-disposed with municipal solid waste, and the extraction methods attempt to replicate some of the key factors affecting leaching in the municipal solid waste environment to predict the concentrations which will leach within the landfill (Kosson et al., 2002). The use of one disposal scenario to evaluate and regulate waste has been criticized previously, and according to the Science Advisory Board of the USEPA in order for the leaching procedure to be accurate and reasonably related to the leachability of a waste under actual conditions, multiple leaching tests may need to be developed (Kosson et al., 2002). The toxicity of various electronics products such as light-emitting diodes (Lim et al., 2011), personal computer components (Li et al., 2009a; Komilis et al., 2013) and other household electronic waste (Musson et al., 2006) have been characterized using the standard as well as modified leaching methodologies.

Criticisms of the TCLP include its inability to evaluate and regulate wastes while assuming a single, worst-case test condition which has been shown to be both over-regulating and inadequately protective of the environment (Kosson et al., 2002). Leaching of metals and anions, which can vary as a function of pH, is not accounted for in the regulatory methods (Karamalidis and Voudrias, 2007). The acid neutralizing capacity of some wastes impede a true assessment of leaching potential by the TCLP which has implications for the assessment of long-term leaching after the acid neutralizing capacity diminishes (Poon and Lio, 1997). For arsenic leaching,

comparing landfill leachate to regulatory methods, the TCLP and the WET, shows much higher arsenic concentrations for the actual landfill leachate than for the regulatory methods, and equilibrium is not reached within the 18 hour TCLP duration (Ghosh et al., 2004). Increased lead concentrations for a solidified waste are found for increasing the leachate contact time, and decreased concentrations are found for applying a minimum particle size of 8 mm in addition to the maximum of 9.5 mm (Janusa et al., 1998).

In addition to the previous criticisms of the regulatory methods, Zimmermann et al. investigated the long-term leaching of thin-film photovoltaic cells using natural waters and showed that due to long-term releases of metals and metalloids from CIGS cells, leaching procedures need revision to account for the long-term releases (Zimmermann et al., 2013). The current study expands the scope of the previous study to investigate leaching using regulatory methods in the United States and includes PV cells and modules.

4.2 Materials and Methods

The goal of this study was to investigate the risk of module disposal in landfills, and for this reason, the modules chosen for this work were not subject to manufacturer take-back programs or legislation regulating their disposal. Because of this, these modules will likely be disposed of in landfills at end-of-life where their environmental impacts have not been quantified (Goe and Gaustad, 2014). These modules were obtained through eBay. The results of the leaching tests using these PV modules are not meant to represent all currently available technologies but are useful for investigating the sensitivity of the methods used for classifying the toxicity of PV modules at end-of-life. For this study, multi-crystalline silicon (mc-Si) cells which constitute the active layer of a mc-Si module, a 20 watt Sun Solar mc-Si module, and a 12 watt Global Solar copper indium gallium diselenide (CIGS) module were chosen for testing (Figure 4.1a).

Two methods, EPA Method 1311 and California WET, and modifications of these methods were used to investigate the potential toxicity of PV modules. EPA Method 1311, which is the Toxicity Characteristic Leaching Procedure (TCLP), and the California WET describe sample preparation for determining the toxicity of waste from a regulatory standpoint. Modifications were made to these methods to determine the sensitivity of the results to method conditions and to examine the applicability of the current regulatory methods to PV waste. Variations in time, acidity, maximum particle size, and fluid-to-sample ratio are investigated. All chemicals were purchased through VWR International and Fisher Scientific and used as received. Standards from EMD Millipore and Ultra Scientific were used for inductively coupled plasma optical emission spectrometry (ICP-OES) analysis.

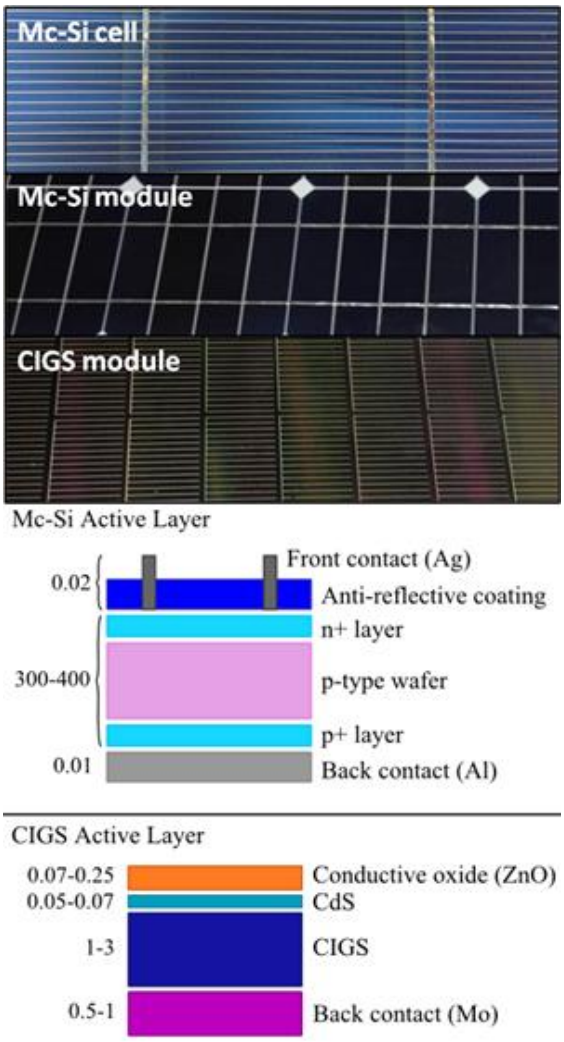

Figure 4.1: (a) Images of mc-Si cell, mc-Si module, and CIGS module and (b) associated material structure with typical layer thickness in micrometers (Goe and Gaustad, 2014).

4.2.1 EPA Method 1311 (TCLP)

For the TCLP, samples were crushed to a particle size of less than 9.5 mm, an extraction fluid was added at a 20-to-1 fluid-to-sample ratio, and samples were rotated in an extraction fluid for 18 hours. One liter of the TCLP extraction fluid consisted of 5.7 mL glacial acetic acid, 64.3 mL

1 N sodium hydroxide, and 930 mL of reagent water. The pH of the extraction fluid was 4.93 ± 0.05. After rotating, the samples were filtered and acidified with nitric acid. The samples were analyzed by ICP-OES (Perkin Elmer Optima 3100RL) to determine the concentrations of metals and metalloids present, which were compared to the regulatory limits. Elements regulated by the TCLP include arsenic, barium, cadmium, lead, mercury, selenium, and silver (USEPA, 1992). The regulatory limits were set to account for the likely dilution and attenuation that will occur in subsurface transport by multiplying the drinking water standards of 1986 by a factor of 100 (USEPA, 1995). Although the drinking water standards have changed since 1986 (USEPA, 2014), the regulatory limits for the TCLP have not.

4.2.2 California WET

For the California WET, samples were crushed to less than 2 mm particle size, sodium citrate extraction fluid was added at a 10-to-1 fluid-to-sample ratio, and samples were rotated in extraction fluid for 48 hours. The extraction fluid was 0.2 M sodium citrate at a pH of 5.0 ± 0.1. After rotating, the samples were filtered, acidified with nitric acid, and analyzed by ICP-OES (Perkin Elmer Optima 3100RL). Elements regulated by the WET in addition to the elements regulated by the TCLP include antimony, beryllium, chromium, cobalt, copper, molybdenum, nickel, thallium, vanadium, and zinc (DTSC, 2005).

4.2.3 Extraction Test Variations

To test the sensitivity of the results to the experimental conditions, sample preparation was varied by changing the extraction fluid ratio, the acidity of the extraction fluid, the rotation time, and the maximum particle size. The concentrations of regulated metals and metalloids were expected to increase by decreasing the extraction fluid-to-sample ratio, by decreasing the acidity of the extraction fluid, by increasing the rotation time with more time for metals and metalloids to leach

from the samples, and by decreasing the particle size with more surface area for leaching to occur.

For the mc-Si cells, both the TCLP and WET methods were altered to understand the leaching processes associated with the specific testing protocols. Extraction times for the TCLP were extended to 48 hours, which corresponds with the WET method time, and 72 hours, which is four times the TCLP standard of 18 hours, to understand the time dependence of the leaching process. The maximum particle size for the TCLP was reduced to 2.0 mm, and the extraction fluid ratio was reduced to 10-to-1, both corresponding to the WET protocols to compare the dependence of each specific protocol on the leaching results. For the WET, the extraction time was shortened to 18 hours, which corresponds to the TCLP method time, and increased to 72 hours, which is similar to the TCLP samples, and increased to 96 hours which is twice the standard WET time of 48 hours. The maximum particle size for the WET was increased to 9.5 mm from 2.0 mm, and the extraction fluid ratio was increased to 20-to-1, both corresponding to the TCLP protocols. For both the TCLP and WET, samples were also heated at 50 degrees Celsius for 8 hours.

For the mc-Si and CIGS modules, one set of samples was rotated up to 35 days. These samples were prepared at a 10-to-1 ratio with the extraction fluids more acidic at pH of 4.91 and 3.71 for the TCLP and WET, respectively, than pH of 4.96 and 5.0 which the regulatory methods specify. The volume of acetic acid for the TCLP method was increased 200 percent from the standard procedure, which resulted in a pH decrease of 0.05. Whereas the citric acid in the WET fluid was increased 200 percent and resulted in a pH decrease of 1.29. Because actual pH values for landfill leachate can vary from 4.5 to 7.5 during the acid phase (Kjeldsen et al., 2002), the tests were altered to show the sensitivity in the concentrations with slightly different pH values compared to the standard procedure values. Additional samples were rotated up to 60 days for the

CIGS module and up to 27 days for the mc-Si module. These samples were prepared following the standard procedures of the TCLP and California WET methods. By increasing the rotation time, it is possible to see if there is a lag before leaching occurs from the samples which has implications for the required rotation time specified in the regulatory methods. Increasing the rotation time also gives a better picture of the leaching kinetics for the metals and metalloids extracted from the PV modules to observe equilibrium concentrations and when they occur. The module samples were rotated for up to 60 days as opposed to 96 hours for the PV cells because it was theorized the layered structure of the modules would delay leaching compared to the non-encapsulated cells.

In addition to considering the concentrations of the regulated metals and metalloids, other potentially toxic metals and metalloids should be considered because of the possibility of future regulation. Studies have indicated the potential toxicity of gallium and indium (Tanaka, 2004; Chitambar, 2010) which are used in some PV modules. Thus, data for gallium and indium was collected during the leaching tests.

Table 4.1 summarizes the testing parameters for the TCLP and the WET and the extraction text variations which were performed for the multi-crystalline silicon cells, the multi-crystalline silicon module, and CIGS module.

4.3 Results

4.3.1 Multi-crystalline Silicon Cell

Using the TCLP and California WET methods for the mc-Si cells showed that cells would not be classified as hazardous waste, but the results from the leaching tests with modifications showed that concentrations significantly varied with slight changes to the procedures (Figure 4.2). The concentration of lead leached from the cells was 0.0 mg/L for both unmodified testing

Table 4.1: Summary of toxicity testing conditions.

T.C.L.P. (Reference Conditions)	Particle size of less than 9.5 mm 20-to-1 extraction fluid to sample ratio Rotation time of 18 hours pH of 4.93 ± 0.05 Acetic acid, NaOH, and reagent water extraction fluid		
W.E.T. (Reference Conditions)	Particle size of less than 2.0 mm 10-to-1 extraction fluid to sample ratio Rotation time of 48 hours pH of 5.0 ± 0.1 Sodium citrate extraction fluid		
	mc-Si Cells	**mc-Si Module**	**CIGS Module**
T.C.L.P. modifications	Particle size of less than 2.0 mm 10-to-1 extraction fluid to sample ratio Rotation times of 48 and 72 hours Heated at 50°C for 8 hours	Rotation time of 28 days pH of 4.91 10-to-1 extraction fluid to sample ratio	Rotation time of 35 and 60 days pH of 4.91
W.E.T. modifications	Particle size of less than 9.5 mm 20-to-1 extraction fluid to sample ratio Rotation times of 18, 72, and 96 hours Heated at 50°C for 8 hours	Rotation time of 28 days pH of 3.71	Rotation time of 35 and 60 days pH of 3.71

procedures. A decrease in the California WET rotation time from 48 hours to 18 hours showed an increase in lead concentration but did not exceed the regulatory limit. By decreasing the extraction fluid ratio from 20-to-1 to 10-to-1 for the TCLP, the lead concentration exceeded the regulatory limit of 5.0 mg/L with an average concentration of 5.3 mg/L and a standard deviation of 2.5 mg/L. By decreasing the maximum particle size from 9.5 mm to 2.0 mm for the TCLP, lead concentration increased but did not exceed the regulatory limit. The modified procedures for which the samples were heated at 50 degrees Celsius for 8 hours resulted in lead concentrations of 7.1 mg/L for the TCLP and 14.8 mg/L for the California WET, both of which exceeded the regulatory limit.

To show the variability in the concentrations leached from the mc-Si cells with the different test conditions, aluminum concentrations were analyzed (Figure 4.3). Aluminum was chosen because it was expected to readily leach from the samples from its use as the back contact for the mc-Si cells (Figure 4.1b). For the TCLP, the aluminum concentration was 16.5 mg/L with

a standard deviation of 4.2 mg/L. When the rotation time for the TCLP was extended to 48 and 72 hours, the concentration increased to 172 mg/L and 348 mg/L, respectively. This significant increase in aluminum leached from the mc-Si cells demonstrates that equilibrium was not reached within the standard rotation time of 18 hours. For the California WET, the aluminum concentration was 24.6 mg/L with a standard deviation of 0.3 mg/L. When the rotation time for the California WET was extended to 72 and 96 hours, the concentration increased to 39.1 mg/L and 49.6 mg/L, respectively. When the extraction fluid-to-sample ratio was reduced to 10-to-1 for the TCLP, the aluminum concentration increased to 59.3 mg/L. An increase in the maximum particle size for the California WET to 9.5 mm resulted in an increase in concentration to 40.2 mg/L, and although the concentration increase is unexpected, the results demonstrated the variability concentrations leaching under different conditions and potential differences among samples of the same type selected for regulatory testing. When the maximum particle size for the

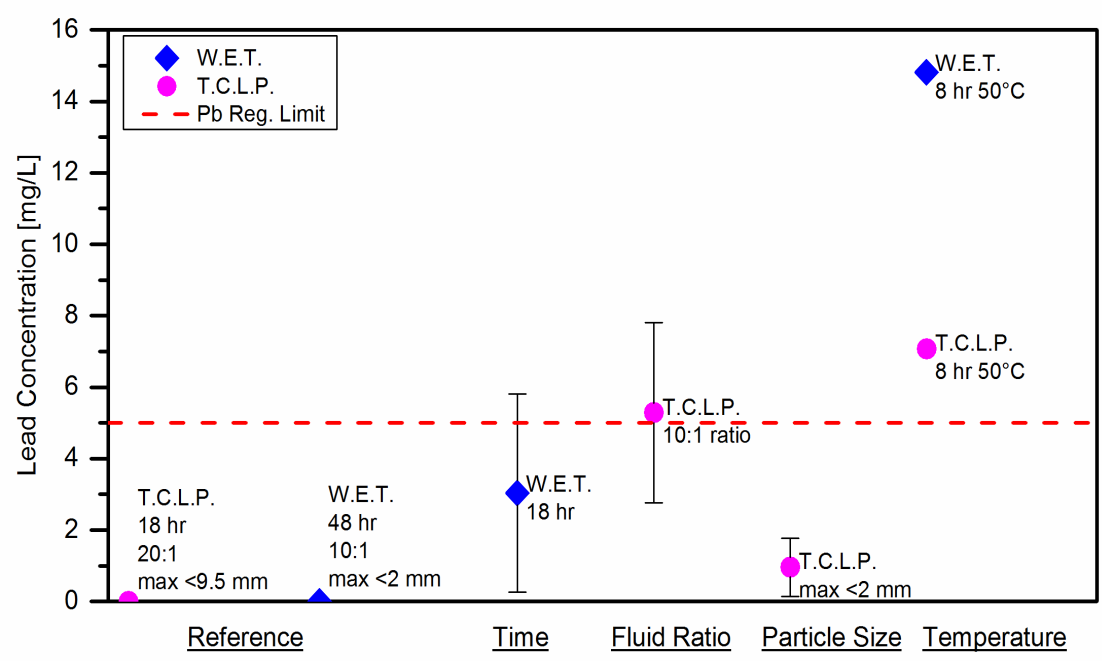

Figure 4.2: Lead concentrations from variations of the TCLP and California WET leaching methods for mc-Si cells.

TCLP was reduced to 2.0 mm, the aluminum concentration increased to 34.2 mg/L. This concentration is more than double the concentration when using the standard maximum particle size, which demonstrated the dependency of the results on the particle size. Aluminum concentrations of 62.5 mg/L and 55.5 mg/L for the TCLP and the California WET, respectively, occurred when the samples were heated at 50 degrees Celsius for 8 hours.

4.3.2 Multi-crystalline Silicon Module

Results from the TCLP method for the mc-Si module showed that lead exceeded the regulatory limit of 5 mg/L with a concentration of 34.9 mg/L when the test was performed without modification. The California WET results showed that the regulatory limit for lead was exceeded with a concentration of 32.4 mg/L. While not used in the absorber layer of mc-Si cells, lead can be used in solder and contacts within the module.

With modifications to the methods, including extended rotation time to 28 days and more

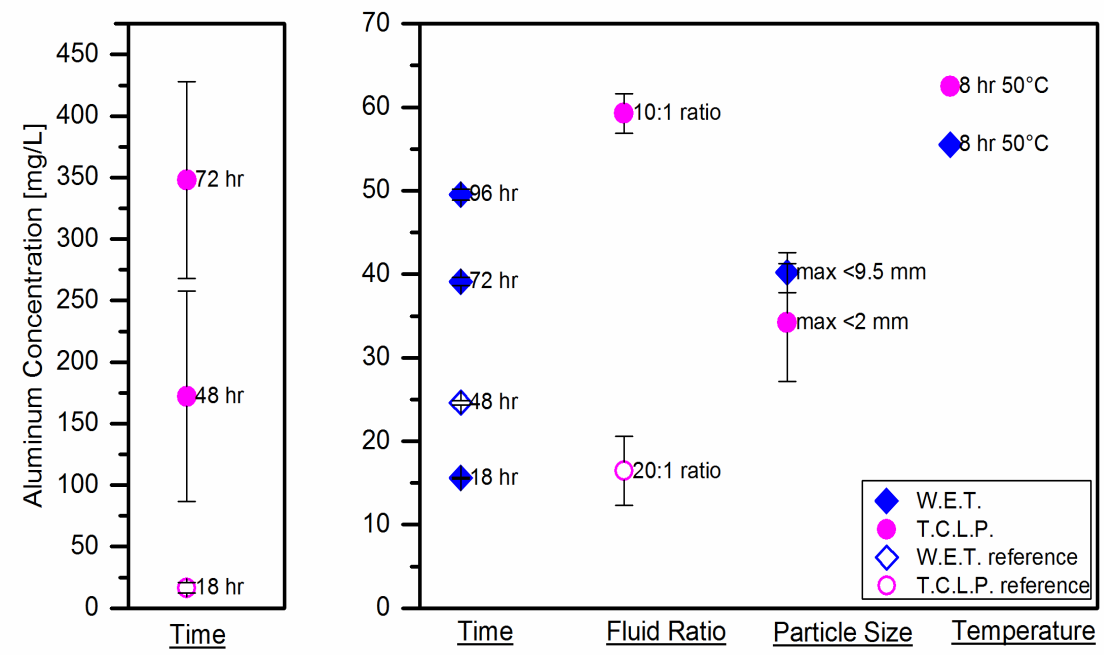

Figure 4.3: Aluminum concentrations from variations of the TCLP and California WET leaching methods for mc-Si cells.

acidic extraction fluid for both the TCLP and WET, lead concentrations for the mc-Si module were greater than regulatory limits (Figure 4.4a). Although the concentration was still increasing at day 28, the change in concentration for both the TCLP and WET modified tests from day 13 to day 28 was less than 15 percent.

Using modified TCLP and WET methods, concentrations of copper leached from the mc-Si module exceeded the California regulatory limit of 25 mg/L with a concentration of 94.8 mg/L at 27 days in the TCLP fluid (Figure 4.4b). Concentrations of aluminum and iron, which are not regulated, increased with time to 223.5 mg/L and 1.55 mg/L, respectively.

Table 4.2 shows the TCLP and WET regulatory limits, concentrations from the TCLP and WET procedures for the mc-Si module, and maximum concentrations leached from the mc-Si module during the extended rotation times.

4.3.3 Copper Indium Gallium Diselenide Module

The TCLP and WET results for the CIGS module showed that no elements exceeded regulatory limits for either sample preparation method

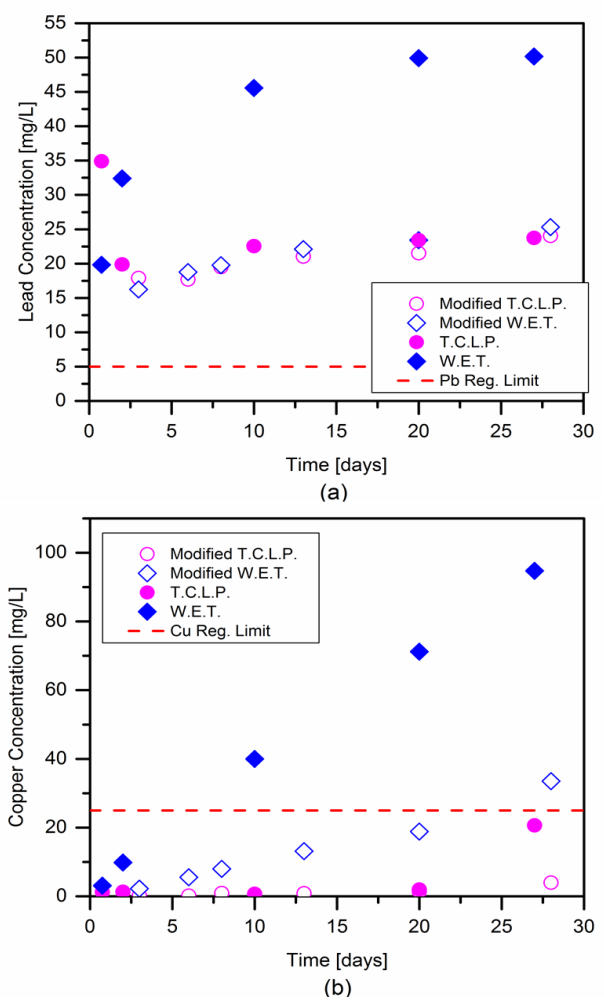

Figure 4.4: (a) Lead concentrations versus time and (b) copper concentrations versus time for the multi-crystalline silicon module using the TCLP and WET modified and unmodified extraction fluids.

Table 4.2: Summary of regulatory limits and concentrations for each regulatory test and maximum concentrations for each module with extended rotation time.
Note: Values in bold exceed the regulatory limits.

Element	Regulatory Limits [mg/L]		mc-Si Module [mg/L]	mc-Si Module [mg/L]	CIGS Module [mg/L]	CIGS Module [mg/L]	mc-Si Module [mg/L]	CIGS Module [mg/L]
	T.C.L.P.	W.E.T.	T.C.L.P.	W.E.T.	T.C.L.P.	W.E.T.	Max	Max
Al	--	--	3.72	3.32	1.36	0.49	223.5	134.5
Cd	1.0	1.0	--	--	0.10	0.52	--	**3.52**
Cu	--	25	1.23	9.81	0.07	10.7	**94.8**	**254.9**
Fe	--	--	0.21	1.18	24.8	170	1.55	560.1
Ga	--	--	--	--	--	--	--	0.98
In	--	--	--	--	0.02	0.34	--	9.56
Pb	5.0	5.0	**34.9**	**32.4**	0.50	0.01	**50.2**	3.43
Se	1.0	1.0	--	--	--	--	--	**1.55**

without modification. For the TCLP and California WET methods, the cadmium concentrations were 0.10 mg/L and 0.52 mg/L, respectively. These concentrations did not exceed the cadmium regulatory limit of 1 mg/L. The cadmium likely leached from the cadmium sulfide buffer layer, and concentrations of cadmium were expected to increase as the zinc oxide conductive layer dissolved.

With modifications to the methods, including extended rotation time and more acidic extraction fluid for both the TCLP and WET, results showed concentrations greater than regulatory limits for cadmium (Figure 4.5a). Although cadmium concentrations were still increasing for the modified procedures, the increase was less than three percent from day 27 to day 35 for the modified TCLP which had the highest cadmium concentration. Unmodified TCLP and WET extraction fluids were used with samples rotated for 60 days. For these samples, concentrations did not reach the levels from using the modified extraction fluids for cadmium (Figure 4.5a) or for selenium until after day 35 (Figure 4.5b).

The modified tests showed concentrations of copper exceeded the regulatory limit over the extended sample time period. The results from the modified TCLP and WET methods also

showed concentrations of unregulated elements including aluminum, iron, gallium, and indium increasing with time (Figure 4.6).

Table 4.2 shows the concentrations from the TCLP and WET procedures for the CIGS module and maximum concentrations leached from the CIGS module during the extended rotation times.

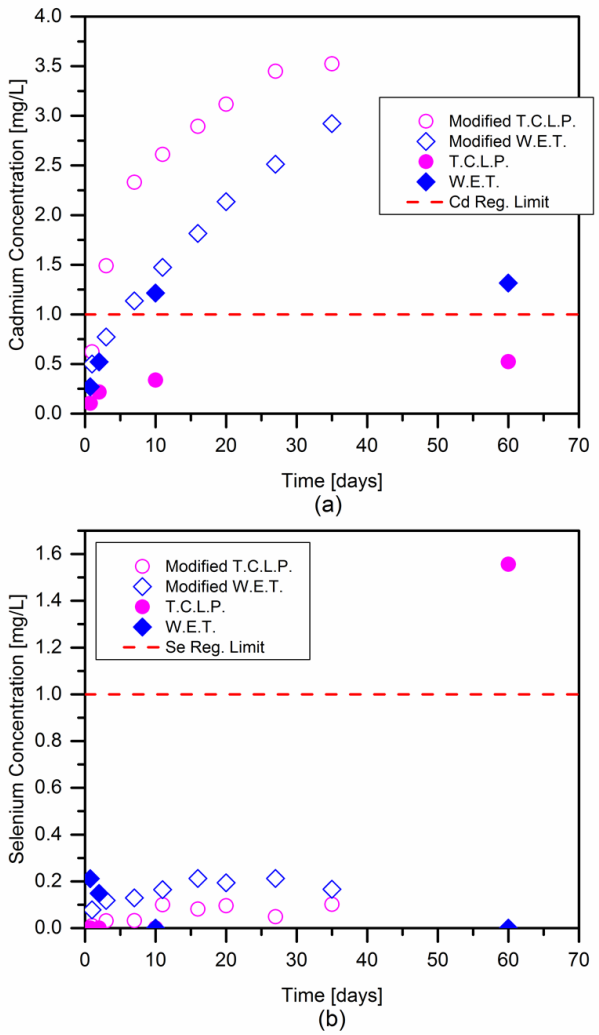

Figure 4.5: (a) Cadmium concentrations versus time and (b) selenium concentrations versus time for the CIGS module using the TCLP and WET modified and unmodified extraction fluids

4.4 Discussion

Because solar energy is perceived as a green technology, any harmful environmental issues arising from the use and end-of-life phases of PV modules will be detrimental to solar energy's long-term success. Solar energy and PV modules provide a source of sustainable, renewable energy while concerns exist for traditional, non-renewable energy sources, but at the end of their useful life, PV modules could be considered hazardous waste due to the leaching of metals and metalloids when disposed of in landfills. Modules may be regarded as recyclable resources due to the value associated with these materials but if these materials have little economic value this may inhibit recycling efforts (Anctil and Fthenakis,

2013). End-of-life pathways for recycling or safe disposal of PV waste must be developed to ensure the continued growth and cost reduction of solar energy as a sustainable energy option.

Methods for PV waste characterization need to be developed to prevent toxic wastes from entering municipal landfills if the current regulatory methods have the potential to underestimate the concentrations of regulated elements leached from the PV waste. Because the regulatory limits were set to account for the likely dilution and attenuation that occurs in subsurface transport by multiplying the drinking water standards of 1986 by a factor of 100 to obtain the regulatory limits (USEPA, 1995), the limits for every element may or may not be protective of the environment under different scenarios. The factor of 100 used was originally an estimated factor not derived from models or empirical data, but was later deemed adequate by the USEPA through subsurface fate and transport modeling (USEPA, 1995). Additionally, the drinking water standards have become more stringent since 1986 (USEPA, 2014), but the regulatory limits for the TCLP have not. Therefore, modifications to the regulatory methods have been used to examine the variability in the concentrations of metals and metalloids leached from the PV samples when changes occur to the testing procedures.

4.4.1 Multi-crystalline Silicon Cell

Results from TCLP and California WET methods for the mc-Si cells showed that the cells would not be classified as hazardous waste, but the results from the modified tests showed that concentrations vary significantly with slight changes to the procedures. The motivation of this study was not to classify the mc-Si cells as hazardous waste at end-of-life but rather to investigate the differences in concentrations that occur with slight modifications to the testing procedures. Thus, the appropriateness of the testing procedures applied to PV waste can be investigated.

Results from the modified testing showed lead concentrations above the regulatory limit of 5 mg/L for the samples heated to 50 degrees Celsius for 8 hours. Aluminum concentrations

increased when increasing the sample rotation time, decreasing the TCLP maximum particle size, and heating the samples to 50 degrees Celsius for 8 hours.

Increased concentrations with slight changes in testing conditions demonstrated that the current regulatory methods may not be suitable for properly characterizing PV wastes which have slower dissolution rates and could represent a long-term source for metals and metalloid leaching in landfills. As shown in Figure 4.1b, in order to access the interior layers, the outside layers including the aluminum back contact and the anti-reflective coating first need to be leached. Although samples are shredded or crushed for the regulatory methods, the epoxy used to keep the layers together is not easily separated by these mechanical techniques, so the interior layers are difficult to access even when samples are shredded or crushed. This is similar to liquid-crystal display glass where extraction occurs in stages due to the material layers (Yang et al., 2013). The variability in the results from changing the testing procedures emphasizes the dependence of hazardous waste characterization on specific testing conditions.

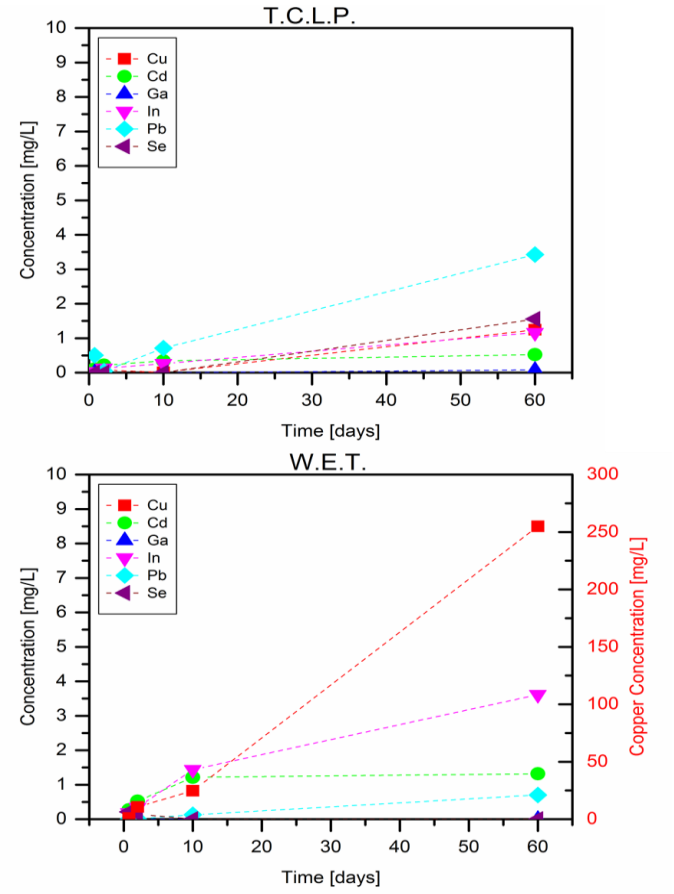

Figure 4.6: (a) Cu, Cd, Ga, In, Pb, and Se concentrations versus time for the CIGS module using an unmodified TCLP extraction fluid. (b) Cu, Cd, Ga, In, Pb, and Se concentrations versus time for the CIGS module using an unmodified WET extraction fluid.

4.4.2 Multi-crystalline Silicon Module

The multi-crystalline silicon module in this study exceeded the regulatory limit for lead of 5 mg/L, but the results cannot be considered representative of all multi-crystalline silicon modules. As can be seen in Figure 4.4 and Table 4.2, leaching does not occur instantaneously and continues beyond the time periods defined by the regulatory procedures. Additional testing is needed to examine the trends in leaching over longer times. When determining the toxicity of PV waste, longer leaching times should be considered by the regulatory methods to account for the slower leaching kinetics due to the layering of the material. Additional testing is needed to characterize the waste stream resulting from the various types modules installed.

4.4.3 Copper Indium Gallium Diselenide Module

Although results showed that the CIGS module did not exceed regulatory limits for the TCLP or WET methods, the concentration of cadmium leached from the module in short period of time in a weak acid demonstrates the need for further testing of CIGS modules and the possibility of cadmium leaching in concentrations greater than anticipated by the leaching tests in an actual landfill setting. Concentrations of copper and selenium increased with time and exceeded their regulatory limits. Currently unregulated elements including gallium and indium leached from the CIGS module. Studies have been conducted investigating the toxicity of gallium and indium (Tanaka, 2004; Chitambar, 2010), which could eventually be regulated in waste. Due to the layering of the materials in CIGS modules, as shown in Figure 4.1b, exterior layers must leach prior to the interior layers which can continue beyond the timeframe specified by the regulatory methods. Because this study is not meant to represent all available CIGS modules, additional CIGS and other types of thin-film modules need to be tested to characterize the waste stream that will result from their installation.

4.4.4 Implications

By conducting the TCLP and WET leaching tests, the toxicity of PV modules from metal and metalloid leaching was examined. By modifying these methods and observing concentration trends over time, the applicability of the methods to PV waste was investigated. The results from the modified methods showed that leaching continues beyond the time specified in the regulatory methods and that concentrations for some elements exceeded the regulatory limits to be considered hazardous waste.

Results from the modified testing procedures demonstrated that the regulatory methods might not be valid for PV waste, and therefore, additional studies are needed to determine actual concentrations in landfill leachate in environmentally-relevant conditions which should be compared to the results of regulatory testing. Similar studies have been conducted to characterize the leaching of metals and metalloids from household electronic waste in simulated municipal solid waste landfills (Li et al., 2009b; Kiddee et al., 2013). Comparisons of the TCLP and WET with actual and simulated landfill leachate in laboratory conditions has shown that actual landfill leachate can extract a ten-fold greater arsenic concentration than the TCLP for arsenic-bearing solid residuals from adsorption processes in water treatment (Ghosh et al., 2004). This is beyond the scope of this study but should be considered in future work to determine the actual environmental impacts from disposing of PV modules in landfills.

The possibility of modules being categorized as hazardous waste at end-of-life needs to be considered when implementing manufacturer take-back programs and legislating and managing recycling programs in the United States. These findings are important to the PV industry because the classification of PV modules as hazardous waste will restrict end-of-life options in the United States and could impact PV manufacturers if take-back programs and recycling are required. The toxicity of PV waste will determine the fate of the waste as potentially hazardous waste which affects the ability to landfill the waste with municipal waste and could

encourage recycling PV waste from both an environmental stewardship perspective and an economic perspective because of higher landfill tipping fees for hazardous waste landfills. In the European Union member states, the Waste Electrical and Electronic Equipment (WEEE) Directive now includes PV modules, so PV modules are collected for recycling and no longer discarded as waste (European Parliament and Council of the European Union). Recycling technologies are being developed and implemented for thin-film technologies (Marwede et al., 2013) and silicon cells (Klugmann-Radziemska et al., 2010), but collection programs will need to be implemented to ensure all modules are recycled. The potential of PV modules to be classified as hazardous waste could lead to adopting take-back programs and recycling even if they are currently economically and logistically infeasible in the United States. Temporal and spatial boundaries should be considered when implementing take-back and recycling programs, and mathematical models which include varying material prices, transportation, and external costs have been developed to aid in maximizing profits for recycling PV modules (Choi and Fthenakis, 2010, 2014).

Although the modified procedures cannot substitute for the regulatory procedures, they provide insight into the concentrations of metals and metalloids that could leach from PV waste which is the aim of the regulatory methods. Implications of the results from the modified testing procedures show that the regulatory methods might not be valid for characterizing PV waste, and additional testing is needed to quantify concentrations leached in a landfill setting with comparisons to the results of regulatory testing. Waste characterization is needed to find appropriate end-of-life procedures for PV modules which will be necessary to sustain the current growth of PV and cost reduction trends. While the PV industry is relatively young, positive steps can be taken to ensure the entire life cycle is sustainable and avoid an e-waste problem with regard to solar energy.

4.5 References

Anctil, A.; Fthenakis, V. Critical Metals in Strategic Photovoltaic Technologies: Abundance versus Recyclability. *Prog. Photovoltaics Res. Appl.* **2013**, *21* (6), 1253–1259.

Chitambar, C. R. Medical Applications and Toxicities of Gallium Compounds. *Int. J. Environ. Res. Public Health* **2010**, *7* (5), 2337–2361.

Choi, J.-K.; Fthenakis, V. Economic Feasibility of Recycling Photovoltaic Modules. *J. Ind. Ecol.* **2010**, *14* (6), 947–964.

Choi, J.-K.; Fthenakis, V. Crystalline Silicon Photovoltaic Recycling Planning: Macro and Micro Perspectives. *J. Clean. Prod.* **2014**, *66*, 443–449.

Dinçer, F. The Analysis on Photovoltaic Electricity Generation Status, Potential and Policies of the Leading Countries in Solar Energy. *Renew. Sustain. Energy Rev.* **2011**, *15* (1), 713–720.

DTSC. *California Waste Extraction Test*; **2005**.

EPIA. *Global Market Outlook for Photovoltaics until 2016*; EPIA, **2012**.

European Parliament and Council of the European Union. Official Journal of the European Union. *55* (L197), 1–71.

Feldman, D.; Barbose, G.; Margolis, R.; James, T.; Weaver, S.; Darghouth, N.; Fu, R.; Davidson, C.; Booth, S.; Wiser, R. *Photovoltaic System Pricing Trends: Historical, Recent, and Near-Term Projections. 2014 Edition (Presentation). Sunshot, U.S. Department of Energy (DOE).*; **2014**.

Fthenakis, V.; Kim, H. C.; Frischknecht, R.; Raugei, M.; Sinha, P.; Stucki, M. *Life Cycle Inventories and Life Cycle Assessment of Photovoltaic Systems*; International Energy Agency, **2011**; Vol. T12–02:201.

Ghosh, A.; Mukiibi, M.; Ela, W. TCLP Underestimates Leaching of Arsenic from Solid Residuals under Landfill Conditions. *Environ. Sci. Technol.* **2004**, *38* (17), 4677–4682.

Goe, M.; Gaustad, G. Strengthening the Case for Recycling Photovoltaics: An Energy Payback Analysis. *Appl. Energy* **2014**, *120*, 41–48.

Jäger-Waldau, A. *PV Status Report 2012*; European Commission, **2012**.

Janusa, M. A.; Bourgeois, J. C.; Heard, G. E.; Kliebert, N. M.; Landry, A. A. Effects of Particle Size and Contact Time on the Reliability of Toxicity Characteristic Leaching Procedure for Solidified/Stabilized Waste. *Microchem. J.* **1998**, *59* (2), 326–332.

Karamalidis, A. K.; Voudrias, E. A. Release of Zn, Ni, Cu, SO4(2-) and CrO4(2-) as a Function of pH from Cement-Based Stabilized/solidified Refinery Oily Sludge and Ash from Incineration of Oily Sludge. *J. Hazard. Mater.* **2007**, *141* (3), 591–606.

Kiddee, P.; Naidu, R.; Wong, M. H. Metals and Polybrominated Diphenyl Ethers Leaching from Electronic Waste in Simulated Landfills. *J. Hazard. Mater.* **2013**, *252–253*, 243–249.

Kjeldsen, P.; Barlaz, M. A.; Rooker, A. P.; Baun, A.; Ledin, A.; Christensen, T. H. Present and Long-Term Composition of MSW Landfill Leachate: A Review. *Crit. Rev. Environ. Sci. Technol.* **2002**, *32* (4), 297–336.

Klugmann-Radziemska, E.; Ostrowski, P.; Drabczyk, K.; Panek, P.; Szkodo, M. Experimental Validation of Crystalline Silicon Solar Cells Recycling by Thermal and Chemical Methods. *Sol. Energy Mater. Sol. Cells* **2010**, *94* (12), 2275–2282.

Komilis, D.; Tataki, V.; Tsakmakis, T. Leaching of Heavy Metals from Personal Computer Components: Comparison of TCLP with a European Leaching Test. *J. Environ. Eng.* **2013**, *139* (11), 1375–1381.

Kosson, D. S.; van der Sloot, H. A.; Sanchez, F.; Garrabrants, A. C. An Integrated Framework for Evaluating Leaching in Waste Management and Utilization of Secondary Materials. *Environ. Eng. Sci.* **2002**, *19* (3), 159–204.

Li, Y.; Richardson, J. B.; Niu, X.; Jackson, O. J.; Laster, J. D.; Walker, A. K. Dynamic Leaching Test of Personal Computer Components. *J. Hazard. Mater.* **2009a**, *171* (1–3), 1058–1065.

Li, Y.; Richardson, J. B.; Bricka, R. M.; Niu, X.; Yang, H.; Li, L.; Jimenez, A. Leaching of Heavy Metals from E-Waste in Simulated Landfill Columns. *Waste Manag.* **2009b**, *29* (7), 2147–2150.

Lim, S.-R.; Kang, D.; Ogunseitan, O. A.; Schoenung, J. M. Potential Environmental Impacts of Light-Emitting Diodes (LEDs): Metallic Resources, Toxicity, and Hazardous Waste Classification. *Environ. Sci. Technol.* **2011**, *45* (1), 320–327.

Marwede, M.; Berger, W.; Schlummer, M.; Mäurer, A.; Reller, A. Recycling Paths for Thin-Film Chalcogenide Photovoltaic Waste – Current Feasible Processes. *Renew. Energy* **2013**, *55* (0), 220–229.

McDonald, N. C.; Pearce, J. M. Producer Responsibility and Recycling Solar Photovoltaic Modules. *Energy Policy* **2010**, *38* (11), 7041–7047.

Musson, S. E.; Vann, K. N.; Jang, Y.-C.; Mutha, S.; Jordan, A.; Pearson, B.; Townsend, T. G. RCRA Toxicity Characterization of Discarded Electronic Devices. *Environ. Sci. Technol.* **2006**, *40* (8), 2721–2726.

Poon, C. S.; Lio, K. W. The Limitation of the Toxicity Characteristic Leaching Procedure for Evaluating Cement-Based Stabilised/solidified Waste Forms. *Waste Manag.* **1997**, *17* (1), 15–23.

Robinson, B. H. E-Waste: An Assessment of Global Production and Environmental Impacts. *Sci. Total Environ.* **2009**, *408* (2), 183–191.

Sanaeepur, S.; Sanaeepur, H.; Kargari, A.; Habibi, M. H. Renewable Energies: Climate-Change Mitigation and International Climate Policy. *Int. J. Sustain. Energy* **2013**, *33* (1), 203–212.

Solangi, K. H.; Islam, M. R.; Saidur, R.; Rahim, N. A.; Fayaz, H. A Review on Global Solar Energy Policy. *Renew. Sustain. Energy Rev.* **2011**, *15* (4), 2149–2163.

Tanaka, A. Toxicity of Indium Arsenide, Gallium Arsenide, and Aluminium Gallium Arsenide. *Toxicol. Appl. Pharmacol.* **2004**, *198* (3), 405–411.

Timilsina, G. R.; Kurdgelashvili, L.; Narbel, P. A. Solar Energy: Markets, Economics and Policies. *Renew. Sustain. Energy Rev.* **2012**, *16* (1), 449–465.

USEPA. Method 1311 Toxicity Characteristic Leaching Procedure.

USEPA. *Applicability of the Toxicity Characteristic Leaching Procedure to Mineral Processing Wastes*; **1995**.

USEPA. National Primary Drinking Water Regulations
http://water.epa.gov/drink/contaminants/#List.

Yang, J.; Retegan, T.; Ekberg, C. Indium Recovery from Discarded LCD Panel Glass by Solvent Extraction. *Hydrometallurgy* **2013**, *137*, 68–77.

Zimmermann, Y.-S.; Schäffer, A.; Corvini, P. F.-X.; Lenz, M. Thin-Film Photovoltaic Cells: Long-Term Metal(loid) Leaching at Their End-of-Life. *Environ. Sci. Technol.* **2013**, *47* (22), 13151–13159.

Chapter 5: Metal Leaching from Lithium-ion and Nickel-metal Hydride Batteries and PV Modules in Simulated Landfill Leachates and Municipal Solid Waste Materials

Abstract

As the use of energy technologies, including photovoltaic modules and batteries, rapidly increases to meet the growing worldwide energy demand, so does the waste stream of these products at end-of-life. Most studies of the end-of-life of these products focus on recycling and not municipal waste disposal, which is likely to occur in locations without sufficient recycling laws or take-back programs. To study the potential metal leaching that could occur during landfill disposal, the Toxicity Characteristic Leaching Procedure (TCLP), microwave digestions, and batch leaching tests in two simulated leachates sampled over a period of 100 days were conducted for seven types of lithium-ion (Li-ion) batteries, one type of nickel-metal hydride (NiMH) battery, and two types of photovoltaic (PV) modules. Additionally, one product of each type (Li-ion battery, NiMH battery, and PV module) was mixed with municipal solid waste (MSW) components and a simulated landfill leachate to compare leaching in a more realistic waste matrix to the batch leaching tests. Results from the TCLP showed that one of the two PV modules and three of the eight batteries would be classified as hazardous waste in the US, with two of the batteries leaching mercury at concentrations an order of magnitude higher than the regulatory limit. For some of the e-wastes which would not be classified as hazardous waste, the metal concentrations observed in the batch leaching tests were much greater than observed for the TCLP, signaling that

the TCLP might not be adequate at predicting metal concentrations leached from some types of e-wastes in landfill conditions. For the batch tests with e-waste mixed with MSW, both lower (Pb for all three waste types and Hg for the NiMH power tool battery) and higher (Co and Ni for the Li-ion laptop battery) metal leachate concentrations were observed than for the batch tests without MSW. The results from the leaching tests highlight the complexity of characterizing PV and battery e-waste and developing end-of-life recycling or disposal regulations and procedures that are applicable to each e-waste category. Appropriate characterization tools and techniques that ensure adequate protection of the environment are necessary to avoid a growing e-waste problem while simultaneously promoting renewable energy sources.

5.1 Introduction

Renewable energy resources, including solar energy, represent a sustainable way to meet growing energy requirements while minimizing long-term environmental effects. Solar photovoltaic (PV) installation is increasing in the US and is forecasted to continue to rise due to the increased number of renewable portfolio standards and policies (Dinçer, 2011; Solangi et al., 2011; Timilsina et al., 2012). The increase in solar PV installation will result in an increase in energy storage to be able to use the energy produced at any time, and Li-ion batteries are a viable option for energy storage in homes and at the utility scale (Chen et al., 2009; USDOE, 2013; Scott and Simon, 2015). In addition to solar related applications, Li-ion batteries are increasing in use in consumer electronics and electric vehicles (Lithium Batteries: Markets and Materials, 2013; USEPA, 2013).

The increase in solar PV installation globally from 306.5 gigawatts installed as of 2016 to a moderate outlook of 700 gigawatts installed by 2021 (SolarPower Europe, 2017), as well as the increase in Li-ion battery usage, will lead to an enormous waste stream in the future (McDonald

and Pearce, 2010). The diversity of the technologies for both PV modules and batteries will lead to diverse electronic waste streams which can impede recycling processes. Worldwide, approximately 85% of PV production is wafer-based silicon modules, but thin-film technologies, which use Cu(In, Ga)(Se, S), CdTe, or dye as absorber materials, are emerging and represented 10% of the market share in 2007 (Jäger-Waldau, 2012). Cathode materials in Li-ion batteries vary and are shifting from cobalt to iron phosphate and manganese compounds, which can reduce the incentive to recycle due to the decrease in profitability of recovering relatively low value materials when the costs for recovery are relatively high (Wang et al., 2014b). The waste stream from automotive Li-ion batteries is expected to reach 750,000 batteries by 2030 in North America (Commission for Environmental Cooperation, 2015); however, automotive batteries are more likely to have infrastructure and policies in place to ensure their collection and recycling at end-of-life unlike batteries in portable consumer products (Commission for Environmental Cooperation, 2015). For batteries in portable devices, consumers currently only return 20-40% of spent batteries for recycling in the US (BU-705: How to Recycle Batteries, 2015) with most of the batteries that would be available for recycling either sequestered in homes and businesses or entering the municipal solid waste stream (Goonan, 2012).

There is a limited understanding of the end-of-life phase of PV modules and Li-ion batteries and the associated risks to human and environmental health (Hawkins et al., 2012; Kang et al., 2013). Li-ion battery manufacturing has been the subject of recent research, but the risks from toxic metal emissions from disposal have not been quantified (Gaustad et al., 2012). Disposing of Li-ion batteries in landfills could present environmental risks from leaching of organic electrolytes, toxic metals, lithium salts, and carbonaceous material (Richa et al., 2014). Similarly, PV modules are not subject to regulations mandating manufacturer take-back programs

or recycling in the United States (US), and their environmental impacts from disposal at end-of-life have not been quantified.

US Environmental Protection Agency (EPA) regulations and some individual state regulations are used to determine the toxicity of potentially hazardous waste by simulating contaminant release when the waste is co-disposed with municipal solid waste. The extraction methods attempt to replicate the factors affecting leaching in a municipal solid waste landfill environment to predict concentrations which will leach from the wastes within the landfill (Kosson et al., 2002). EPA Method 1311 (USEPA, 1992), which outlines the Toxicity Characteristic Leaching Procedure (TCLP), has been previously used to categorize the toxicity of electronics including light-emitting diodes (Lim et al., 2011), personal computer components (Li et al., 2009a; Komilis et al., 2013), mobile phones (Yadav and Yadav, 2014), and other household e-waste (Musson et al., 2006). However, the use of current regulatory leaching methods to assess the toxicity of different e-wastes may be less than accurate (Poon and Lio, 1997; Kosson et al., 2002; Ghosh et al., 2004; Karamalidis and Voudrias, 2007). Specifically, the TCLP may be inadequate due to evaluating and regulating wastes using a single, worst-case test condition leading to both over-regulation and inadequate protection of the environment (Kosson et al., 2002). The TCLP does not account for a range of pH values, which is known to affect the leaching of metals and anions (Karamalidis and Voudrias, 2007). Additionally, the TCLP is ill-suited to account for the acid neutralizing capacity of landfill wastes and to assess long-term leaching after the acid neutralizing capacity diminishes (Poon and Lio, 1997). Additionally, the regulatory limits were set to account for the likely dilution and attenuation that will occur in subsurface transport by multiplying the drinking water standards of 1986, authorized by the Safe Drinking Water Act (SDWA), by a factor of 100 (USEPA, 1995). Although the drinking water standards have changed since 1986 (USEPA, 2014), the regulatory limits for the TCLP have not.

Thus, there is a need to compare TCLP results for e-waste with leaching that occurs over time and within a representative municipal solid waste matrix to determine if the TCLP is adequate at evaluating hazardous waste classification for e-waste.

5.2 Materials and Methods

5.2.1 Li-ion and NiMH batteries and PV modules

For this study, seven types of Li-ion batteries, one type of NiMH battery, and two types of PV modules, one crystalline silicon and one multi-crystalline silicon, were purchased from retailers within the US (Table 5.1). The batteries include both cylindrical and prismatic forms and were marketed for use in laptops, power tools, cell phones, flashlights, solar lights, digital cameras, and watches. The selected batteries reflect the shift in technology for electric vehicles (Catenacci et al., 2013; USEPA, 2013) and portable devices (Wang et al., 2014a). The plastic housings for the power tool and laptop batteries were removed, and their interior cells and circuit boards were separated (Figure 5.1) for the TCLP, digestions, and batch leaching tests. The procedures are briefly described in Table 5.2. The frames from the PV modules were removed for the leaching tests.

5.2.2 TCLP

EPA Method 1311, the Toxicity Characteristic Leaching Procedure (TCLP), was conducted for each of the battery and PV module types. The TCLP is used to classify unlisted wastes as hazardous wastes based on concentrations leached during the procedure (USEPA, 1992). For the batteries, the outer housing was removed using hand tools, and samples of the electrodes (rolled anode and cathode) were used for testing. The TCLP sample preparation steps involve mechanically reducing the sample to a particle size of less than 9.5 mm, adding an extraction fluid at a 20:1 fluid-to-sample ratio, and rotating the sample in extraction fluid for 18 hours on a

tumbler. A preliminary evaluation determines which of two extraction fluids to use for each of the PV and battery samples. One liter of TCLP extraction fluid consists of either 5.7 mL glacial acetic acid, 64.3 mL 1 N sodium hydroxide, and 930 mL of reagent water resulting in a solution pH of 4.93 ± 0.05 (TCLP #1), or 5.7 mL glacial acetic acid and 994.3 mL reagent water resulting in a solution pH of 2.88 ± 0.05 (TCLP #2) (USEPA, 1992). After rotating, the samples are filtered with 0.2

Table 5.1: Product descriptions for the Li-ion and NiMH batteries and PV modules

	Product Description	**E-waste Type**
1	Suniva OPT245-60-4-100 c-Si PV module	c-Si module
2	Suniva MVP240-60-5-401 mc-Si PV module	mc-Si module
3	Lenmar LBZ378D laptop battery	Li-ion battery
4	Lenmar PTD9094 power tool battery	NiMH battery
5	Rayovac CTL10293 power tool battery	Li-ion battery
6	Empire BLP-1277-1.4 iPhone 5 replacement battery	Li-ion battery
7	Nuon NURE18650 flashlight battery	Li-ion battery
8	Ultralast UL14430SL solar light battery	Li-ion battery
9	Rayovac RL123A digital camera battery	Li-ion battery
10	Energizer CR2450 watch battery	Li-ion battery
11	Lenmar LBZ378D laptop battery circuit board	circuit board
12	Rayovac CTL10293 power tool battery circuit board	circuit board

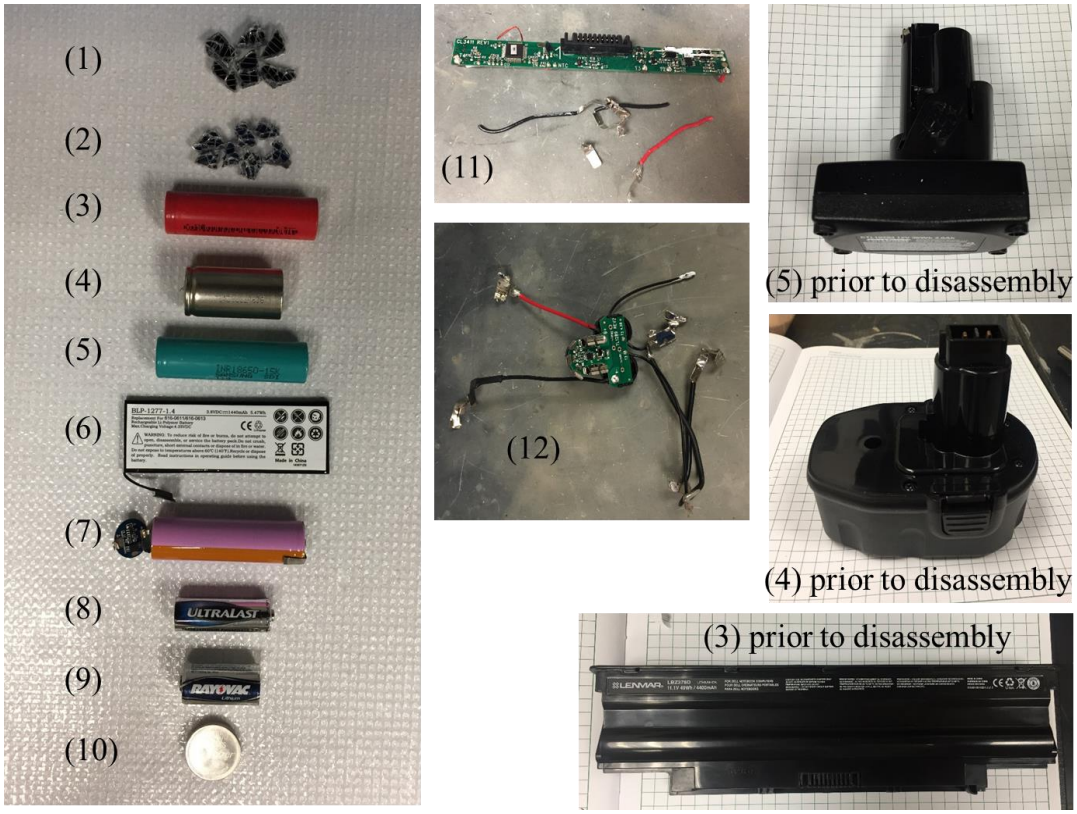

Figure 5.1: Li-ion and NiMH batteries and PV module pieces for batch leaching tests. Numbers correspond to products in Table 5.1.

micrometer pore diameter nylon filters. The filtrate is then acidified with nitric acid and analyzed by inductively coupled plasma optical emission spectrometry (ICP-OES, Perkin Elmer Optima 3100RL) to determine the concentrations of metal ions present. Elements regulated by the TCLP include As, Ba, Cd, Cr, Pb, Hg, Se, and Ag (USEPA, 1992).

5.2.3 Digestions

Battery electrodes and PV module pieces were digested to determine extractable amounts of metals for comparison with the other leaching tests and to identify the metals used in the cathodes for the batteries. For the batteries, the outer housing was removed using hand tools. Samples of 500 mg of the electrodes (rolled anode and cathode) for the batteries and particle size reduced pieces of the PV modules were placed in digestion tubes containing 10 mL of concentrated nitric acid. The samples were digested with a ramp up time of 4.5 minutes and held at 175°C for 8.5 minutes using a MARS microwave digester. The digestate was filtered with a 0.2 micrometer

Table 5.2: Test procedures with brief description and purpose

Test Procedure	**Brief Description**	**Purpose**
TCLP (USEPA, 1992)	Leaching test with specifications for particles passing through a 9.5 mm sieve, an extraction fluid added at a 20:1 fluid-to-sample ratio, and rotating samples for 18 hours	US regulatory procedure (EPA Method 1311) used to classify unlisted wastes as hazardous wastes based on concentrations leached
Digestions	Samples microwave digested in concentrated nitric acid	To determine total extractable amounts of metals for comparison with the other leaching tests
Batch Tests	Samples in original and damaged conditions were submerged in two landfill leachate simulants with aliquots removed over time to monitor changes in metal ion concentrations	To compare metal leaching in two extraction fluids (TCLP and a simulated landfill leachate) over time for samples in original and damaged conditions
Batch Tests with MSW	Samples in damaged condition mixed with MSW and saturated with a simulated landfill leachate with aliquots removed over time to monitor changes in metal ion concentrations	To compare leaching within a more realistic waste matrix to the results of the batch tests and the TCLP

pore diameter nylon filter, diluted with DDI water, then acidified to a concentration of two percent nitric acid and analyzed by ICP-OES (Perkin Elmer Optima 3100RL) to determine the amounts of extractable metals present.

5.2.4 Batch leaching tests in simulated landfill leachates

PV module pieces and Li-ion and NiMH batteries in original and damaged housing were submerged in two landfill leachate simulants, and aliquots were removed to monitor changes in metal ion concentrations over time. For the original condition for the PV modules, pieces which passed through a 9.5 mm sieve and with all the layers intact were chosen, and for the damaged condition, the layers (back material, active materials layer, and glass) were mechanically separated. For the laptop and power tool batteries, the plastic housing was disassembled and the individual cells within the battery were used for testing. For the original housing condition, the batteries, or the cells from the laptop and power tool batteries, were discharged and placed in the leachates whole. For the damaged condition, the batteries or cells were discharged, the electrodes were removed from the housing and unrolled, and both the housing and the electrodes were cut into pieces of less than approximately one centimeter in length before placing in the leachates.

The samples were submerged in two extraction fluids: the TCLP extraction fluid (either TCLP #1 or #2) determined from conducting the preliminary evaluation on the samples and a simulated landfill leachate (Sim. Leachate) (Ghosh et al., 2004), which was chosen to minimize the variability from microbial influences and focus on the chemical/physical changes (Table 5.3). For most of the samples, the ratio of leachate to waste by mass was 10; however, for some of the samples with less mass (specified in Table 5.4), a ratio of 20 was used to ensure that the percent of the leachate removed by aliquots by the end of the experiment was kept to less than 15 percent of the starting volume.

Leaching kinetics were determined via aliquot sampling to monitor changes in the leachate compositions over time. The leachates were added to the jars on Day 0, and aliquots of approximately 1.5 mL were removed from each jar on Days 1, 2, 5, 9, 12, 14, 23, 30, 37, 44, 58, 72, 86, and 100. For the iPhone 5

Table 5.3: Simulated landfill leachate composition

Component	Concentration [mg/L]
Calcium carbonate	1100
Sodium carbonate	11500
Ammonium chloride	650
Acetic acid*	6876
Propionic acid	192
Butyric acid	422
Pentanoic acid	163
Hexanoic acid	232
Sodium citrate	46400
Hydroxylamine hydrochloride	31.7
*Acetic acid concentration differs from Ghosh et al. (2004)	

Table 5.4: Batch leaching test conditions including leachate type, sample condition, number of samples, mass of samples, and ratio of the mass of leachate to the mass of waste

E-waste Type	Leachate Type	Original or Damaged Housing	# of Samples	Average Sample Mass (g)	Ratio of Leachate to Waste
Suniva OPT245-60-4-100 c-Si PV module	TCLP #1	original	3	45	10
Suniva OPT245-60-4-100 c-Si PV module	Sim. Leachate	original	3	45	10
Suniva OPT245-60-4-100 c-Si PV module	TCLP #1	damaged	3	45	10
Suniva OPT245-60-4-100 c-Si PV module	Sim. Leachate	damaged	3	45	10
Suniva MVP240-60-5-401 mc-Si PV module	TCLP #1	original	3	45	10
Suniva MVP240-60-5-401 mc-Si PV module	Sim. Leachate	original	3	45	10
Suniva MVP240-60-5-401 mc-Si PV module	TCLP #1	damaged	3	45	10
Suniva MVP240-60-5-401 mc-Si PV module	Sim. Leachate	damaged	3	45	10
Lenmar LBZ378D laptop battery	TCLP #1	original	3	42.5	10
Lenmar LBZ378D laptop battery	Sim. Leachate	original	3	42.5	10
Lenmar LBZ378D laptop battery	TCLP #1	damaged	3	42.5	10
Lenmar LBZ378D laptop battery	Sim. Leachate	damaged	3	42.5	10
Lenmar PTD9094 power tool battery	TCLP #2	original	2	56.2	10
Lenmar PTD9094 power tool battery	Sim. Leachate	original	2	56.2	10
Lenmar PTD9094 power tool battery	TCLP #2	damaged	3	56.2	10
Lenmar PTD9094 power tool battery	Sim. Leachate	damaged	3	56.2	10
Rayovac CTL10293 power tool battery	TCLP #1	original	3	40.7	10
Rayovac CTL10293 power tool battery	Sim. Leachate	original	3	40.7	10
Rayovac CTL10293 power tool battery	TCLP #1	damaged	3	40.7	10
Rayovac CTL10293 power tool battery	Sim. Leachate	damaged	3	40.7	10
Empire BLP-1277-1.4 iPhone 5 replacement battery	TCLP #2	original	1	25.4	10
Empire BLP-1277-1.4 iPhone 5 replacement battery	Sim. Leachate	original	1	25.4	10
Empire BLP-1277-1.4 iPhone 5 replacement battery	TCLP #2	damaged	1	25.4	10
Empire BLP-1277-1.4 iPhone 5 replacement battery	Sim. Leachate	damaged	1	25.4	10
Nuon NURE18650 flashlight battery	TCLP #1	damaged	3	45.9	10
Nuon NURE18650 flashlight battery	Sim. Leachate	damaged	3	45.9	10
Ultralast UL14430SL solar light battery	TCLP #1	original	1	14.85	20
Ultralast UL14430SL solar light battery	Sim. Leachate	original	1	14.85	20
Ultralast UL14430SL solar light battery	TCLP #1	damaged	3	14.85	20
Ultralast UL14430SL solar light battery	Sim. Leachate	damaged	3	14.85	20
Rayovac RL123A digital camera battery	TCLP #2	original	1	16.35	20
Rayovac RL123A digital camera battery	Sim. Leachate	original	1	16.35	20
Rayovac RL123A digital camera battery	TCLP #2	damaged	3	16.35	20
Rayovac RL123A digital camera battery	Sim. Leachate	damaged	3	16.35	20
Energizer CR2450 watch battery	TCLP #2	damaged	3	6.65	20
Energizer CR2450 watch battery	Sim. Leachate	damaged	3	6.65	20
Lenmar LBZ378D laptop battery circuit board	Sim. Leachate	original	3	7.15	20
Rayovac CTL10293 power tool battery circuit board	Sim. Leachate	original	3	14.3	20

replacement battery, additional aliquots were removed on Day 128, and for the PV modules, additional aliquots were removed on Days 128 and 156. Each aliquot was filtered with a 0.2 micrometer pore diameter nylon filter, then acidified to a concentration of two percent nitric acid and analyzed by ICP-OES (Perkin Elmer Optima 3100RL) to determine the concentrations of metals present. Redox potential and pH measurements were taken in the jars at the time of sampling.

5.2.5 Leaching tests in simulated landfill leachates and municipal solid waste components

Three of the e-waste types (the Suniva c-Si PV module, the Lenmar NiMH power tool battery, and the Lenmar Li-ion laptop battery) from the previously described tests were chosen to mix with municipal solid waste (MSW) components and simulated landfill leachate (Table 5.3) to compare leaching within a more realistic waste matrix to the results of the batch leaching tests and the TCLP. For the c-Si PV module, pieces which passed through a 9.5 mm sieve and with all the layers intact were chosen. For the power tool and laptop batteries, the plastic housing was disassembled and cut into approximately two centimeter square pieces, and for the individual cells within the batteries, cells were discharged, the electrodes were removed from the housing and unrolled, and both the housing and the electrodes were cut into pieces of less than approximately one centimeter in length. The MSW mixture contains paper products, plastics, metal, glass, and food (Table 5.5) mixed at the same ratio as the typical US MSW (Khan et al., 2013; USEPA, 2015). To simulate a daily cover of soil being added to the landfill, the MSW was mixed with a previously characterized sandy loam soil (Montgomery et al., 2017), with 75 percent by mass MSW and 25 percent by mass soil. Each e-waste type was mixed with the MSW

Table 5.5: Municipal solid waste composition

Component	Percentage by Weight (not including e-waste)	Materials Used
Paper products	45.5	Foam board
Plastics	16.4	Plastic beads
Metal	10.9	Aluminium beads
Glass	9.6	Glass beads
Food	17.6	Rabbit feed

and soil mixture, placed in containers, and covered with a layer of pea gravel to keep the less dense materials from separating from and floating on top of the other waste materials. The simulated landfill leachate was added to saturate the waste materials, simulating a potential "worst case" scenario of the e-waste materials in constant contact with the leachate (Table 5.6).

Leaching kinetics were determined via aliquot sampling to monitor changes in the leachate composition over time. The simulated landfill leachate was added on Day 0, and 5 mL aliquots were removed using syringes from three different locations within the waste matrix on Days 1, 2, 5, 9, 12, 14, 23, 30, 37, 43, 58, 72, 86, and 100. The aliquots were filtered with 0.2 micrometer pore diameter nylon filters, then acidified to a concentration of two percent nitric acid and analyzed by ICP-OES (Perkin Elmer Optima 3100RL) to determine the concentrations of metals present. Redox potential and pH measurements were taken at each sampling event. Additionally on Day 100, samples of the biofilm present in each container were removed and dried. Three 200 mg (dry weight) biofilm samples from each container were digested in 2 mL of concentrated nitric acid and 2 mL of 30 percent hydrogen peroxide to determine the uptake of metals in the biofilms.

5.3 Results

5.3.1 TCLP

Metal concentration results from TCLP testing show that one of the two PV modules and three of the eight batteries would be classified as hazardous waste in the US (Table 5.7). The c-Si module would be classified as hazardous waste due to Pb, but the mc-Si module would not. The NiMH

Table 5.6: Masses of e-waste, MSW, and leachate for simulated landfill leaching tests

E-waste type	Mass of E-waste (g)	Mass of MSW & Soil (g)	E-waste % by Mass	Mass of Sim. Leachate (g)
Suniva OPT245-60-4-100 c-Si PV module	750.00	1250.00	37.5	1800
Lenmar PTD9094 power tool battery	797.66	1202.34	39.9	3700
Lenmar LBZ378D laptop battery	293.28	1706.72	14.7	3300

Table 5.7: TCLP results for the PV module pieces, battery electrodes, and battery circuit boards. Waste labels and numbers correspond to Table 5.1. Values bolded and in red exceeded regulatory limits for the US or CA. Ag and Cd measured but not detected in any samples.

	Detection Limit	1 c-Si module	2 mc-Si module	3 laptop battery	4 NiMH power tool battery	5 Li-ion power tool battery	6 phone replacement battery	7 flashlight battery	8 solar light battery	9 camera battery	10 watch battery	11 circuit board	12 circuit board	TCLP Limits	SDWA Limits
	[mg/L]	[mg/L]	[mg/L]	[mg/L]	[mg/L]	[mg/L]	[mg/L]	[mg/L]	[mg/L]	[mg/L]	[mg/L]	[mg/L]	[mg/L]	[mg/L]	[mg/L]
As	0.053	ND	ND	ND	**28.9**	ND	ND	ND	ND	ND	ND	ND	ND	5	0.010
Ba	0.004	ND	0.01	0.07	0.03	0.01	ND	0.01	ND	ND	ND	1.58	1.27	100	2.0
Cr	0.007	ND	ND	ND	ND	ND	ND	0.05	0.01	ND	ND	ND	ND	5	0.1
Hg	0.061	ND	ND	ND	ND	ND	**7.83**	**4.26**	ND	ND	ND	ND	ND	0.2	0.002
Pb	0.042	**20.2**	0.07	0.11	0.89	ND	2.15	0.11	ND	ND	ND	ND	ND	5	0.015
Se	0.075	ND	ND	0.11	ND	0.62	ND	ND	ND	ND	0.17	ND	ND	1	0.05
														CA only	
Co	0.007	ND	ND	33.6	**541**	7.55	**1655**	**262**	1.04	ND	ND	0.08	0.07	80	-
Cu	0.010	ND	ND	**730**	ND	**644**	**1746**	**134**	**74.7**	ND	ND	0.17	0.15	25	1.3
Ni	0.015	ND	ND	17.4	**1412**	17.4	ND	**52.7**	1.14	ND	ND	**27.5**	**40.6**	20	-
Zn	0.006	0.40	0.05	ND	5.95	ND	1.35	ND	1.12	ND	ND	102	0.41	250	-

ND: not detected/below detection limits

power tool battery exceeded the regulatory limit for As, as well as limits set by California for Co and Ni. The Li-ion phone replacement and flashlight batteries exceeded the regulatory limit for Hg, in spite of the intention of the Mercury-Containing and Rechargeable Battery Management Act of 1996 to phase out the usage of Hg in batteries in the US (USEPA, 2017). Three other Li-ion batteries (laptop, power tool, and solar light batteries) did not exceed regulatory limits for the US but did exceed limits set by California, which is in line with the landfill disposal ban of Li-ion batteries in California.

5.3.2 Digestions

Battery electrodes without battery housing and PV module pieces without the module frames were digested to determine extractable amounts of metals, which were compared with the amounts of metals leached in the TCLP and the batch leaching tests. For the c-Si and mc-Si modules, only 2.4 and 2.5 percent, respectively, of the total mass was accounted for by the elements analyzed by ICP-OES, which is likely due to not measuring Si, a major component of the modules in the active layer and glass. For the batteries, 31.2 to 74.9 percent of the electrode masses were accounted for by the elements analyzed by ICP-OES analysis (Table A.1).

5.3.3 Batch leaching tests in simulated landfill leachates

PV module pieces and Li-ion and NiMH batteries in original and damaged housing were submerged in two leachates, either TCLP #1 or #2 and the simulated leachate (Sim. Leachate) (Table 5.3), and changes in metal ion concentrations, redox potential, and pH were observed over a 100 day period. For the PV module pieces, circuit boards, and the original condition for the batteries, the pH did not vary significantly over time from the initial pH on Day 0. For the damaged condition for the batteries, the pH increased with time. The most notable increases occurred for the digital camera and watch batteries in the TCLP #2 leachate, which increased from pH 2.88 on Day 0 to pH 11.9 and 11.8, respectively, on Day 100, which demonstrates the ability of battery e-waste to control the surrounding pore conditions within the waste matrix and in this instance contribute to reducing the solubility of cations. Redox potential measurements for the Sim. Leachate samples were generally lower than the redox potential of the TCLP leachate samples over the 100 days, with only one exception: for the digital camera battery, the TCLP #2 damaged samples redox conditions were very similar to the redox conditions of the Sim. Leachate samples.

When comparing the original condition to the damaged condition samples within each leachate type, the metal concentrations leached for the damaged condition were higher than for the original condition except for iron concentrations for most of the batteries. Although metal concentrations leached for the whole batteries did not reach the concentration levels of the damaged condition on the time scale sampled, disposing of whole batteries can still pose a risk as the outer casing dissolves or is opened during compaction activities at a landfill.

For two of the four waste types which exceeded the TCLP regulatory limits, Hg concentrations in the Sim. Leachate samples exceeded those of the TCLP leachate samples. For the other two waste types, the Pb and As concentrations were greater for the TCLP leachate samples (Figure 5.2). The Pb concentrations leached from the mc-Si module, which did not

exceed the TCLP regulatory limit, approach similar concentrations to the c-Si, which did exceed the TCLP regulatory limit, over time in the batch leaching tests (Figure 5.3). When the pH of the TCLP and Sim. Leachate samples remained near the initial pH values throughout the sampling time, Pb concentrations were greater for the batch tests with TCLP extraction fluid. However, when the pH increased above 10 from dissolution of components in the e-waste for the Sim. Leachate samples, Pb concentrations were greater for the batch tests with Sim. Leachate than with the TCLP extraction fluid. For the laptop and Li-ion power tool batteries which did not exceed

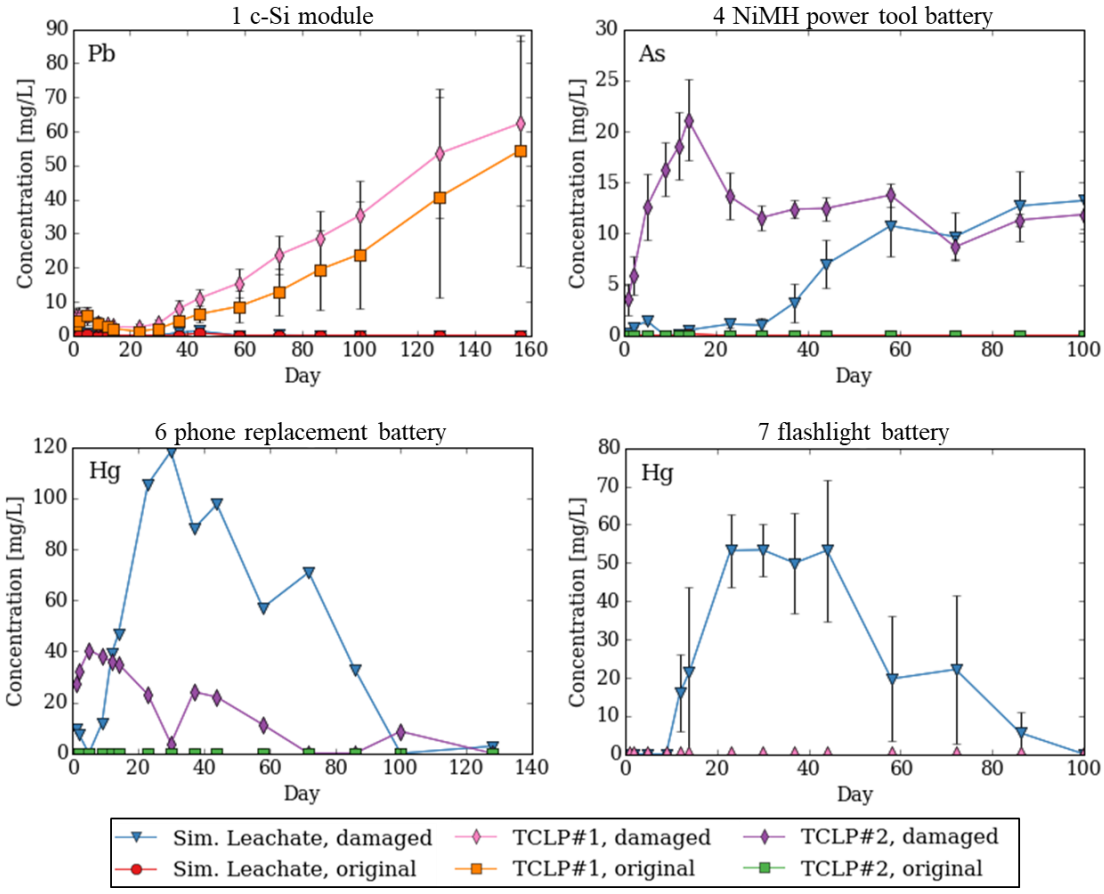

Figure 5.2: Concentrations in leachate over time for the batch leaching tests for lead (c-Si module), arsenic (NiMH power tool battery), and mercury (phone replacement battery and flashlight battery), which exceeded TCLP regulatory limits. Numbers correspond to products in Table 5.1. One liter of the TCLP#1 extraction fluid consists of 5.7 mL glacial acetic acid, 64.3 mL 1 N sodium hydroxide, and 930 mL of reagent water. One liter of TCLP#2 consists of 5.7 mL glacial acetic acid and 994.3 mL reagent water.

the California limit for Co, the Co concentrations were much greater for the Sim. Leachate samples than the TCLP samples, signaling that the TCLP leachate might not be ideal for predicting Co concentrations leaching from e-waste in a landfill setting, especially when the e-waste is capable of altering the pH of the pore water. For the watch battery, which did not leach a detectable amount of Ni during TCLP testing, the Ni concentration in both the Sim. Leachate and TCLP #2 leachate in the batch leaching tests were much higher. One of the watch batteries in Sim. Leachate had a consistently lower Ni concentration (data plotted separately as a dashed line

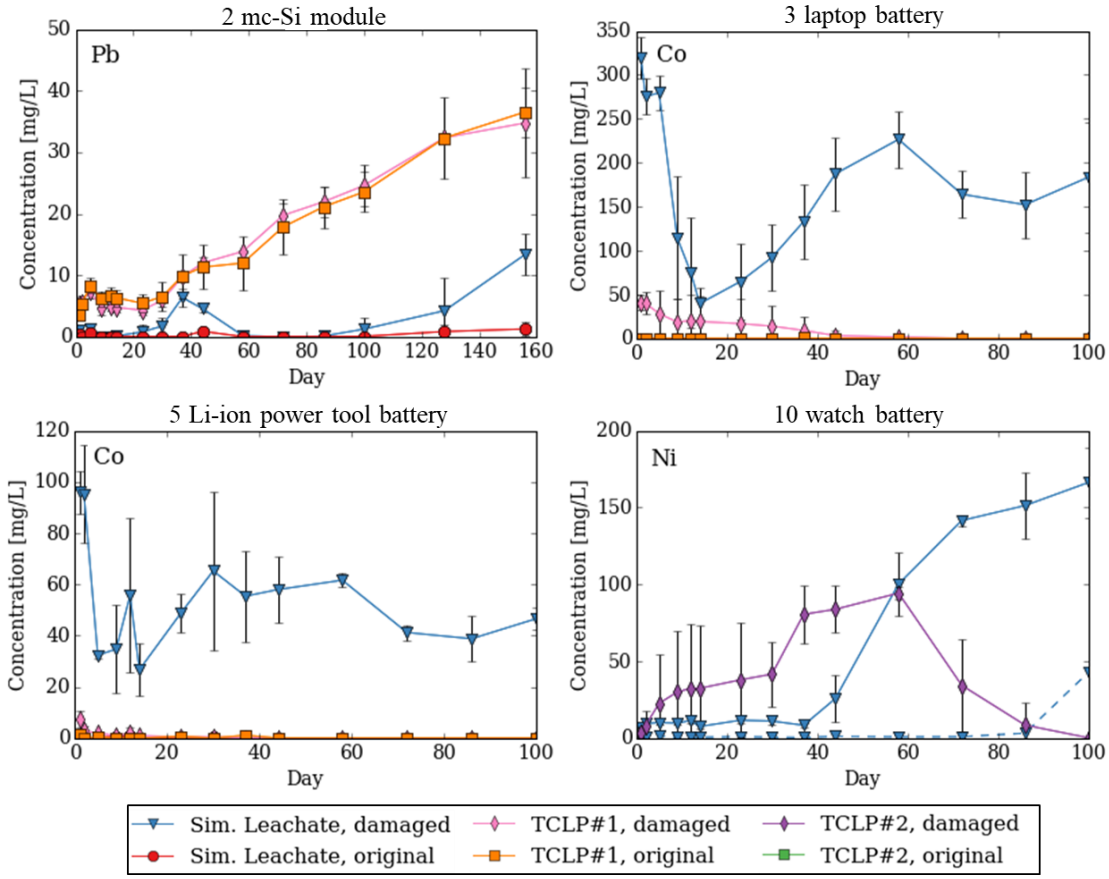

Figure 5.3: Concentrations in leachate over time for the batch leaching tests for lead (mc-Si module), cobalt (laptop battery and Li-ion power tool battery), and nickel (watch battery), which did not exceed regulatory limits. Numbers correspond to products in Table 5.1.

in Figure 5.3), and although all the watch batteries for this study were packaged and marketed the same way, this sample could represent a change in composition for the product, which can add to the complexity of e-waste toxicity characterization and recycling.

5.3.4 Leaching tests in simulated landfill leachates and municipal solid waste components

Three of the e-waste types (c-Si PV module, NiMH power tool battery, and Li-ion laptop battery) from the batch leaching tests were mixed with municipal solid waste (MSW) components and the Sim. Leachate to compare leaching within a more realistic waste matrix to the results of the batch leaching tests and the TCLP. Initially over the first five days in the waste mixtures, pH increased for the two batteries and decreased for the c-Si waste mixture, and after Day 5, pH decreased for the batteries and increased for the c-Si waste mixture (Figure 5.4). Redox potential decreased over the first few days for all three waste mixtures, with anaerobic conditions continuing for the sampling period.

Although the ratio of e-waste to leachate is the highest for the c-Si module out of the three e-waste types, the concentrations of metals leached for the c-Si module were lowest (Figure 5.4). One notable difference from the batch leaching tests and TCLP was that Pb was not detected when the c-Si modules pieces were mixed with MSW, even though 13.2 and 20.3 percent (maximum value reached) of the extractable amount of Pb in the c-Si module pieces leached in the TCLP and batch tests, respectively. Low to undetectable concentrations of Pb in leachate have been observed in other e-waste disposal studies, which found Pb sorbed to waste components near the original source (Li et al., 2009b; Visvanthan et al., 2010). I hypothesize that sorption to the soil or MSW components was responsible for reducing the leachate Pb and other cation concentrations. The soil contains reactive iron oxide and clay minerals (kaolinite and mica), which are known to be strong sorbents for Pb (Bargar et al., 1997; Ostergren et al., 2000; Cruz-Guzmán et al., 2003; Hamidpour et al., 2010). Additionally, humic substances are known to sorb

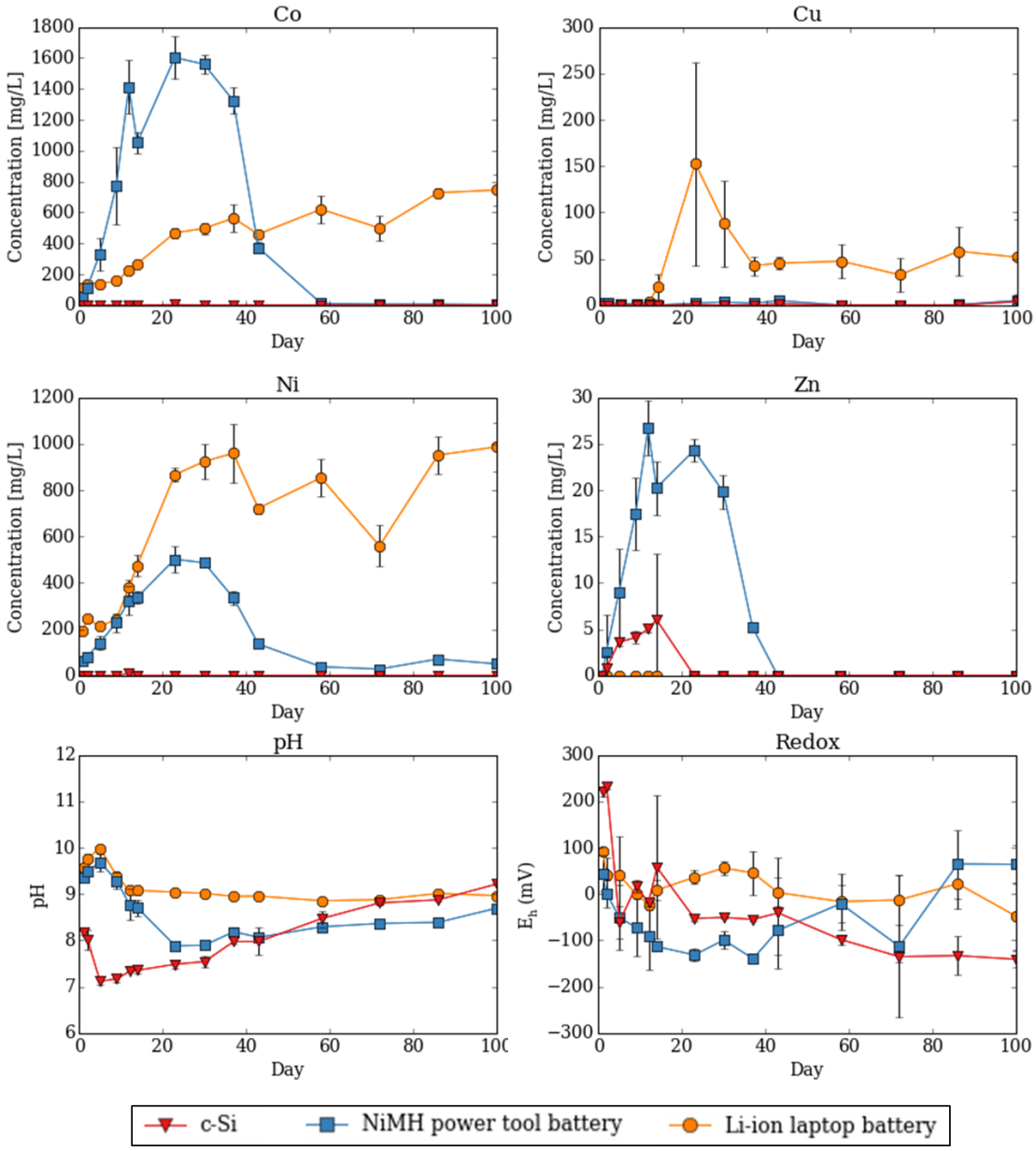

Figure 5.4: Concentrations of metals in leachate, pH, and redox potential for the leaching tests in simulated landfill leachates and municipal solid waste components for the c-Si module, NiMH power tool battery, and Li-ion laptop battery.

metals in landfills (Mårtensson et al., 1999; Bozkurt et al., 2000). For the NiMH power tool battery, the maximum metal leachate concentrations were observed near Day 30, followed by a significant drop in concentrations to near zero by Day 50. Prior to Day 30, the pH and redox potential were decreasing and at Day 30 reached a minimum at which sulfate reduction to sulfide

was possible. Metal ion concentrations decreased for Co, Fe, Mn, Ni, and Zn, which can likely be explained by the formation of metal sulfide minerals (Morse and Luther, 1999). For the Li-ion laptop battery, metal concentrations increased at a slower rate and started to plateau near Day 20. I hypothesize that the changes in leachate concentrations are due to an evolution of the MSW components and microbial growth, which produced additional sorption surfaces. Biofilms were clearly observed in the waste containers, and the decrease in reduction potential is an indication of the microbial activity. To examine the significance of metals sorbed by the biofilms, biofilm samples were harvested from the waste containers, dried, and digested to determine the possibility of metal partitioning to biofilm. Significant concentrations of metal ions were found in all biofilm samples as noted in Table 5.8.

Table 5.8: Metal concentrations [mg metal per g of dry biofilm] in biofilms sampled on Day 100 for the leaching tests mixed with MSW.

	c-Si module	**NiMH power tool battery**	**Li-ion laptop battery**
	mg/g of biofilm	mg/g of biofilm	mg/g of biofilm
Ag	ND	ND	0.003
Al	0.881	6.00	41.1
As	ND	ND	ND
Ba	0.010	0.005	0.015
Be	ND	0.001	ND
Bi	ND	ND	ND
Cd	ND	ND	ND
Co	0.002	14.0	14.5
Cr	ND	0.035	0.007
Cu	0.049	0.144	2.69
Fe	12.7	10.2	7.63
Ga	ND	ND	ND
Hg	ND	ND	ND
In	ND	0.006	0.015
Mn	1.17	0.309	31.6
Ni	ND	17.9	19.4
Pb	ND	ND	ND
Se	ND	ND	ND
Tl	ND	0.038	0.076
Zn	2.46	3.25	2.96

5.4 Discussion

The trends observed in the leaching tests demonstrate the complexity of characterizing PV and battery e-waste. The percentages of the total extractable metals which leached for the TCLP regulatory method compared to the batch tests varied widely for different metals and across the

waste types (Figure 5.5). For most of the waste types, the amounts of metals which leached in the TCLP and batch tests were much lower than the total extractable amounts, demonstrating the potential for additional amounts of metals to leach which have not been accounted for by the TCLP. The results of the TCLP regulatory method showed that only one of the two PV modules and three of the eight batteries would be classified as hazardous waste in the US; however, for some of the other e-wastes, metals of concern including Cr, Cu, Hg, Ni, Pb, and Zn leached during the batch tests but not in the TCLP regulatory method, demonstrating that the TCLP regulatory method might fail at predicting potential leaching and at capturing the complexity of e-waste leaching in landfill conditions. Across the waste types, the batch tests without MSW consistently leached greater amounts of Ba, Co, Hg, and Zn than the TCLP regulatory method. For Cu, Pb, and Ni, no consistent test leached a greater amount than the other across the battery types. For the c-Si module, the maximum amounts of Pb and Zn leached in the batch tests without MSW were similar to the amounts leached in the TCLP regulatory method; however, for the mc-Si module, the maximum amounts of Ba, Pb, and Zn leached in the batch tests were much higher than in the TCLP regulatory method. For the c-Si module batch test with MSW, Pb was not detected in the leachate. Similarly, Pb was not detected in the leachate for the laptop battery batch test with MSW, but larger percentages of Co and Ni leached in the batch test with MSW than the TCLP regulatory method. Conversely, lower percentages of Co and Ni leached in the batch test with MSW for the NiMH power tool battery, which demonstrates how changes in pH and redox conditions and the availability and affinity for sorption sites can drastically change the solubility and potential transport of metal ions. For the phone replacement and flashlight batteries, the batch tests and the TCLP regulatory method leached similar percentages of metals. However, for the Li-ion power tool, camera, and watch batteries, the batch tests leached metals not detected in the TCLP regulatory method.

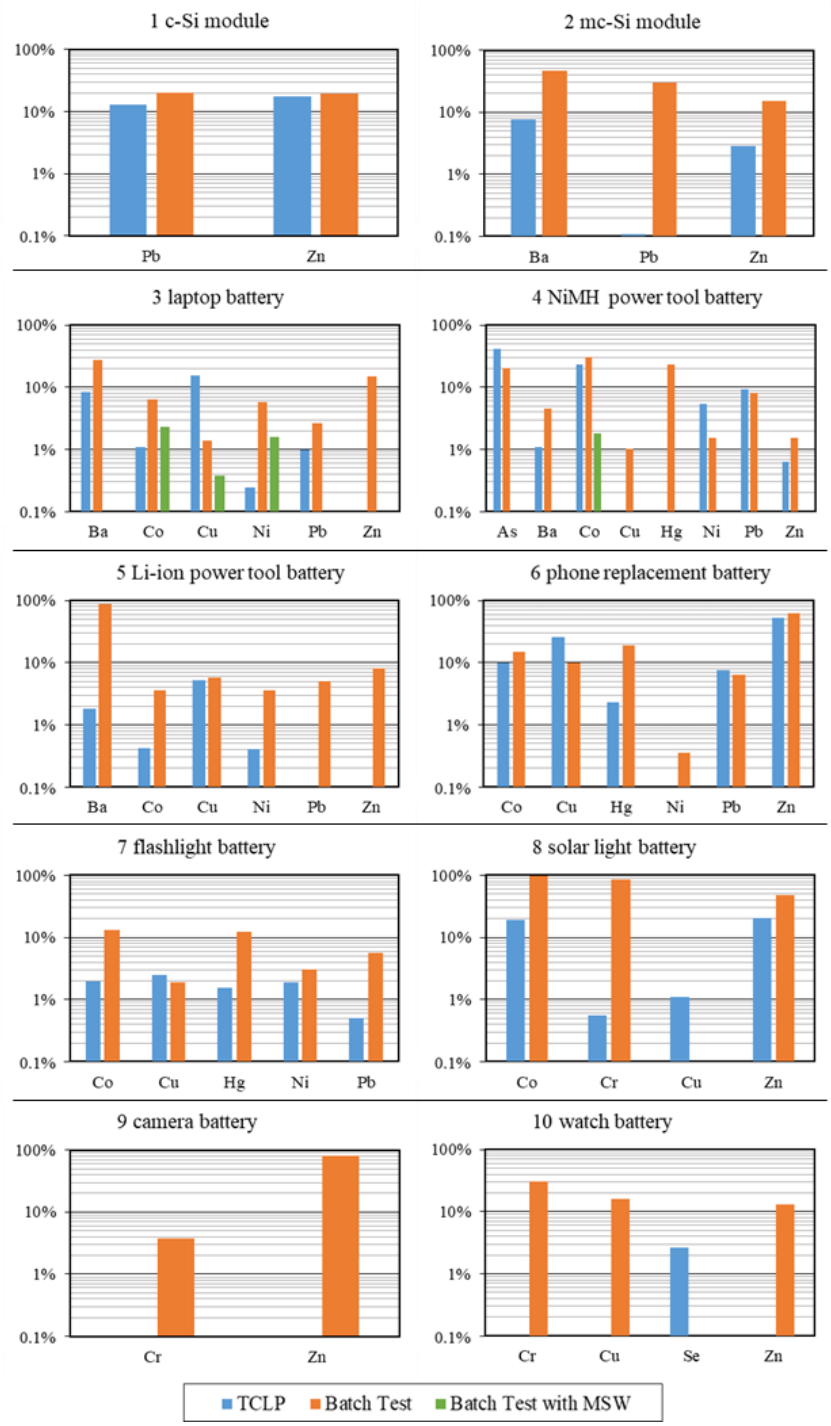

Figure 5.5: Percentages of the total digested amount of each metal leached using the TCLP regulatory method and the maximum from the batch leaching tests. Waste types 1, 3, and 4 were mixed with MSW. Ba and Zn were measured for the Batch Test with MSW but are not plotted because they were also found in the MSW control.

The variability in the results across the batch tests and different simulated landfill leachates demonstrates that one leaching test, the TCLP, might not be sufficient to determine which metals and how much of them will be soluble and potentially mobile in varying landfill conditions. The results highlight the complexity of the characterizing PV and battery e-waste and developing end-of-life recycling or disposal regulations and procedures which are adequately protective of the environment. As an 18 hour leaching test, the TCLP regulatory method is not optimal for capturing the dissolution of metals from e-wastes, as demonstrated by the results of the 100 to 156 day batch tests. The TCLP underpredicted or failed to predict the dissolution of Pb in five and Cr in three of ten e-waste types. In addition to the effect of time on leaching, the use of the more aggressive leachate (Sim. Leachate) resulted in higher metal extraction percentages for most of the waste types, with the exception of Pb and Zn for the PV modules, As for the NiMH power tool battery, and Ni for the phone replacement battery. When mixing the e-wastes with MSW, both lower and higher percentages of the total metals were found in the leachate compared to the TCLP regulatory method, which complicates the development of a predictive test for metal leaching in a MSW landfill. Nevertheless if the aim is to prevent disposal of e-wastes which could leach metals at concentrations of concern, the use of a representative landfill leachate such as Sim. Leachate in this study, in addition to the TCLP leachate, over an amount of time that allows for maximum leachate metal concentrations to be reached would be a preferred alternative to the TCLP regulatory method to reduce the likelihood of disposing of e-wastes leaching metals at concentrations of concern.

In this study, the batch leaching tests occurred in a laboratory setting in an aerobic atmosphere at room temperature, which is not representative of the changing conditions within a solid waste landfill. Although a microbially produced leachate has not been used in this study, future work should consider the influence of a microbially produced leachate compared to the

simulated leachate used. Future work should consider the effects of changes in temperature on leaching kinetics. Although conditions were slightly anaerobic to anaerobic in the containers mixed with MSW, repeating the experiment in an anaerobic atmosphere, which would be more representative of the conditions within a solid waste landfill, could change the metal dissolution observed. The microbial community composition and the physical, chemical, and metabolic structure and functions of the biofilms within the batch tests were not studied, which could affect metal leaching. Future work should also explore if the metals in sulfide minerals remain insoluble over a longer time period than the sampling period for this study or if conditions within the waste matrix can change sufficiently over time for the metals become soluble again. As the composition of landfill waste changes to include less organic material, as composting or incinerating food waste and other organic wastes becomes more prevalent, the capacity for MSW landfills to keep metals immobile could diminish, which should be considered in future work. Knowing the conditions and breakdown of materials that enable metal leaching in landfills could allow material scientists to design products with the potential for less toxic leaching. As the use of energy technologies, including photovoltaic modules and batteries, continues to increase, there is an urgent need to study the end-of-life of these products, both for material recovery through recycling and the consequences of municipal waste disposal, which is likely to occur in locations without sufficient recycling laws or take-back programs, in order to avoid contributing to the growing e-waste problem.

5.5 References

Bargar, J. R.; Brown, G. E.; Parks, G. A. Surface Complexation of Pb (II) at Oxide-Water Interfaces: I. XAFS and Bond-Valence Determination of Mononuclear and Polynuclear Pb (II) Sorption Products on Aluminum Oxides. *Geochim. Cosmochim. Acta* **1997**, *61* (13), 2617–2637.

Bozkurt, S.; Moreno, L.; Neretnieks, I. Long-Term Processes in Waste Deposits. *Sci. Total Environ.* **2000**, *250* (1), 101–121.

BU-705: How to Recycle Batteries http://batteryuniversity.com/learn/article/recycling_batteries (accessed Sep 23, 2015).

Catenacci, M.; Verdolini, E.; Bosetti, V.; Fiorese, G. Going Electric: Expert Survey on the Future of Battery Technologies for Electric Vehicles. *Energy Policy* **2013**, *61*, 403–413.

Chen, H.; Cong, T. N.; Yang, W.; Tan, C.; Li, Y.; Ding, Y. Progress in Electrical Energy Storage System: A Critical Review. *Prog. Nat. Sci.* **2009**, *19* (3), 291–312.

Commission for Environmental Cooperation. *Environmentally Sound Management of End-of-Life Batteries from Electric-Drive Vehicles in North America*; **2015**.

Cruz-Guzmán, M.; Celis, R.; Hermosin, M. C.; Leone, P.; Negre, M.; Cornejo, J. Sorption-Desorption of Lead (II) and Mercury (II) by Model Associations of Soil Colloids. *Soil Sci. Soc. Am. J.* **2003**, *67* (5), 1378–1387.

Dinçer, F. The Analysis on Photovoltaic Electricity Generation Status, Potential and Policies of the Leading Countries in Solar Energy. *Renew. Sustain. Energy Rev.* **2011**, *15* (1), 713–720.

Gaustad, G.; Ganter, M.; Wang, X.; Bailey, C.; Babbitt, C.; Landi, B. Economic and Environmental Trade Offs for Li-Based Battery Recycling. In *Energy Technology 2012: Carbon Dioxide Management and Other Technologies*; **2012**; pp 219–226.

Ghosh, A.; Mukiibi, M.; Ela, W. TCLP Underestimates Leaching of Arsenic from Solid Residuals under Landfill Conditions. *Environ. Sci. Technol.* **2004**, *38* (17), 4677–4682.

Goonan, T. G. *Lithium Use in Batteries Circular 1371*; US Department of the Interior, US Geological Survey, **2012**.

Hamidpour, M.; Kalbasi, M.; Afyuni, M.; Shariatmadari, H.; Holm, P. E.; Hansen, H. C. B. Sorption Hysteresis of Cd (II) and Pb (II) on Natural Zeolite and Bentonite. *J. Hazard. Mater.* **2010**, *181* (1), 686–691.

Hawkins, T.; Gausen, O.; Stromman, A. Environmental Impacts of Hybrid and Electric vehicles—A Review. *Int. J. Life Cycle Assess.* **2012**, *17* (8), 997–1014.

Jäger-Waldau, A. *PV Status Report 2012*; European Commission, **2012**.

Kang, D.; Chen, M.; Ogunseitan, O. Potential Environmental and Human Health Impacts of Rechargeable Lithium Batteries in Electronic Waste. *Environ. Sci. Technol.* **2013**, *47* (10), 5495–5503.

Karamalidis, A. K.; Voudrias, E. A. Release of Zn, Ni, Cu, SO4(2-) and CrO4(2-) as a Function of pH from Cement-Based Stabilized/solidified Refinery Oily Sludge and Ash from Incineration of Oily Sludge. *J. Hazard. Mater.* **2007**, *141* (3), 591–606.

Khan, I. A.; Berge, N. D.; Sabo-Attwood, T.; Ferguson, L.; Saleh, N. B. Single-Walled Carbon Nanotube Transport in Representative Municipal Solid Waste Landfill Conditions. *Environ. Sci. Technol.* **2013**, *47* (15), 8425–8433.

Komilis, D.; Tataki, V.; Tsakmakis, T. Leaching of Heavy Metals from Personal Computer Components: Comparison of TCLP with a European Leaching Test. *J. Environ. Eng.* **2013**, *139* (11), 1375–1381.

Kosson, D. S.; van der Sloot, H. A.; Sanchez, F.; Garrabrants, A. C. An Integrated Framework for Evaluating Leaching in Waste Management and Utilization of Secondary Materials. *Environ. Eng. Sci.* **2002**, *19* (3), 159–204.

Li, Y.; Richardson, J. B.; Niu, X.; Jackson, O. J.; Laster, J. D.; Walker, A. K. Dynamic Leaching Test of Personal Computer Components. *J. Hazard. Mater.* **2009a**, *171* (1–3), 1058–1065.

Li, Y.; Richardson, J. B.; Bricka, R. M.; Niu, X.; Yang, H.; Li, L.; Jimenez, A. Leaching of Heavy Metals from E-Waste in Simulated Landfill Columns. *Waste Manag.* **2009b**, *29* (7), 2147–2150.

Lim, S.-R.; Kang, D.; Ogunseitan, O. A.; Schoenung, J. M. Potential Environmental Impacts of Light-Emitting Diodes (LEDs): Metallic Resources, Toxicity, and Hazardous Waste Classification. *Environ. Sci. Technol.* **2011**, *45* (1), 320–327.

Lithium Batteries: Markets and Materials http://www.bccresearch.com/market-research/fuel-cell-and-battery-technologies/batteries-lithium-fcb028f.html (accessed Sep 23, 2015).

Mårtensson, A. M.; Aulin, C.; Wahlberg, O.; Ågren, S. Effect of Humic Substances on the Mobility of Toxic Metals in a Mature Landfill. *Waste Manag. Res.* **1999**, *17* (4), 296–304.

McDonald, N. C.; Pearce, J. M. Producer Responsibility and Recycling Solar Photovoltaic Modules. *Energy Policy* **2010**, *38* (11), 7041–7047.

Montgomery, D.; Barber, K.; Edayilam, N.; Oqujiuba, K.; Young, S.; Biotidara, T.; Gathers, A.; Danjaji, M.; Tharayil, N.; Martinez, N. The Influence of Citrate and Oxalate on 99TcVII, Cs, NpV and UVI Sorption to a Savannah River Site Soil. *J. Environ. Radioact.* **2017**, *172*, 130–142.

Morse, J. W.; Luther, G. W. Chemical Influences on Trace Metal-Sulfide Interactions in Anoxic Sediments. *Geochim. Cosmochim. Acta* **1999**, *63* (19), 3373–3378.

Musson, S. E.; Vann, K. N.; Jang, Y.-C.; Mutha, S.; Jordan, A.; Pearson, B.; Townsend, T. G. RCRA Toxicity Characterization of Discarded Electronic Devices. *Environ. Sci. Technol.* **2006**, *40* (8), 2721–2726.

Ostergren, J. D.; Trainor, T. P.; Bargar, J. R.; Brown, G. E.; Parks, G. A. Inorganic Ligand Effects on Pb (II) Sorption to Goethite (α-FeOOH): I. Carbonate. *J. Colloid Interface Sci.* **2000**, *225* (2), 466–482.

Poon, C. S.; Lio, K. W. The Limitation of the Toxicity Characteristic Leaching Procedure for Evaluating Cement-Based Stabilised/solidified Waste Forms. *Waste Manag.* **1997**, *17* (1), 15–23.

Richa, K.; Babbitt, C.; Gaustad, G.; Wang, X. A Future Perspective on Lithium-Ion Battery Waste Flows from Electric Vehicles. *Resour. Conserv. Recycl.* **2014**, *83*, 63–76.

Scott, P.; Simon, M. *Utility Scale Energy Storage: Grid-Saver Fast Energy Storage System*; **2015**.

Solangi, K. H.; Islam, M. R.; Saidur, R.; Rahim, N. A.; Fayaz, H. A Review on Global Solar Energy Policy. *Renew. Sustain. Energy Rev.* **2011**, *15* (4), 2149–2163.

SolarPower Europe. *Global Market Outlook for Solar Power 2017-2021*; **2017**.

Timilsina, G. R.; Kurdgelashvili, L.; Narbel, P. A. Solar Energy: Markets, Economics and Policies. *Renew. Sustain. Energy Rev.* **2012**, *16* (1), 449–465.

USDOE. *Grid Energy Storage*; **2013**.

USEPA. Method 1311 Toxicity Characteristic Leaching Procedure.

USEPA. *Applicability of the Toxicity Characteristic Leaching Procedure to Mineral Processing Wastes*; **1995**.

USEPA. *Application of Life-Cycle Assessment to Nanoscale Technology: Lithium-Ion Batteries from Electric Vehicles EPA 744-R-12-001*; **2013**.

USEPA. National Primary Drinking Water Regulations http://water.epa.gov/drink/contaminants/#List.

USEPA. Advancing Sustainable Materials Management: Facts and Figures 2013 http://www.epa.gov/wastes/nonhaz/municipal/msw99.htm (accessed Sep 23, 2015).

USEPA. Environmental Laws that Apply to Mercury https://www.epa.gov/mercury/environmental-laws-apply-mercury#MercuryBattery (accessed Nov 7, 2017).

Visvanthan, C.; Yin, N. H.; Karthikeyan, O. P. Co-Disposal of Electronic Waste with Municipal Solid Waste in Bioreactor Landfills. *Waste Manag.* **2010**, *30* (12), 2608–2614.

Wang, X.; Gaustad, G.; Babbitt, C.; Bailey, C.; Ganter, M.; Landi, B. Economic and Environmental Characterization of an Evolving Li-Ion Battery Waste Stream. *J. Environ. Manage.* **2014a**, *135*, 126–134.

Wang, X.; Gaustad, G.; Babbitt, C.; Richa, K. Economies of Scale for Future Lithium-Ion Battery Recycling Infrastructure. *Resour. Conserv. Recycl.* **2014b**, *83*, 53–62.

Yadav, S.; Yadav, S. Investigations of Metal Leaching from Mobile Phone Parts Using TCLP and WET Methods. *J. Environ. Manage.* **2014**, *144*, 101–107.

Chapter 6: Lysimeter Test Bed Design and Implementation

Abstract

As a part of the Department of Energy's Experimental Program to Stimulate Competitive Research (DOE EPSCoR), a lysimeter test bed (RadFATE) was constructed at Clemson to study transport under natural conditions (Figure 6.1). In flowing systems, spatial and temporal heterogeneity affect the transport of contaminants that cannot be captured in lab-scale batch experiments, which demonstrates the need for lysimeter experiments. The test bed has been utilized for the intermediate-scale degradation studies for Li-ion and nickel metal hydride batteries and PV modules.

6.1 Test Bed Construction

The lysimeter test bed is located near the loading bay of the Clemson Environmental Technologies Laboratory (CETL), as shown in Figure 6.2. The test bed design is modeled after the test bed located at Savannah River Site (SRS). A concrete pad designed to hold approximately 75,000 kg (165,000

Figure 6.1: Lysimeter test bed construction showing the 20 outer casings.

pounds) was poured to support the test bed. The concrete pad is 12” deep and level within a 9’ by 25’ section and has 6” deep by 3.5’ by 25’ sides with a 1% slope for drainage. The overall pad size is 16’ by 25’. Electrical outlets were installed on a post adjacent to the test bed. An 8’ high chain link fence with two 4’ gates was installed surrounding the test bed, which will prevent unauthorized access.

Figure 6.2: Lysimeter test bed located behind CETL.

The test bed was built in a 40 yard steel roll-off container manufactured by Bakers Waste Equipment Incorporated, which houses 20 lysimeters subjected to outdoor conditions. The steel roll-off container dimensions are 7’ by 22’ by 7’ high. A 3’ high safety guardrail was installed on top of the container for staff working with the lysimeters. A platform ladder (McMaster Carr product number 8188T57) was welded to the edge of the container for easy access to the container surface. Two I-beams were welded inside the container for mounting the lysimeters, each consisting of two 11’ sections connected with a bolted plate and piece of angle iron in the center and connected to the floor of the container with two supports at the center. Four additional sets of 2” by 2” by 1/4” thick angle iron were installed to reinforce the I-beams and were located between the second and third, the fourth and fifth, the sixth and seventh, and the eighth and ninth lysimeters (Figure 6.3). The angle iron reinforcement was necessary because the I-beams were not level; therefore, the lysimeter outer casings attached to the beams would not be level without this correction. The angle iron and rusting spots on the container were sprayed with a zinc coating to

Figure 6.3: I-beam and angle iron placement.

resist corrosion (Rust-Oleum product number 7584838). The steel container was manufactured with 20 (10 per side) 5” diameter holes with centers located 2’ from the bottom of the container and evenly spaced along the longer sides of the container, which are for the PVC outer casing pipes to exit and rainwater effluent to be collected. The holes were covered with 5” diameter rubber PVC pipe caps with stainless steel clamps (Cherne product number 270776). A 2” diameter hole was cut in the center of each cap for the PVC pipe to exit the container. The interior of the PVC pipe caps were filled with a gap-and-crack insulating foam sealant (Great Stuff product number 162848) as an extra precaution taken against leakage. The container also has a 6” diameter drainage hole, located on the side of the container close to ground level, for precipitation entering the test bed to drain if it is not captured by the outer casings or lysimeters. While backfilling the container, the drainage hole was temporarily capped with a 6” diameter rubber PVC pipe cap with a stainless steel clamp (Cherne product number 270784), and the interior of the cap was filled with a gap-and-crack insulating foam sealant (Great Stuff product number 162848). Both the cap and the foam sealant surrounding the drainage hole were removed once the backfill dried.

Draining precipitation entering the container is essential to prevent ponding on the surface and overflow into the lysimeters. A layer of gravel (approximately 5.5 cubic yards) was placed at the bottom of the container and graded to guide

Figure 6.4: Gravel graded to promote drainage to the hole on the left side of the tank.

infiltrating precipitation towards the drainage hole (Figure 6.4). Polyester reinforced neoprene rubber sheets (three 48” by 24’ by 1/16” thick sheets, MSC Industrial Supply Company product number 31937311) were placed on top of the gravel to prohibit water from stagnating in the gravel and to provide a surface for the water to travel along to the drainage hole. These sheets have 1000 psi tensile strength and have an acceptable temperature range of -20 to 180 degrees Fahrenheit. In addition to accounting for infiltrating precipitation, a drainage system connecting the surface of the test bed to the drainage hole with 1.5” diameter PVC piping allows precipitation on the surface to drain quickly. The drainage system was built to ensure water does not pool on the surface and flow over the sides of the 10” diameter PVC outer housing. A standpipe was placed near each corner of the container and connected by inclined pipes to the outlet hole, which provides an additional way for water to exit the tank (Figure 6.5).

Figure 6.5: Installation of a drainage system using 1.5” diameter PVC pipes, 2 wyes, 22.5, 45, and 90 degree elbows, and one tee.

Permanent outer casings built of PVC were placed in the container so that the 20 lysimeters can be easily removed and replaced (Figure 6.6). The outer casings also serve as secondary containment for the lysimeters. The outer casings are attached to the I-beams with galvanized steel U-bolts (10 7/8” inner diameter, delivered with the steel roll-off container). From the top down, the outer casings are constructed of a 26 11/16” long piece of 10” inner diameter schedule 40 PVC pipe, a 10” to 6” reducer, a 6” to 2” reducer bushing, a 2 1/4” long piece of 2” inner diameter schedule 40 PVC pipe, a 60 degree elbow, and a 45” long piece of 2” inner diameter schedule 40

PVC pipe, which is used to direct the effluent tubing outside of the container (Figure 6.7). All pieces, except the 10” diameter PVC pipe to the 10” to 6” reducer, are connected with PVC glue. Caps for the outer housing were made from the leftover polyester reinforced neoprene rubber sheet. Three 48” wide by 24’ sheets were ordered (MSC Industrial Supply Company product number 3193731); however, one of the three sheets was longer than 24’. Octagons were cut out of the extra piece to use as temporary covers, while lysimeters are awaiting deployment. Worm-drive clamps (Jupiter Pneumatics product number 85100611176JP) were

Figure 6.6: Outer casings for the lysimeters prior to installation in the test bed.

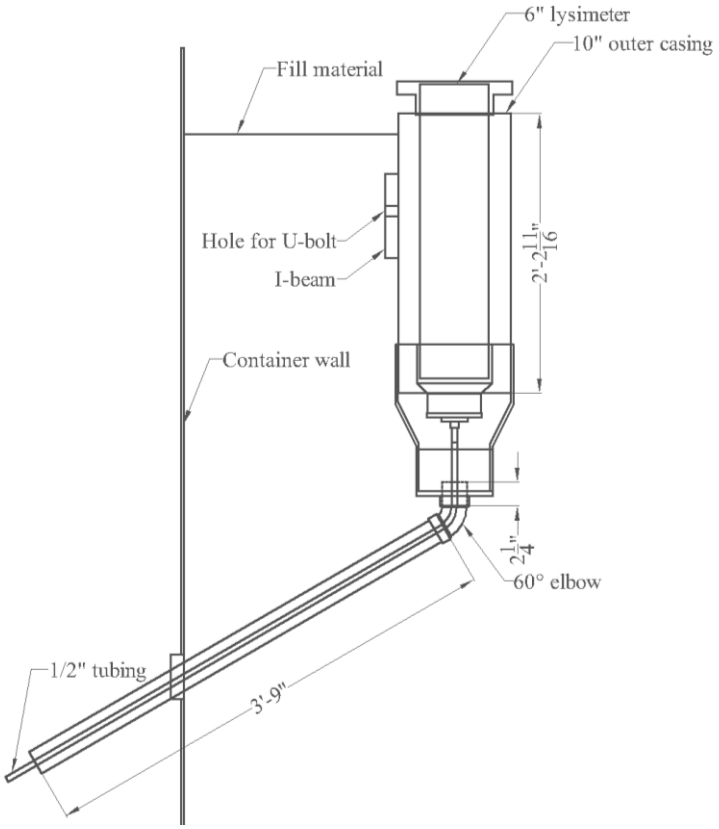

Figure 6.7: Diagram of outer casing with EPSCoR lysimeter.

purchased to secure the covers to the pipes. Storage boxes (Lifetime product number 60012) were purchased to hold the bottles for the lysimeter effluent and secondary containment pans. The inside edges of the storage boxes were sealed with silicone. Holes were drilled in the back of the boxes for the PVC pipes exiting the test bed to enter the boxes, and the area around the holes were sealed with silicone.

After the outer casings were installed, the test bed was ready to be backfilled. Using permanent markers, fill lines were marked on the outer casings that denoted 2" below the top of the 10" diameter pipe. Controlled low-strength material (CLSM)/flowable fill was ordered to backfill the container (Figure 6.8). Although discussed, a sample (smallest amount available was approximately 1 cubic yard) was not ordered prior to filling the tank. A delivery of 28 cubic yards and a pump truck to fill the container were ordered. When almost all the material had been pumped into the container, the container suddenly and markedly bowed outward, and stress cracking at some of the seams became evident. At the greatest point, the container bowed outward 10". Filling the container ceased, and remarkably after 24 hours the container was still intact. After the backfill had dried enough to walk on, the surface was roughed up using a rake and shovel prior to another delivery of backfill. An additional 4 cubic yards and a line pump arrived seven days after the first delivery to finish filling the container. When the backfill dried, the material that was delivered resembled concrete and not CLSM, which should be a much softer material. In hindsight, the tank should have been filled in three lifts, as evidenced by the permanent bowing of the tank

Figure 6.8: Backfilling the test bed, on the left utilizing a pump truck and on the right with a line pump.

walls. After the backfilled solidified, the standpipes for the PVC drainage system were trimmed flush with the surface, and the drainage system was tested with running water from a hose to ensure it was functioning properly.

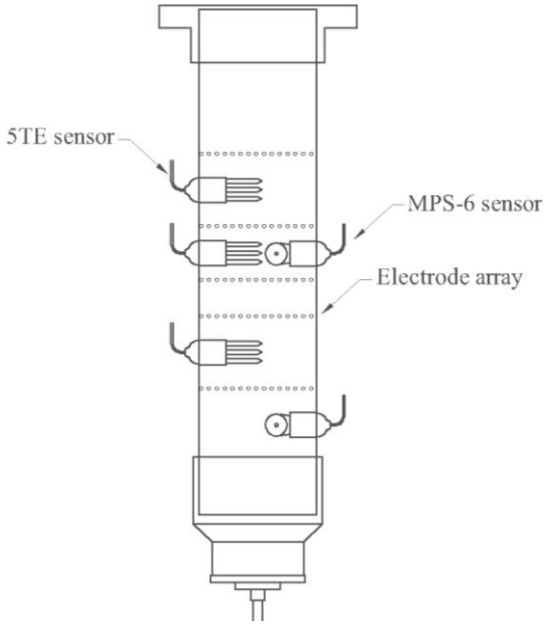

Figure 6.9: Diagram of the EPSCoR lysimeters including Decagon 5TE and MPS-6 sensors and electrode array locations.

The lysimeters deployed in the test bed for the EPSCoR radionuclide transport studies are constructed of 28” long pieces of 6” diameter schedule 40 PVC pipe, which have been drilled to accommodate the sensors described in the following section (Figure 6.9). The bottom end of the pipe has a 6” to 4” reducing coupling, a 4” male to 2” female hex bushing, a 2” male to 1/2” female hex bushing, a 1/2” hose barb, and UV resistant 1/2” inner diameter tubing, which transports the effluent from the container to a collection bottle. The hose barb is wrapped in Teflon tape and the tubing is secured with a hose clamp. Within the lysimeter, a perforated PVC grid supports an 80 x 80 nylon mesh screen, which holds sediment in place during the experiment.

The simulated landfill columns deployed in the test bed containing Li-ion and nickel metal hydride batteries and PV module pieces are constructed of 28” long pieces of 6” diameter schedule 40 PVC pipe, which have been drilled to accommodate the sensors described in the following section (Figure 6.10). The bottom end of the pipe has a 6” to 4” reducing coupling, a 4” male to 2” female hex bushing, a 2” male to 1/2” female hex bushing, a 1/2” male to 1/8” female hex bushing, a 1/8” barbed tube fitting with a 90 degree elbow, and UV resistant 3/16” inner diameter tubing,

which was initially connected to a low-flow peristaltic pump recirculating the effluent from the bottom of the column to the top of the column. The hose barb is wrapped in Teflon tape and the tubing is secured with a hose clamp. Within the column, a perforated PVC grid supports an 80 x 80 nylon mesh screen, which holds the waste components in place during the experiment.

6.2 Test Bed Instrumentation and Data Collection

Sophisticated monitoring of moisture content, temperature, electrical conductivity, and imaging of soil structure, water content, and conductive tracers are part of the data collection for the EPSCoR lysimeters. In addition to effluent collection and sampling, the lysimeters are instrumented with Decagon 5TE sensors (product number 40566), Decagon MPS-6 sensors (product number 40861), Mettler Toledo ORP electrodes (product number LE510), Omega load cells (product number LCAE-1KG), and graphite electrodes (Figure 6.11).

Eight of the 20 lysimeters are equipped with three Decagon 5TE sensors and two Decagon MPS-6 sensors, which operate on SDI-12 protocol. One of the EPSCoR lysimeters and the three landfill columns are equipped with three Decagon 5TE sensors. Decagon 5TE sensors measure apparent dielectric permittivity (unitless range from 1 to 80) using an oscillator running at 70 MHz, which can be converted to volumetric water content (calibration described in Appendix B), electrical conductivity (range of 0 to 23 deciSiemens per meter) using a two-sensor

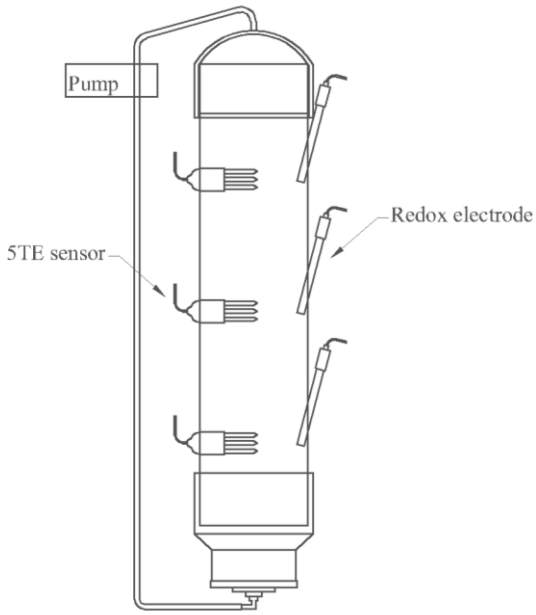

Figure 6.10: Diagram of the simulated landfill columns including Decagon 5TE sensors and Mettler Toledo redox electrode locations.

electrical array, and temperature in Celsius using a surface-mounted thermistor (Decagon Devices, 2016a). Decagon MPS-6 sensors measure water potential in kilopascals using a porous ceramic plate with a moisture release curve and temperature in Celsius using a surface-mounted thermistor (Decagon Devices, 2016b). The SDI-12 addresses of the sensors were updated to an address of "1" from the default "0" address using the SDI-12 command "0A1!" due to compatibility issues using Decagon sensors with a Campbell Scientific datalogger (Decagon Devices).

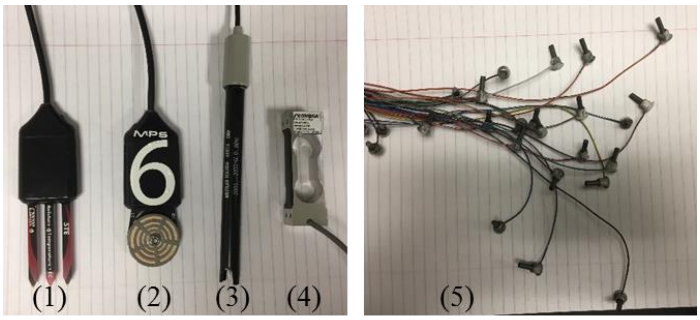

Figure 6.11: (1) Decagon 5TE sensor, (2) Decagon MPS-6 sensor, (3) Mettler Toledo ORP electrode, (4) Omega load cell, and (5) graphite electrode bundle.

Mettler Toledo ORP electrodes are used in one of the EPSCoR lysimeters and the three landfill columns. Measurements are made using the BNC connector on a handheld pH/mV meter. To convert to redox potential, 207 mV at 25 degrees Celsius is added to the measured value.

For five of the EPSCoR lysimeters, Omega load cells are used to monitor changes in mass, mostly due to changes in water content in the columns. The lysimeters are suspended from a balance system constructed out of aluminum and lead blocks with ball bearings for each contact point (Figure 6.12). Each lysimeter is suspended by three load cells. The load cells measure voltage changes that can be related to weight fluctuations (Omega).

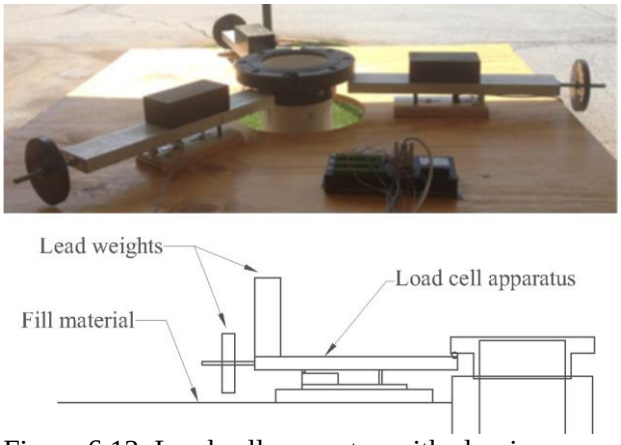

Figure 6.12: Load cell apparatus with aluminum support bars and lead counterweights.

The Decagon 5TE and MPS-6 sensors and Omega load cells are connected to Campbell Scientific CR6 WIFI dataloggers that are used for real-time monitoring (Campbell Scientific, 2016b). Campbell Scientific AM16/32B multiplexers are used to increase the number of sensors that can be recorded per datalogger (Campbell Scientific, 2016a). MicroSD cards (Verbatim product number 44082) were purchased to increase the storage capacity of each datalogger. The Decagon sensors are connected to the multiplexers in 2X32 mode, and the load cells are connected in 4X16 mode, which requires them to be on different multiplexers. Each Decagon sensor has three wires: white (12 volt power) connected to "H" on the multiplexer, red (SDI-12 digital signal) connected to "L" on the multiplexer, and bare (ground) connected to the ground on the multiplexer. Each load cell has five wires: white (white extension) connected to the ground on the multiplexer, red (orange extension) connected to the even "H" on the multiplexer, black (blue extension) connected to the odd "L" on the multiplexer, green (green extension) connected to the odd "H" on the multiplexer, and yellow (brown extension) connected to the ground on the multiplexer.

The first set of lysimeters deployed in the RadFATE facility include four lysimeters with Decagon 5TE sensors and redox electrodes (labeled 1, 11-13), five lysimeters with 5TE and MPS-

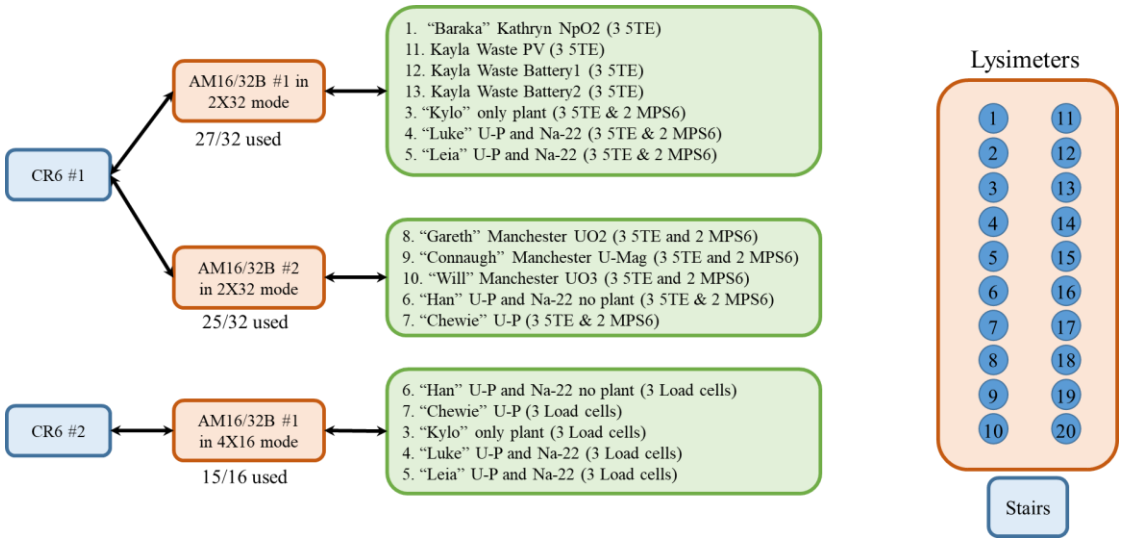

Figure 6.13: CR6 dataloggers, AM16/32B multiplexers, and sensors for each lysimeter for deploying 12 lysimeters.

6 sensors and load cells (labeled 3-7), and three lysimeters with 5TE and MPS-6 sensors (labeled 8-10). To deploy these 12 lysimeters, two CR6 dataloggers and three AM16/32B multiplexers are used (Figure 6.13). The first datalogger (CR6 #1, SN: 3643) has two multiplexers wired in 2X32 mode, with the potential to add a third multiplexer. The second datalogger (CR6 #2, SN: 4478) has one multiplexer in 4X16 mode wired to it, with the potential to add a second multiplexer. To connect each AM16/32B to a CR6, a cable with nine inner wires is necessary. Table C.1 (in Appendix C) contains the wiring guide for connecting the multiplexers to the two dataloggers.

Once the sensors are wired to the multiplexers and the multiplexers are wired to the dataloggers, the dataloggers are connected to a computer using the Campbell Scientific LoggerNet software. To collect and record data from the sensors, the dataloggers require a program written in CRBasic and compiled by the datalogger. The algorithm for writing the CRBasic program is described in Figure 6.14, and the actual CRBasic programs for the dataloggers are located in Appendix C. The computer is connected via Wi-Fi to the CR6 dataloggers and to the internet via Ethernet. The computer that is connected to the dataloggers simultaneously operates a webserver, which displays the 5TE and MPS-6 sensors and load cell data in real time. The website can be accessed by visiting

Using Const, define the following constants:
- Data collection interval
- LoggerNet scanning interval
- Number of lysimeters per multiplexer
- Number of each type of sensor connected to each lysimeter
- Total number of each type of sensor

Using Public, define variables for the data collected for each sensor type in an array.

Using Dim, define variables for the current sensor of each type.

Using Alias, assign labels for data in the data tables.

Construct data tables.

Write subroutines for each of the following tasks:
- Reset counters to zero
- Progress through inputs on each multiplexer
- Turn a sensor on
- Turn a sensor off
- Turn a multiplexer on
- Turn a multiplexer off
- Measure sensors using SDI 12 protocol (or load cells using a full bridge measurement)
- Measure sensors (or load cells) for one lysimeter for each of the multiplexers

Write a program which reads sensors on the multiplexers and writes the data to data tables

Figure 6.14: Algorithm for writing programs for the CR6 dataloggers.

http://130.127.95.40 while connected to the Clemson University network (locally or over the virtual private network). The webserver is also configured to send an email alert when the connection to the dataloggers fails.

In addition to the Decagon sensors and Omega load cells, the EPSCoR lysimeters are equipped with graphite electrodes. Electrical resistivity measurements are made using graphite electrodes constructed in the lab at Clemson. Each electrode is assembled using a piece of graphite and a wire secured by conductive silver epoxy in a small plastic cap. The wire connected to each electrode is one wire of a 50 pin connector. The electrodes are assembled in arrays consisting of 48 electrodes, which are evenly spaced around the circumference of the lysimeter. Each lysimeter has five arrays, for a total of 240 electrodes per lysimeter.

For the EPSCoR lysimeters exposed to rainfall, effluent is collected from the bottom drain of the columns and monitored for contaminants (radionuclides) as well as pH, E_h, dissolved oxygen, major ions, colloids, and dissolved organic carbon. The effluent from the EPSCoR lysimeters and the secondary effluent from the outer casings are collected in separate high-density polyethylene sample bottles, which are exchanged and analyzed monthly or more frequently due to rain events. For the simulated landfill columns, which are capped, there is no effluent due to rainfall nor sample bottle collection, and the leachate sampling procedure is described in Chapter 7.

6.3 Weather Stations

Site-specific weather data including precipitation, humidity, temperature, atmospheric pressure, solar radiance, wind speed, and wind direction are collected and used in the FAO Penman-Monteith equation to estimate a daily site-specific evapotranspiration rate for a hypothetical grass reference crop (Allen et al., 1998). Two weather stations equipped with Decagon sensors have been deployed at the site. The Decagon VP-4 sensor (product number 40023) collects temperature, relative

humidity, and barometric pressure data. The ECRN-50 sensor (product number 40655) measures precipitation with a single-spoon tipping rain gauge that tips at 1 mm of precipitation. The Davis Cup anemometer (product number 40030) measures wind speed and direction. The PYR Solar Radiation sensor (product number 40006) measures the solar radiation flux density in watts per square meter. Each weather station has one of each of the sensors, and the sensors for each weather station are connected to a Decagon Devices EM50 datalogger that is set to record data every five minutes. Additionally, two Decagon 5TE sensors are buried in holes filled with Savannah River Site (SRS) soil, which is a sandy loam soil used in the EPSCoR lysimeters and characterized previously in Montgomery et al. (2017), near the test bed and are connected to the Decagon dataloggers to compare ground temperature at two depths with the air temperature and the lysimeter temperatures (Appendix D).

The weather data collected on site has been compared to data from the Anderson Regional Airport (located approximately 9 miles away) for February 3, 4, 11, 15, and 22, 2016; March 9 and 17, 2016; and April 1, 6, and 16, 2016. The average values for wind speed were approximately 70 to 90% lower at the site than at the Anderson Regional Airport. Precipitation, relative humidity, temperature, and barometric pressure varied from 0 to 39% between the site and the Anderson Regional Airport over these 10 days, which justifies the use of site weather stations in place of relying on data from far away from the site.

The two weather stations were originally placed in separate locations at the site, with one located on the corner of the test bed container and one located approximately 50 feet away from the container and the CETL building (Figure 6.15). The data from these two locations were compared to see if the building was affecting the weather conditions experienced at the test bed. The data for the two weather stations at CETL had small variations in precipitation, relative humidity, maximum and minimum temperatures, wind speed, and average solar radiation. The

variation could not directly be attributed to the location of the stations. Therefore, the weather station located away from the building was moved to within a few feet of the other weather station to compare data gathered at the same time and location. Over three days (July 22 to 25, 2016) data were collected at five minute intervals for both weather stations, and the data were compared without rounding. The precipitation data agreed for 99.63% the five minute intervals, which was less than 100% due to one instance of precipitation registering in different but consecutive time intervals for each station and one instance of one station registering precipitation while the other station did not. Relative humidity, temperature, pressure, solar radiance, wind speed, wind gust speed, and wind direction were different for each station for 48 to 82% of the five minute intervals. Relative humidity values between the stations did not vary by more than 5% over the time interval. Temperature varied more than 1% during only 4.76% of the intervals, but the temperature values never varied more than 10% between the two stations. Barometric pressure did not vary more than 1%. Solar radiance varied by more than 5% for 25.4% of the intervals, more than 10% for 13.5% of the intervals, and more than 20% for 6.7% of the intervals. Wind speed, wind gust speed and wind direction varied by more than 20% for 39.4%, 40.9%, and 44.3% of the intervals, respectively.

Figure 6.15: Weather station locations (1) on the corner of the test bed and (2) on the ground away from the building.

Five minute intervals over three additional days (February 8 to 10, 2017) were compared, and similar variations were observed. The precipitation data agreed 99.31% of the five minute

intervals; the variation was due to two instances of precipitation registering in different but consecutive time intervals for each station and two instances of one station registering precipitation while the other station did not. Relative humidity, temperature, pressure, solar radiance, wind speed, wind gust speed, and wind direction were different for each station for 39 to 90% of the five minute intervals. Relative humidity values varied by more than 5% during only 1.85% of the intervals and did not vary more than 10% during any of the intervals. Temperature varied more than 5% during only 7.06% of the intervals and more than 20% for only 1.04% of the intervals. Barometric pressure did not vary more than 1%. Solar radiance varied by more than 5% for 27.3% of the intervals, more than 10% for 18.9% of the intervals, and more than 20% for 11.2% of the intervals. Wind speed, wind gust speed and wind direction varied by more than 20% for 30.6%, 35.3%, and 31.1% of the intervals, respectively. Due to the variations in the data when the weather stations are placed side-by-side, each calculated value for site-specific evapotranspiration from each weather station should not be attributed to either side of the test bed even when the weather stations are located on opposite sides of the test bed. A better approach would be to average the evapotranspiration values calculated by each weather station.

6.4 Site-specific Evapotranspiration Calculations

Weather data collected at the site for temperature, relative humidity, wind speed, and solar radiation are used in the FAO Penman-Monteith equation to calculate daily evapotranspiration rates (Eq. 6.1) (Allen et al., 1998).

$$ET_O = \frac{0.408\Delta(R_n - \mathrm{G}) + \gamma\frac{900}{T+273}u_2(e_s - e_a)}{\Delta + \gamma(1 + 0.34u_2)} \qquad \text{(Eq. 6.1)}$$

ET_O is the reference evapotranspiration [mm/day], R_n is the net radiation at the crop surface [MJ/m^2/day], G is the soil heat flux density [MJ/m^2/day], T is the mean daily air temperature at 2 m height [degrees Celsius], u_2 is the wind speed at 2 m height [m/s], e_s is the saturation vapor

pressure [kPa], e_a is the actual vapor pressure [kPa], Δ is the slope of the vapor pressure and temperature curve [kPa/degree Celsius], and γ is the psychrometric constant [kPa/degree Celsius]. The daily ET_O values for 2016 and 2017 at the test bed are shown in Figure 6.16. The equations needed to calculate the ET_O as well as a Python script, which performs the calculations can be found in Appendix E.

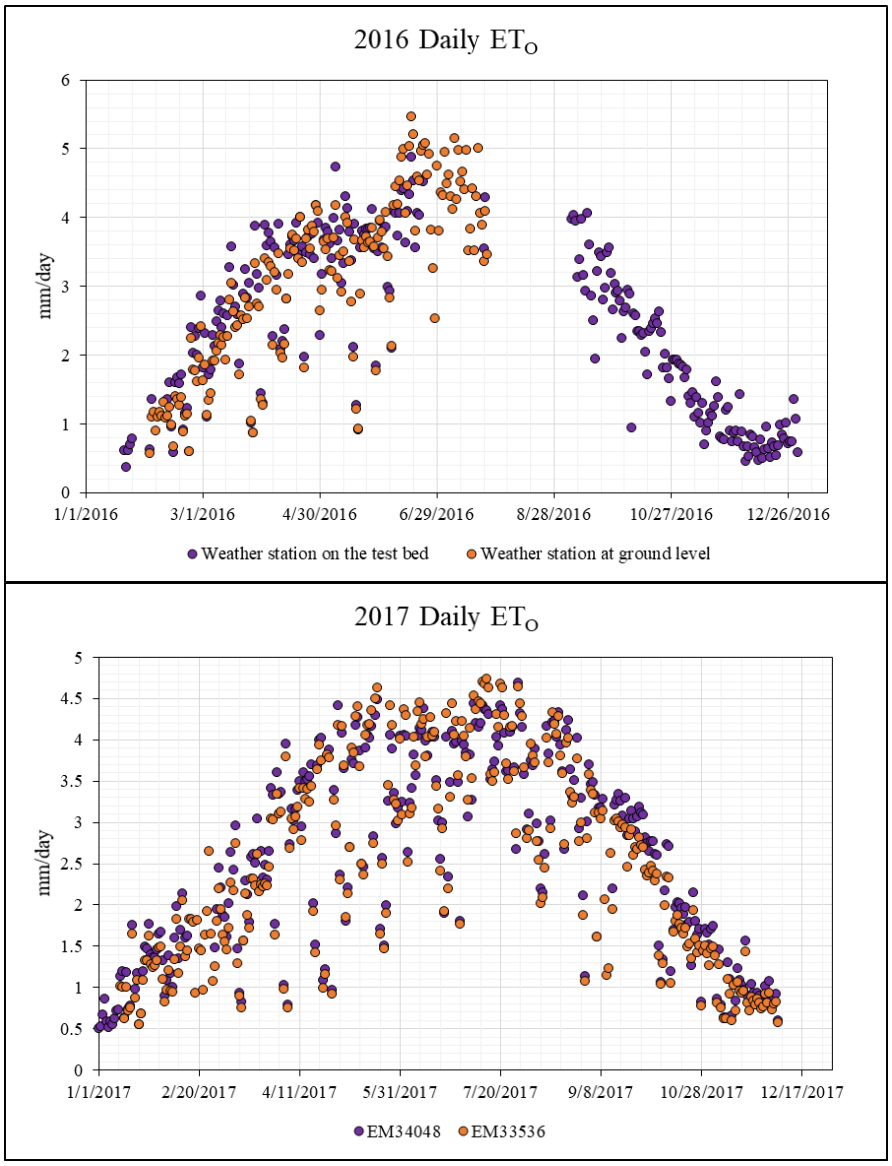

Figure 6.16: Daily ET_O for 2016 and 2017 from weather station data measured at the test bed site. During 2016, one weather station was located on the test bed and the other was located at ground level. During 2017, both weather stations were located on the test bed.

6.5 References

Allen, R. G.; Pereira, L. S.; Raes, D.; Smith, M. *Crop Evapotranspiration - Guidelines for Computing Crop Water Requirements - FAO Irrigation and Drainage Paper 56*; **1998**.

Campbell Scientific. AM16/32B Relay Multiplexer Instruction Manual https://s.campbellsci.com/documents/us/manuals/am16-32b.pdf (accessed Feb 23, 2017a).

Campbell Scientific. CR6 Measurement and Control System Operator's Manual https://s.campbellsci.com/documents/us/manuals/cr6.pdf (accessed Feb 23, 2017b).

Decagon Devices. 5TE Sensor Integrator Guide http://manuals.decagon.com/Integration Guides/5TE Integrators Guide.pdf (accessed Jan 2, 2017).

Decagon Devices. 5TE Water Content, EC and Temperature Sensor http://manuals.decagon.com/Manuals/13509_5TE_Web.pdf (accessed Feb 23, 2017a).

Decagon Devices. MPS-2 & MPS-6 Dielectric Water Potential Sensors http://manuals.decagon.com/Manuals/13755_MPS-2and6_Web.pdf (accessed Feb 23, 2017b).

Montgomery, D.; Barber, K.; Edayilam, N.; Oqujiuba, K.; Young, S.; Biotidara, T.; Gathers, A.; Danjaji, M.; Tharayil, N.; Martinez, N. The Influence of Citrate and Oxalate on 99TcVII, Cs, NpV and UVI Sorption to a Savannah River Site Soil. *J. Environ. Radioact.* **2017**, *172*, 130–142.

Omega. Economical, OEM-style Single Point Load Cells http://www.omega.com/pressure/pdf/LCAE.pdf (accessed Feb 23, 2017).

Chapter 7: Degradation and Metal Leaching of Lithium-ion and Nickel-Metal Hydride Batteries and PV Modules in Simulated Landfill Columns

Abstract

Previous results from the batch tests described in Chapters 4 and 5 demonstrate the need to study metal leaching from photovoltaic (PV) module and battery e-waste in a more realistic disposal scenario to determine if the batch test results can be considered representative of e-waste disposal with municipal solid waste (MSW). Three columns, which have been deployed in the lysimeter test bed described in Chapter 6, were built to simulate the conditions within a bioreactor solid waste landfill and were subjected to outdoor temperature fluctuations. One column containing c-Si module pieces, one column containing a dismantled nickel-metal hydride (NiMH) power tool battery, and one column containing a dismantled lithium-ion (Li-ion) laptop battery were each mixed with a representative MSW and simulated landfill leachate. The experiment was designed to evaluate plausible concentrations of metals that could leach from e-waste in a landfill operated as a bioreactor or a landfill which recirculates leachate for liquid management over an initial period. Measurements taken by Decagon 5TE sensors showed that the portion of the columns mixed with e-waste maintained a moisture content of approximately 44 percent and contained higher amounts of dissolved salts than the other locations within each column. The redox potential measured by electrodes inserted in the portion of the columns mixed with e-waste showed conditions were reducing (ranging from -293 to -56 mV) over the data collection period, and the pH of the leachate ranged from 6.5 to 8.0. For the column with the c-Si module pieces, Pb was not detected in the leachate even though Pb was observed in the TCLP testing and batch tests

without MSW described in Chapter 5. For the column with the NiMH power tool battery, Co, Cu, and Ni were measured in the leachate, but As, Hg, Pb, and Zn were not detected in the column leachate samples even though they were observed in the previous batch tests. For the column with the Li-ion laptop battery, Co, Cu, and Ni were measured in the leachate samples and were also found in the previous batch tests. The difference observed between the column and batch tests for metal concentrations is likely due to sorption to MSW components and biofilm surfaces within the columns. Although As, Hg, and Pb were not found in the leachate samples, the other soluble and potentially mobile metals, including Co, Cu, and Ni, found in the leachate could be of concern in an improperly managed landfill and could cause contamination of soils and aquifers. Future work will include dissecting the waste columns to examine the physical and chemical degradation of the e-waste after additional aging has occurred.

7.1 Introduction

Most studies of the end-of-life of PV modules and batteries focus on recycling and not municipal waste disposal, which is likely to occur in locations without sufficient recycling laws or take-back programs. Additionally, to determine if an unregulated waste can be landfilled with MSW in the US, the Environmental Protection Agency (EPA) Toxicity Characteristic Leaching Procedure (TCLP) is used typically, with some states having more stringent regulations (e.g., California). However, the use of regulatory leaching methods to assess the toxicity of different e-wastes may be less than accurate (Poon and Lio, 1997; Kosson et al., 2002; Ghosh et al., 2004; Karamalidis and Voudrias, 2007), and the TCLP uses a single, worst-case test condition which has been shown to be both over-regulating and inadequately protective of the environment (Kosson et al., 2002). Because batch leaching tests have been shown to be unreliable at predicting or

determining what actually occurs in landfills, researchers have turned to waste-filled columns or lysimeters to study e-waste degradation.

Previous studies have constructed waste-filled columns, or lysimeters, to simulate landfill conditions to understand the degradation of household e-waste co-disposed with MSW. Waste lysimeters have been used to study metal leaching from personal computer components and cathode ray tubes (Li et al., 2009; Visvanthan et al., 2010) and also from spent zinc-carbon, alkaline, nickel-cadmium, and nickel-metal hydride batteries (Karnchanawong and Limpiteeprakan, 2009; Komilis et al., 2011). Over a two year period, Pb was not detected in the leachate circulating through columns containing personal computers and cathode ray tubes; however, increased levels of Pb were observed within the material beneath the e-waste, so Pb might eventually migrate into the leachate (Li et al., 2009). Over 280 days in another lysimeter e-waste study containing computer parts, Fe and Zn concentrations from the lysimeters were comparable to TCLP leaching concentrations; however, the Pb concentration from the lysimeters was much lower than the TCLP concentration (Visvanthan et al., 2010). In another study, broken and intact cathode ray tubes, central processing units, and fluorescent tubes were added to outdoor columns filled with MSW and then exposed to rain, and although sampling showed a slow, continuous leaching of Al, Ba, Be, Cd, Co, Cr, Cu, Ni, Pb, Sb and V, the concentrations of the regulated metals were far below TCLP limits (Kiddee et al., 2013). In a similar study using synthetic and excavated MSW, Pb concentrations within columns containing computer parts, smoke detectors, and cell phones did not significantly differ from control columns over a monitoring period of 440 days (Spalvins et al., 2008).

Although these studies mostly show that the proper management of landfills can prevent inorganic pollutants (most often Pb) from e-waste from contaminating soils and aquifers, few consider how the composition of PV modules and Li-ion and NiMH batteries differ from the

average e-waste of computer parts and cathode ray tubes often studied. Additionally, improper management of landfills can cause environmental contamination of soils and aquifers from e-waste disposal (Komilis et al., 1999). Furthermore, in a previous study, the difference in metal leaching behavior observed in columns and conducting the TCLP (Visvanthan et al., 2010) demonstrates the need for both column and batch tests simulating e-waste disposal.

For this study, columns have been constructed to simulate conditions within a bioreactor landfill, in which leachate was initially recirculated. Recirculating leachate can increase metal mobility in the early phase of a landfill; however, the recirculation can facilitate reaching the methanogenic phase sooner which reduces metal mobility (Qu et al., 2008). The optimal moisture content for bioreactor landfills is near field capacity, which is typically between 35 to 65 percent and is a much higher moisture content than a conventional landfill (USEPA, 2017). Bioreactor landfills can optimize waste stabilization and have advantages over conventional landfills; however, the operation of bioreactor landfills is dependent on increased moisture content, which can lead to issues not typically encountered for conventional landfills such as increased pressure on liners, side seeps, clogging in collection pipes, managing additional leachate production in wet weather, and reduced slope stability, which must be accounted for in the design and maintenance (Reinhart et al., 2002). Studying the degradation and metal leaching from e-waste in landfills with higher moisture content is important due to the increased potential for groundwater and soil contamination.

7.2 Materials, Methods, and Timeline

7.2.1 MSW materials, simulated leachate, and e-wastes

For this study, three different e-wastes were chosen: a c-Si PV module, a NiMH power tool battery, and a Li-ion laptop battery, which were previously used in TCLP and other batch

leaching tests in Chapter 5 (Table 7.1). To examine a worst-case scenario, the e-wastes were broken into pieces to maximize the possibility of interaction with the leachate solution and waste matrix. For the c-Si PV module, pieces which passed through a 9.5 mm sieve and with all the layers intact were used. For the two batteries, the plastic housing was disassembled and cut into approximately two centimeter square pieces. For the individual cells within the batteries, cells were discharged, the electrodes were removed from the housing and unrolled, and both the housing and the electrodes were cut into pieces of less than approximately one centimeter in length (Figure 7.1). The e-wastes were mixed with MSW containing paper products, plastics, metal, glass, and food (Table 7.2 and Figure 7.2) at the same ratio as the typical US MSW (Khan et al., 2013; USEPA, 2015a). To simulate cover soil added to the landfill, the MSW components were mixed with a previously characterized sandy loam soil (characteristics reported by (Montgomery et al., 2017)), with 75 percent by mass MSW and 25 percent by mass soil. Different from previous column e-waste studies which used a rainfall simulant in columns (Li et al., 2009; Kiddee et al., 2013), a representative leachate (Ghosh et al., 2004) was used to simulate the leachate produced within an acid-phase landfill, essentially accelerating the process of organic acid formation which occurs in young landfills and

Table 7.1: E-waste product descriptions for the columns deployed in the lysimeter test bed.

Column	Product Description	E-waste Type
1	Suniva OPT245-60-4-100 c-Si PV module	c-Si module
2	Lenmar PTD9094 power tool battery	NiMH battery
3	Lenmar LBZ378D laptop battery	Li-ion battery

Figure 7.1: Disassembled and shredded NiMH outer casings (top left), Li-ion outer casings (bottom left), NiMH electrodes (top right), and Li-ion electrodes (bottom right).

representing the leachate percolating through a landfill or recirculated in a bioreactor design (Table 7.2). Additionally, a batch laboratory control of the MSW and soil mixture in simulated leachate was monitored to determine metal leaching from the waste materials without e-waste.

Table 7.2: Municipal solid waste (MSW) and simulated leachate compositions.

MSW Component (product)	Percentage by Mass
Paper (foam board)	45.5
Plastics (plastic beads)	16.4
Metal (aluminium beads)	10.9
Glass (glass beads)	9.6
Food (rabbit feed)	17.6

Leachate Component	Concentration [mg/L]
Calcium carbonate	1100
Sodium carbonate	11500
Ammonium chloride	650
Acetic acid*	6876
Propionic acid	192
Butyric acid	422
Pentanoic acid	163
Hexanoic acid	232
Sodium citrate	46400
Hydroxylamine hydrochloride	31.7
*Acetic acid concentration differs from (Ghosh et al., 2004)	

7.2.2 Packing the columns

The columns were built with PVC pipe and fittings, as described in Chapter 6. Each column holds approximately 11.4 liters of the waste mixture (15.4 cm inner diameter, 61 cm height). When packing the columns, 850 grams of pea gravel (approximately 2.5 cm deep) were added to the bottom of each column. Next, four layers of the MSW/soil were added, with the top of these layers approximately 45 cm from the top of the column. Then, two layers with the e-wastes split equally by mass per layer and mixed with the MSW/soil were added to the columns, with a depth between 10 to 20 cm. The batteries and PV pieces were kept to less than 10% of the total mass of the waste mixture added to the columns (Figure 7.3 and Table 7.3), which parallels the ratio reported in the US MSW stream (USEPA, 2015b). Next, three more layers of the MSW/soil mixture were added. A layer of pea

Figure 7.2: MSW components: from left to right: paper, plastic, metal, glass, and food.

gravel of approximately 2500 grams (approximately 7.5 cm deep) was added at the top of the columns. The columns were capped to prevent infiltrating rainwater when placed outdoors and to limit evaporation of leachate from the columns. Holes were drilled into the caps to place vertical soil water samplers and then sealed with silicone sealant as described below.

7.2.3 Instrumentation and data collection

After each column was packed, three Decagon 5TE sensors and three Mettler Toledo ORP electrodes were inserted in opposite sides of each column and sealed with marine epoxy (Figure 7.4). Decagon 5TE sensors measure apparent dielectric permittivity (unitless range from 1 to 80) using an oscillator running at 70 MHz, which can be converted to volumetric water content (calibration described in Appendix B), electrical conductivity (measured in deciSiemens per meter) using a two-sensor electrical array, and temperature in Celsius using a surface-mounted thermistor (Decagon Devices, 2016). In addition to the 5TE sensors and redox electrodes, three soil water samplers were installed to periodically sample the leachate at three different depths in the waste columns. At each sampling time, the first 2 mL of leachate removed with each sampler were discarded, and approximately 3 mL samples were removed. Redox potential and pH measurements were made of the samples. Samples were filtered with a 0.2 micrometer pore diameter nylon filter, diluted with DDI water, acidified to a concentration of two percent nitric acid, and analyzed by inductively coupled plasma optical emission spectrometry (ICP-OES,

Figure 7.3: E-wastes (left to right: c-Si module, NiMH battery, Li-ion battery) mixed with MSW components and soil before packing in columns.

Table 7.3: MSW, soil, and e-waste added to the columns.

Column	MSW [g]	Soil [g]	E-waste [g]	E-waste [%]
1 c-Si module	6187.50	2062.50	750.00	8.3%
2 NiMH battery	5409.34	1803.12	787.58	9.8%
3 Li-ion battery	5630.56	1876.86	292.60	3.8%

Perkin Elmer Optima 3100RL) to determine metal ion concentrations.

7.2.4 Timeline

After the columns were packed and the sensors inserted and epoxied in place, simulated leachate was added to each column and low-flow pumps were used to recirculate the leachate in each column, as described in Table 7.4. Due to the amount of organic matter in the columns, the water holding capacity of the wastes was high and the infiltration rate through the columns was considerably less than the pumping rate; therefore, leachate could not be continuously recirculated in the columns. Leachate initially leaked from the columns, and the leaks were stopped by adding additional epoxy around the sensors, electrodes, and PVC joints. On day 11, one additional liter of simulated leachate was added to each column to compensate for leaking and to ensure saturation had been reached. On day 35, additional simulated leachate was added to

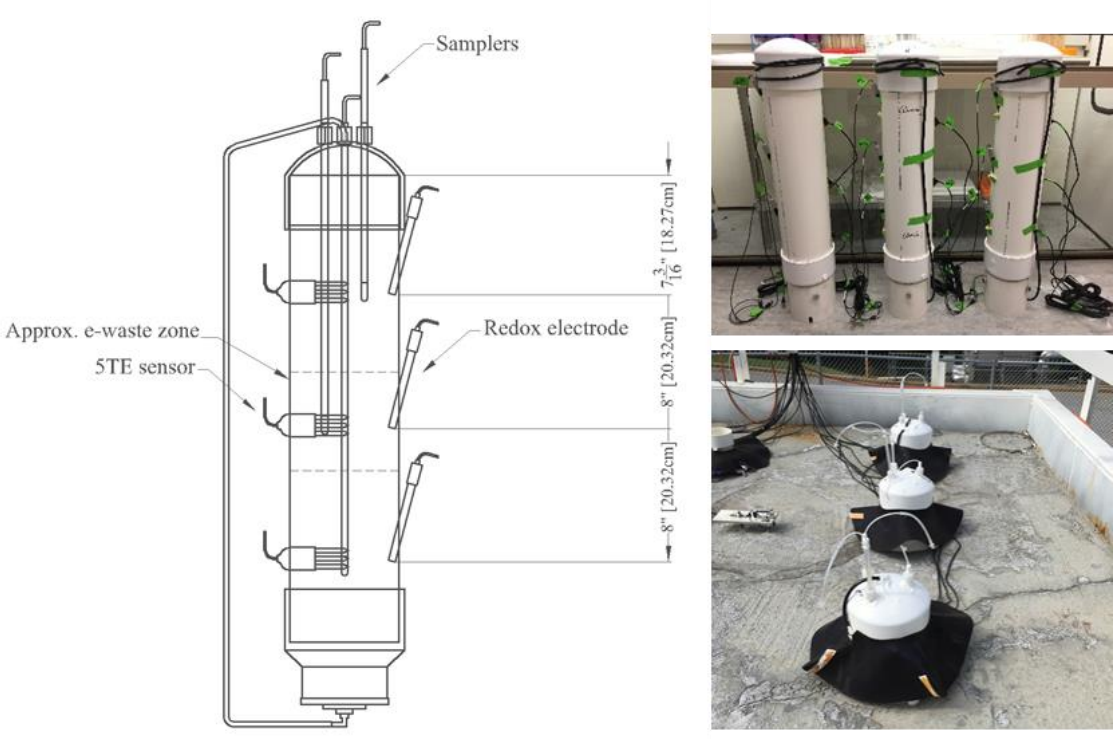

Figure 7.4: Column design with 5TE sensors, redox electrodes, and samplers (left) and photos of columns before and after deployment in the test bed (right).

Table 7.4: Timeline for column activities.

Day	Activity
0	4 liters of simulated leachate added to each column Low-flow pumps set up to recirculate leachate at 1 L/day Additional epoxy added around sensors, electrodes, PVC joints
11	1 liter of simulated leachate added to each column
35	1 liter added to Column 1 (c-Si PV) 0.5 liters added to Column 2 (NiMH battery) 1.5 liters added to Column 3 (Li-ion battery)
0 to 41	Leachate intermittenly recirculated
41	Columns placed in outdoor test bed described in Chapter 6 5TE data collection started
69	Soil water samplers installed
70	1 liter added to Column 3 (Li-ion battery); 5TE sensor indicated e-waste zone no longer saturated
72	First set of samples taken with soil water samplers
93	Top and middle soil water sampler heights adjusted

each column so that each had standing leachate at the top. From day 0 to day 41, the leachate was intermittently recirculated in all three columns indoors, and on day 41, the columns were taken outdoors. On day 72, the first set of samples were taken with the soil water samplers, and additional samples were taken on days 79, 86, 93, 99, 107, 114, 123, 135, 149, 171, and 190. On day 93, the upper and e-waste zone soil water samplers were adjusted so that the sampling height matched the locations of the 5TE sensors and redox electrodes; they were previously collecting samples from slightly below that height.

7.3 Results and Discussion

Starting on day 41 when the columns were taken outdoors, 5TE sensor data for water content, electrical conductivity, and temperature were collected every two hours (Figure 7.5). The water content measured by the 5TE sensors located in the e-waste zone of each column stayed saturated at a water content of approximately 44 percent for most of the data collection period for all three columns. The upper 5TE sensors for Columns 1 and 2 showed that the water content was less than saturated, which was also demonstrated by the inability to collect leachate samples from the

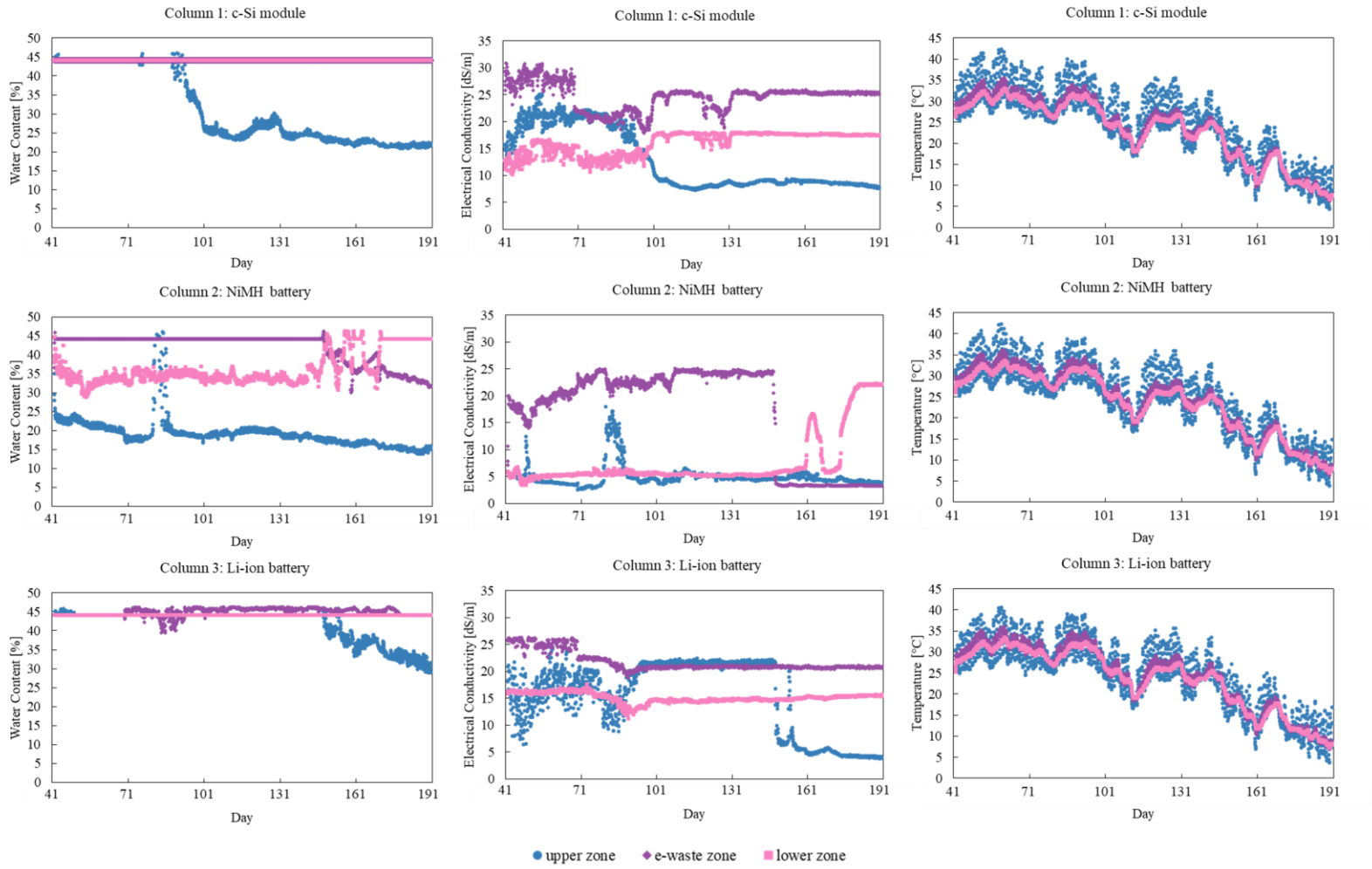

Figure 7.5: Water content, electrical conductivity, and temperature graphs measured by the 5TE sensors for each column.

upper locations after day 86. Having the section of the columns with the e-waste saturated for the duration of the study allowed for maximum contact time, which would likely lead to greater concentrations of the metals in the e-wastes solubilizing than in an intermittently saturated case. The electrical conductivity measurements for dissolved salts were higher for the e-waste zone 5TE sensor than the upper and lower 5TE sensors throughout the data collection period for Column 2 and were mostly higher for the e-waste zone 5TE sensor for Columns 1 and 3. Components leaching from the e-wastes could explain the higher measurements, but it is unclear if the consistency in the measurement values can be attributed to slow diffusion through the waste matrix or a constant rate of dissolution from the e-wastes. The upper 5TE sensors showed the most variation in temperature, with approximately 10 degree Celsius daily variations. The e-waste zone 5TE sensors measured temperatures that were slightly higher than the lower 5TE sensors throughout the data collection time, but both had much lower daily variations than the upper 5TE sensors. The decrease in temperature from approximately day 80 to 110 corresponds to a decrease in metal concentrations in the leachate samples. However, the temperature continued to decrease from day 140 onward, but some metal concentrations increased over this period, demonstrating that in column experiments many factors, including pH, redox potential, and availability of complexing agents, in addition to temperature affect leaching behavior (Bozkurt et al., 2000).

Redox potential and pH measurements of the leachate samples and redox potential measurements from the electrodes inserted in the columns were made at the sampling times (Figure 7.6). Differences were observed in the redox potential of the samples removed using the samplers, which were exposed to oxygen in the air in the process of removing samples from the columns, and the redox potential measured by electrodes inserted into the columns. The redox potential measured by the electrodes inserted in the e-waste zone of the columns showed conditions were anaerobic for all three columns over the entire data collection period. The pH of

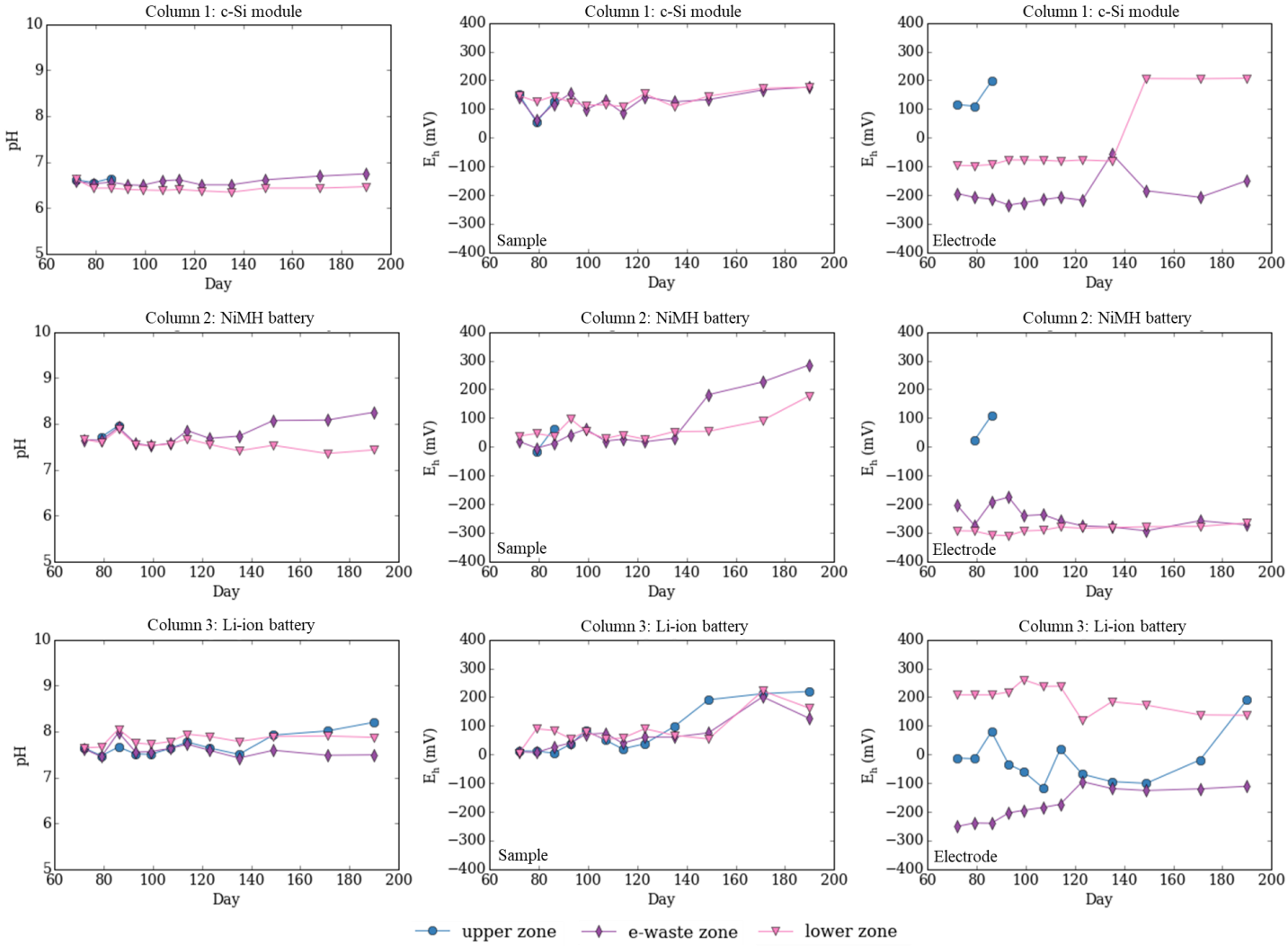

Figure 7.6: Redox and pH measurements for each column. “Sample” labels refer to the redox potential measurements made of the leachate samples removed from the columns, and “Electrode” labels refer to the measurements from the electrodes inserted in the columns.

the leachate samples from Column 1 with the c-Si module pieces was approximately 6.5 for the data collection period, which was lower than the other two columns with batteries where the pH ranged from 7 to 8 over the data collection period.

Metal concentrations were measured in the leachate samples removed from the columns with the soil water samplers. For Column 1 with the c-Si module pieces, Al, Fe, and Mn were measured in the leachate (Figure 7.7). These metals were also detected in the control MSW and soil mixture without e-waste and are not regulated by the TCLP. For Column 2 with the NiMH power tool battery, Al, Co, Cu, Fe, Mn, and Ni were measured in the leachate samples (Figure 7.8). While none of these metals are regulated by the TCLP, Co, Cu, and Ni in wastes are regulated by California. For Column 3 with the Li-ion laptop battery, Al, Co, Cu, Fe, Mn, and Ni were measured in the leachate samples (Figure 7.9).

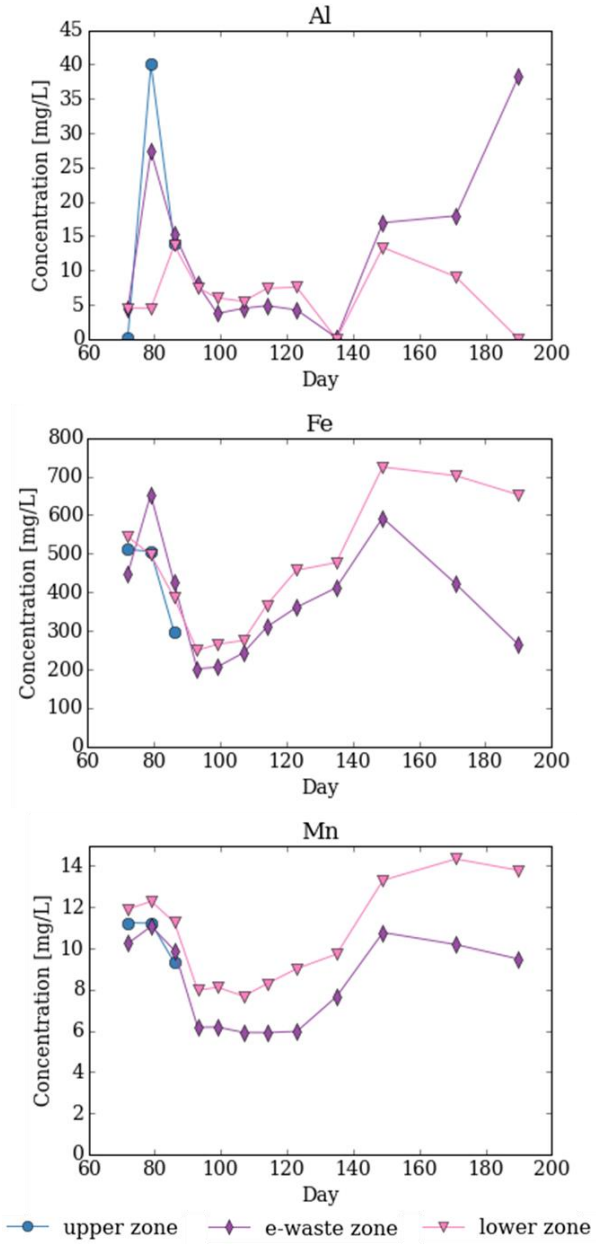

Figure 7.7: Al, Fe, and Mn concentrations in the leachate samples removed from Column 1 with the c-Si module pieces. Note: maximum y-axis values differ for the three plots.

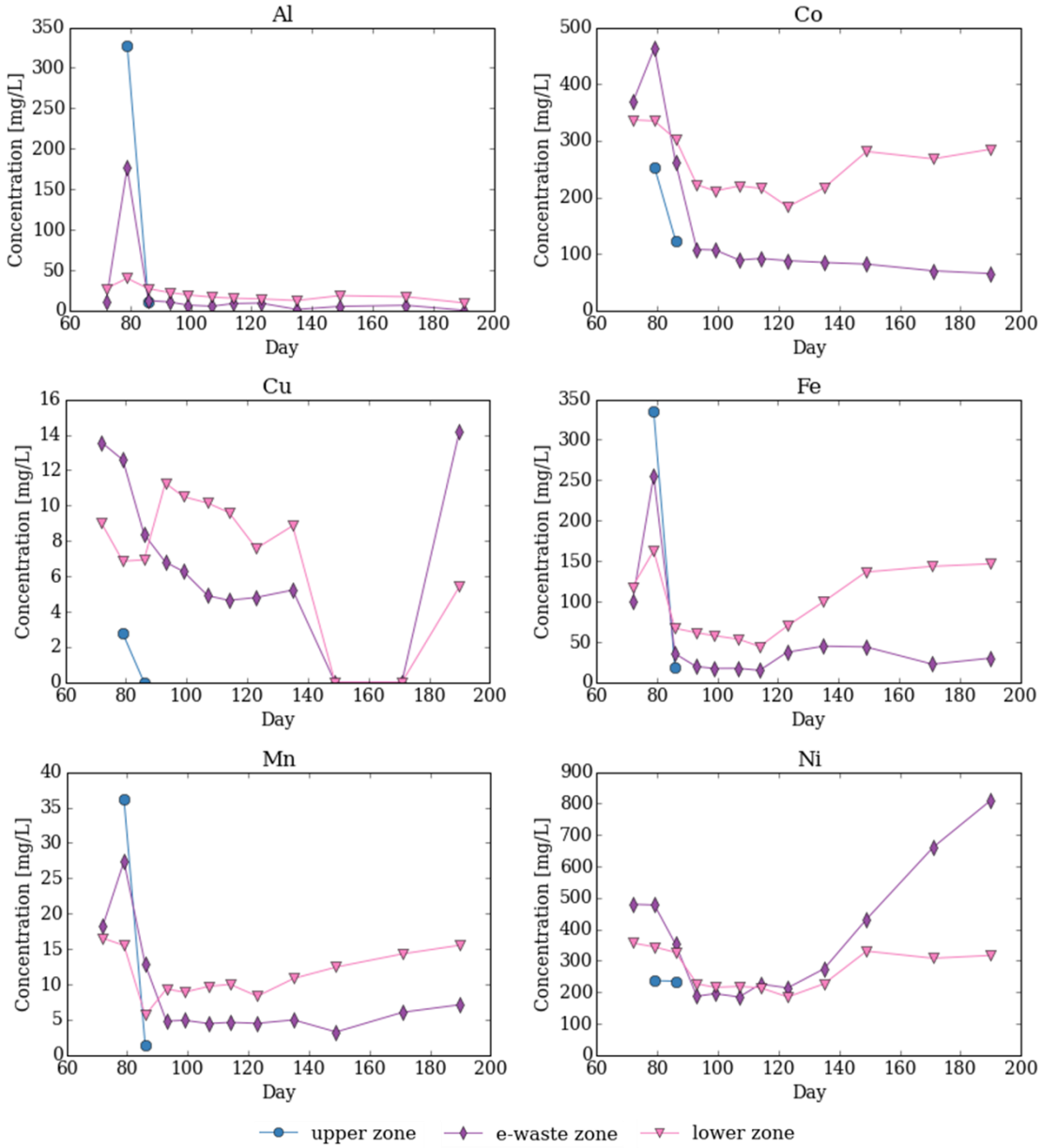

Figure 7.8: Al, Co, Cu, Fe, Mn, and Ni concentrations in the leachate samples removed from Column 2 with the NiMH power tool battery. Note: maximum y-axis values differ for the six plots.

For the columns, changes in metal concentrations were observed over the sampling time, likely due to changes in redox potential. In Column 3 with the Li-ion laptop battery, the E_h for the e-waste zone started low, near -250 mV, and gradually increased to approximately -100 mV by day 120. At first, iron was present in its more soluble form (Fe(II)), but as oxygen migrated into

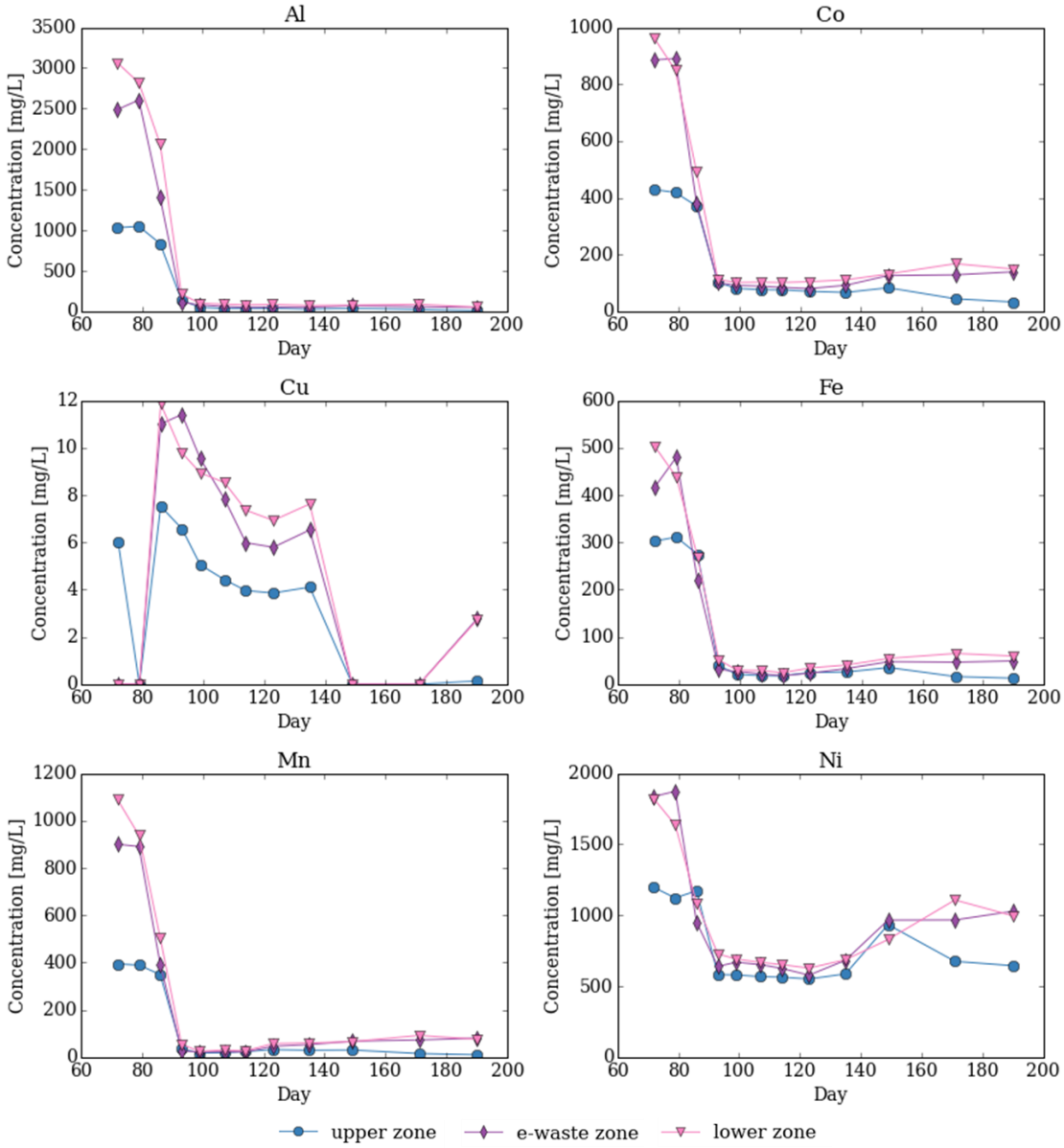

Figure 7.9: Al, Co, Cu, Fe, Mn, and Ni concentrations in the leachate samples removed from Column 3 with the Li-ion laptop battery. Note: maximum y-axis values differ for the six plots.

the e-waste zone from the upper and lower sections of the column (the E_h values of the upper and lower zones were more aerobic), iron oxides in the Fe(III) oxidation state likely formed. As Fe precipitated, co-precipitation or sorption of the other metals to the newly formed Fe(III) mineral phase reduced the concentrations of the metals in the leachate. The observed drop in Al, Co, Cu, Fe, Mn, and Ni concentrations near day 90 is shown in Figure 7.9. For Column 2 with the NiMH

power tool battery, the E_h for the e-waste and lower zones remained low at approximately -300 to -200 mV throughout the sample collection period; therefore, less oxygen migrated into the e-waste zone as in Column 3, and metal concentrations did not exhibit a pronounced drop as observed in Column 3 (Figure 7.8). For Column 1 with the c-Si module pieces, the E_h for the lower zone started near -100 mV and increased quickly to approximately 200 mV near day 150, after which oxygen could migrate into the e-waste zone from the lower zone; however, only a slight increase in E_h was observed for the e-waste zone, which started near -200 mV and remained mostly constant with time. Consequently, the Al, Fe, and Mn concentrations observed in the leachate fluctuated around their initial concentrations, as shown in Figure 7.7.

Table 7.5 compares the regulated metals observed in the column leachate samples to previous testing of these products described in Chapter 5. Of the metals regulated by the US and CA, Ba and Zn were observed in the MSW/soil control. For the c-Si module, Pb and Zn were observed in the TCLP testing and batch tests without MSW; however, neither was observed in the column leachate. For the NiMH power tool battery, As, Ba, Pb, and Zn were observed in the TCLP testing but not observed in the column leachate, and Cu was observed in the column leachate but not in the TCLP testing. For the Li-ion laptop battery, Ba and Pb were observed in the TCLP testing but not in the column leachate. The metal leaching observed in this study is similar to previous e-waste column studies simulating the co-disposal of e-waste with MSW. In the two columns where Pb was expected to leach from the e-waste based on TCLP testing, Pb was not detected in the leachate. This observation can likely be explained by sorption to the soil (Ostergren et al., 2000; Hamidpour et al., 2010) and MSW components (Mårtensson et al., 1999), which has been observed in other column e-waste studies (Li et al., 2009; Visvanthan et al., 2010). Observing Ni and Cu in the leachate but not Pb is supported by a previous study of metal solubility in MSW, which found that the metal adsorption for Ni in the 6.5 to 8 pH range was

Table 7.5: Observations of regulated metals in the MSW/soil control and each e-waste column, and from Chapter 5, previous batch tests with MSW, batch tests without MSW, and TCLP regulatory testing. Observations are denoted by an "X" and shading.

Column 1: c-Si module pieces	Observed in MSW/Soil Control	Observed in Column	Observed in batch tests with MSW (Ch 5)	Observed in batch tests without MSW (Ch 5)	Observed in TCLP testing (Ch 5)
Pb				X	X
Zn	X		X	X	X
Column 2: NiMH power tool battery					
As				X	X
Ba	X		X		X
Co		X	X	X	X
Cu		X	X	X	
Hg				X	
Ni		X	X	X	X
Pb				X	X
Zn	X		X	X	X
Column 3: Li-ion laptop battery					
Ba	X		X	X	X
Co		X	X	X	X
Cu		X	X	X	X
Ni		X	X	X	X
Pb					X

approximately 50 percent, Cu was approximately 75 percent, but Pb was close to 100 percent (Lo et al., 2009).

The differences observed in the metal leaching data for the batch tests and the columns cast doubt upon the validity of either method to assess the long-term risk of contamination of soil and groundwater. With short durations compared to the lifetime of landfills, both batch and columns tests are not designed to extrapolate leaching data to account for future conditions. However, the column study was designed to assess plausible leachate metal concentrations during the initial stages of the landfill when concentrations and metal mobility are assumed to be highest with the greatest potential for soil and groundwater contamination (Qu et al., 2008). Although the column experiment was designed to evaluate plausible concentrations of metals that could leach from e-waste in a landfill operated as a bioreactor, the results are relevant to "open dumping" situations in a wet or temperate climate where moisture entering the discarded waste is not controlled, and Co, Cu, and Ni leaching from the batteries could be of concern.

7.4 Future Work

To allow for additional aging of the wastes, the columns remain in the test bed as of May 2018. The additional time will simulate actual landfill conditions more closely than the short-term sampling period of this study. Future work will involve dissecting the waste columns to examine the physical degradation of the e-wastes. Prior to removing and dissecting the waste columns, additional leachate samples should be taken, with one set processed as described previously and an additional set acidified immediately upon collection without taking redox or pH measurements to determine if metal ions were precipitating in the short time prior to acidifying the samples. Samples of the e-wastes will be examined using optical microscopy and electron microscopy to determine physical and chemical changes compared to samples of the e-wastes not aged in the columns. Additionally, samples of the MSW and soil mixture will be digested using a sequential extraction method to determine metal partitioning to the different components of the waste matrix, and if Pb, not detected in the leachates, dissolved from the e-waste to be sorbed by other waste components or remained in its original form in the e-waste. Overall, dissecting the columns will provide additional insight into the rate and extent of metal leaching from e-wastes and the potential mobility of metals in landfill conditions.

7.5 References

Bozkurt, S.; Moreno, L.; Neretnieks, I. Long-Term Processes in Waste Deposits. *Sci. Total Environ.* **2000**, *250* (1), 101–121.

Decagon Devices. 5TE Water Content, EC and Temperature Sensor http://manuals.decagon.com/Manuals/13509_5TE_Web.pdf (accessed Feb 23, 2017).

Ghosh, A.; Mukiibi, M.; Ela, W. TCLP Underestimates Leaching of Arsenic from Solid Residuals under Landfill Conditions. *Environ. Sci. Technol.* **2004**, *38* (17), 4677–4682.

Hamidpour, M.; Kalbasi, M.; Afyuni, M.; Shariatmadari, H.; Holm, P. E.; Hansen, H. C. B. Sorption Hysteresis of Cd (II) and Pb (II) on Natural Zeolite and Bentonite. *J. Hazard. Mater.* **2010**, *181* (1), 686–691.

Karamalidis, A. K.; Voudrias, E. A. Release of Zn, Ni, Cu, SO4(2-) and CrO4(2-) as a Function of pH from Cement-Based Stabilized/solidified Refinery Oily Sludge and Ash from Incineration of Oily Sludge. *J. Hazard. Mater.* **2007**, *141* (3), 591–606.

Karnchanawong, S.; Limpiteeprakan, P. Evaluation of Heavy Metal Leaching from Spent Household Batteries Disposed in Municipal Solid Waste. *Waste Manag.* **2009**, *29* (2), 550–558.

Khan, I. A.; Berge, N. D.; Sabo-Attwood, T.; Ferguson, L.; Saleh, N. B. Single-Walled Carbon Nanotube Transport in Representative Municipal Solid Waste Landfill Conditions. *Environ. Sci. Technol.* **2013**, *47* (15), 8425–8433.

Kiddee, P.; Naidu, R.; Wong, M. H. Metals and Polybrominated Diphenyl Ethers Leaching from Electronic Waste in Simulated Landfills. *J. Hazard. Mater.* **2013**, *252–253*, 243–249.

Komilis, D.; Bandi, D.; Kakaronis, G.; Zouppouris, G. The Influence of Spent Household Batteries to the Organic Fraction of Municipal Solid Wastes during Composting. *Sci. Total Environ.* **2011**, *409* (13), 2555–2566.

Komilis, D. P.; Ham, R. K.; Stegmann, R. The Effect of Landfill Design and Operation Practices on Waste Degradation Behavior: A Review. *Waste Manag. Res.* **1999**, *17* (1), 20–26.

Kosson, D. S.; van der Sloot, H. A.; Sanchez, F.; Garrabrants, A. C. An Integrated Framework for Evaluating Leaching in Waste Management and Utilization of Secondary Materials. *Environ. Eng. Sci.* **2002**, *19* (3), 159–204.

Li, Y.; Richardson, J. B.; Bricka, R. M.; Niu, X.; Yang, H.; Li, L.; Jimenez, A. Leaching of Heavy Metals from E-Waste in Simulated Landfill Columns. *Waste Manag.* **2009**, *29* (7), 2147–2150.

Lo, H. M.; Lin, K. C.; Liu, M. H.; Pai, T. Z.; Lin, C. Y.; Liu, W. F.; Fang, G. C.; Lu, C.; Chiang, C. F.; Wang, S. C. Solubility of Heavy Metals Added to MSW. *J. Hazard. Mater.* **2009**, *161* (1), 294–299.

Mårtensson, A. M.; Aulin, C.; Wahlberg, O.; Ågren, S. Effect of Humic Substances on the Mobility of Toxic Metals in a Mature Landfill. *Waste Manag. Res.* **1999**, *17* (4), 296–304.

Montgomery, D.; Barber, K.; Edayilam, N.; Oqujiuba, K.; Young, S.; Biotidara, T.; Gathers, A.; Danjaji, M.; Tharayil, N.; Martinez, N. The Influence of Citrate and Oxalate on 99TcVII, Cs, NpV and UVI Sorption to a Savannah River Site Soil. *J. Environ. Radioact.* **2017**, *172*, 130–142.

Ostergren, J. D.; Trainor, T. P.; Bargar, J. R.; Brown, G. E.; Parks, G. A. Inorganic Ligand Effects on Pb (II) Sorption to Goethite (α-FeOOH): I. Carbonate. *J. Colloid Interface Sci.* **2000**, *225* (2), 466–482.

Poon, C. S.; Lio, K. W. The Limitation of the Toxicity Characteristic Leaching Procedure for Evaluating Cement-Based Stabilised/solidified Waste Forms. *Waste Manag.* **1997**, *17* (1), 15–23.

Qu, X.; He, P.-J.; Shao, L.-M.; Lee, D.-J. Heavy Metals Mobility in Full-Scale Bioreactor Landfill: Initial Stage. *Chemosphere* **2008**, *70* (5), 769–777.

Reinhart, D. R.; McCreanor, P. T.; Townsend, T. The Bioreactor Landfill: Its Status and Future. *Waste Manag. Res.* **2002**, *20* (2), 172–186.

Spalvins, E.; Dubey, B.; Townsend, T. Impact of Electronic Waste Disposal on Lead Concentrations in Landfill Leachate. *Environ. Sci. Technol.* **2008**, *42* (19), 7452–7458.

USEPA. Advancing Sustainable Materials Management: Facts and Figures 2013 http://www.epa.gov/wastes/nonhaz/municipal/msw99.htm (accessed Sep 23, 2015a).

USEPA. Statistics on the Management of Used and End-of-Life Electronics http://www.epa.gov/wastes/conserve/materials/ecycling/manage.htm (accessed Sep 23, 2015b).

USEPA. Bioreactor Landfills https://www.epa.gov/landfills/bioreactor-landfills (accessed Nov 22, 2017).

Visvanthan, C.; Yin, N. H.; Karthikeyan, O. P. Co-Disposal of Electronic Waste with Municipal Solid Waste in Bioreactor Landfills. *Waste Manag.* **2010**, *30* (12), 2608–2614.

Chapter 8: Improving Life Cycle Assessments of Lithium-ion and Nickel-metal Hydride Batteries and PV Modules by Modeling Landfill Disposal as an End-of-Life Option

Abstract

Conducting life cycle assessments (LCAs) of lithium-ion (Li-ion) and nickel-metal hydride (NiMH) batteries and photovoltaic (PV) modules are useful to understand the environmental impacts at each product stage; however, many LCA studies of these products focus on recycling at end-of-life (EOL) and neglect to consider landfill disposal. To incorporate landfill disposal as an EOL option, a crystalline silicon Suniva OPT245-60-4-100 PV module, a NiMH Lenmar PTD9094 power tool battery, and a Li-ion Lenmar LBZ378D laptop battery were disassembled and digested to determine composition to build their assemblies, and leaching tests were performed to quantify metal leaching in landfill conditions (described in Chapters 5 and 7). The product assembly materials were compared to similar products in the ecoinvent database. For the PV module, updating the product assembly resulted in a reduction in the calculated effects for both toxicity and non-toxicity categories. For the NiMH battery, updating the assembly resulted in greater toxicity effects but lower effects in non-toxicity categories. For the Li-ion battery, updating the assembly resulted in greater effects in both toxicity and non-toxicity categories. After comparing the differences in the assemblies, product-specific waste scenarios were developed and compared to the generic waste disposal scenario. Scenarios of metal emissions to groundwater were built based on the metal leaching data collected previously and analyzed for

toxicity effects. The results showed that the worst-case scenario effects exceeded those of the assemblies, and with notable effects for the other scenarios, the inclusion of the potential for EOL metal leaching is merited in LCAs of these products.

8.1 Introduction

The use of lithium ion (Li-ion) and nickel-metal hydride (NiMH) batteries and photovoltaic (PV) modules is growing to meet the increasing worldwide energy demand, but the end-of-life (EOL) phase, especially disposal with other solid wastes, of these products is poorly understood and typically not fully incorporated in life cycle assessments (LCAs). Many of the studies of Li-ion and NiMH batteries and PV modules at EOL focus on recycling, and few consider landfill disposal. Understanding of the EOL phase of these products and the associated risks to human and environmental health is limited (Hawkins et al., 2012; Kang et al., 2013). Li-ion battery manufacturing has been the subject of recent research, but the risks from toxic metal emissions from disposal have not been quantified (Gaustad et al., 2012). Disposing of Li-ion batteries in landfills could present environmental risks from leaching of organic electrolytes, toxic metals, lithium salts, and carbonaceous material (Richa et al., 2014). Similarly, PV modules are not subject to regulations mandating manufacturer take-back programs or recycling in the United States (US), only a voluntary take-back program exists (SEIA National PV Recycling Program), and their environmental impacts from disposal at EOL have not been quantified.

8.1.1 Previous Li-ion and NiMH battery LCAs

Recently LCA has been used to analyze the manufacturing, use, and disposal stages of Li-ion and NiMH batteries; however, the assumptions and the quality of the incorporated data within these studies vary widely. For example in several Li-ion battery LCAs, material inventory was used from either Li-ion battery manufacturing processes or identified during battery disassembly, was

assumed to remain unaltered during the battery lifetime and upon disposal, and potentially excluded materials with small masses, including some metals, that could alter the results (Gaustad et al., 2012). In a LCA of lithium manganese oxide batteries, little data was provided for disposal (Notter et al., 2010). In a 2011 LCA study of both Li-ion and NiMH batteries, no EOL scenarios were included in the analysis because battery recycling was believed to be not widely implemented, and not including EOL was assumed to be the worst-case scenario (Majeau-Bettez et al., 2011). The authors neglected that the EOL phase can have negative contributions in addition to benefits from recycling metals. In another LCA, Li-ion batteries were assumed to be dismantled and cryogenically shattered at EOL, but specific information about the process was not provided (Hawkins et al., 2013). In a LCA study of Li-ion and NiMH batteries, recycling and incineration were included as EOL treatments; however, landfilling was not (Yu et al., 2014). In a LCA of Li-rich cathode material, the EOL impact was found to be small compared to the other life cycle stages, but a lack of data was noted for the EOL phase (Wang et al., 2017). Several LCAs have assumed high recycling rates for Li-ion batteries (Olofsson and Romare, 2013; USEPA, 2013), which is an overly optimistic assumption for the US. Elucidating the entire Li-ion battery life cycle requires determining and characterizing the metal emissions at the EOL phase to ensure an accuracy of results (Gaustad et al., 2012). However, little is currently known about the fate and potential risks of Li-ion and NiMH battery emissions caused by leaching during disposal (Hawkins et al., 2012). Past battery LCAs mostly report impacts for metrics related to energy and global warming potential, but more recent LCAs have also considered health and environmental impacts (Larcher and Tarascon, 2015); however, only one of the referenced studies considered landfill disposal as an EOL option. In that study, leaching data for Li-ion cell phone batteries was used to determine resource depletion and toxicity potentials, but it was incomplete for determining the occurrence of Li-ion battery leaching in landfills and did not consider the

diversity in the composition of Li-ion batteries (Kang et al., 2013). Nonetheless, when the data were included in a LCA, cobalt, copper, nickel, thallium, and silver leaching contributed to potential freshwater and terrestrial eco-toxicities, possible abiotic resource depletion, and human toxicity (Kang et al., 2013), which validates the need to identify the leaching mechanisms and the fate of metal emissions during disposal.

8.1.2 Previous PV LCAs

While PV installations are considered clean energy because they are non-polluting during the use phase, impacts occur from their production, transportation, and EOL recycling or disposal. Life cycle inventories for a small sampling of PV modules have been assembled from manufacturing data (Fthenakis et al., 2011), but these studies exclude minority materials and usually do not consider disposal at EOL. A literature review of LCAs of PV systems published in 2014 noted only three studies which consider EOL in the analysis (Gerbinet et al., 2014). In one of these studies, the authors included three decommissioning scenarios for a PV plant in Italy: landfilling, recycling only glass and aluminum, and recycling all components; however, only the impact categories from the complete recycling scenario were presented in the results (Desideri et al., 2012), likely due to the lack of data for landfilling. In another LCA of PV plants with and without axis tracking, an EOL scenario was discussed, but no specific EOL results were presented (Bayod-Rújula et al., 2011). In a study comparing a polycrystalline PV module and wind turbine, landfill disposal of all components and recycling of glass, plastic, and metal components were compared (Zhong et al., 2011). For the landfilling scenario, 51.2% of the impacts were found to be from the plastic components, and the PV cells were assumed to be inert waste (Zhong et al., 2011). A LCA of the balance of system components (all necessary components not including the PV modules) for a power plant PV installation included disposal of the plant components at EOL and assumed a transportation distance of 160 km (Mason et al., 2006), but the study did not

consider the actual PV materials and their fate at EOL. Another study of a roof installation in Rome, Italy, recognized that impacts from system disposal at EOL need to be considered, however disposal was assumed to have a negligible impact (Battisti and Corrado, 2005), most likely due to a lack of data. Similarly, a LCA study of crystalline and thin film technologies installed in Europe recognized that recycling and disposal of PV modules needs be included in LCA studies, but they were not included or discussed as part of the hazardous emissions results (Alsema et al., 2006). A study of four commercially available PV systems showed very promising results for reducing greenhouse gas emissions by producing modules using PV solar energy sources, but limited their scope to cradle to gate (raw materials to manufacturing) and considered heavy metal emissions from direct sources (losses during manufacturing or disposal) to be minute compared to the indirect emissions from electricity and fuel use in manufacturing (Fthenakis et al., 2008).

8.1.3 ecoinvent data for Li-ion and NiMH batteries and PV modules

In addition to the published LCAs for Li-ion and NiMH batteries and PV modules, the ecoinvent database (Ecoinvent Centre) contains datasets for each of these products. Both Li-ion and NiMH rechargeable batteries are described within the documentation for electric and electronic equipment (Hischier et al., 2007), and PV modules are described within the documentation for energy systems (Jungbluth et al., 2009). Disposal for the electric and electronic equipment is limited to recycling. The EOL treatment for the NiMH batteries is recycling with a pyrometallurgical process, and for the Li-ion batteries, treatment is recycling with both pyrometallurgical and hydrometallurgical processes. Additionally, the battery chemistries are limited to one type of NiMH battery ($LaNi_5$ with $Ni_{94}Co_3Zn_3$) and one type of Li-ion battery ($LiMn_2O_4$ with LiC_6) although several chemistries exist for both battery types (Hischier et al., 2007). The EOL treatment for PV modules is not included in the documentation due to a lack of

sufficient data (Jungbluth et al., 2009). The datasets for these products focus on manufacturing and exclude minority metals and other components, which could have an impact on toxicity assessments using these datasets.

8.2 Objectives

The previous LCAs of Li-ion and NiMH batteries and PV modules highlight the knowledge gap in potential emissions from disposal of these products and that LCA practitioners lack the necessary data to properly model landfill disposal as an EOL option. Additionally, the datasets available in ecoinvent for these products do not include landfill disposal as an option at EOL. To address this knowledge gap, three products (a Li-ion laptop battery, a NiMH power tool battery, and a crystalline silicon PV module) were chosen, and metal leaching in landfill conditions was determined through the use of batch leaching tests and columns in an outdoor test bed facility, described previously in Chapters 5 and 7. The metal leaching and disassembly and digestion data have been combined with literature and database data to build new assemblies and waste scenarios for these products in SimaPro (PRé, 2018). The new product assemblies have been compared with the database product assemblies, and the toxicity effects from metal leaching at EOL from batch and column tests from these products have been compared to recycling and average municipal solid waste (MSW) scenarios. By adding missing data in the material inventories and creating product-specific waste scenarios, the validity of the LCAs of these products can be improved. By building these waste scenarios, the potential impacts from landfill disposal at EOL can be compared with other life cycle stages to determine if they truly are negligible as assumed in previous LCAs.

8.3 Materials and Methods

8.3.1 Product descriptions and material inventories

The three products chosen for this study are a crystalline silicon Suniva OPT245-60-4-100 PV module, a NiMH Lenmar PTD9094 power tool battery, and a Li-ion Lenmar LBZ378D laptop battery (Table 8.1). All three products were purchased new: the PV module in 2013 and batteries in 2015. For the PV module, the balance of system is not included. For the batteries, the products the batteries would be used within (i.e. laptop, power tool) are not included. The material inventories for the products have been created through disassembly and digestion data (described in Chapter 5) and have been supplemented by data for similar products in the ecoinvent database (Ecoinvent Centre). The records for the products in the ecoinvent database were copied and edited to reflect the material inventories measured in this study. For the c-Si module, the material composition was estimated by taking measurements to determine layer thicknesses and masses and by digestion of the active materials (Figure 8.1, Table 8.2). Due to lamination, measuring the individual masses of the photovoltaic cells, solder, ethylvinylacetate, and backing materials was not possible. Therefore, the masses of each component were estimated using ecoinvent data and literature sources (Jungbluth et al., 2009; DuPont, 2014; Polman et al., 2016). Two assembly scenarios were considered: updating the ecoinvent record including changing the mass of the crystalline silicon used in the production of solar cells to account for a thinner wafer and updating everything but the mass of the crystalline silicon, so that the effects from updating the crystalline silicon mass can be isolated. The metals measured via digestion of the active layer not accounted

Table 8.1: Product descriptions for the three e-wastes in this study and ecoinvent product descriptions for reference.

	This Study			Reference Products			
	c-Si PV Module	**NiMH Power Tool Battery**	**Li-ion Laptop Battery**	**c-Si PV Module** (ecoinvent 3)	**NiMH Battery** (ecoinvent 3)	**Li-ion Battery** (ecoinvent 3)	**Li-ion Battery** (ecoinvent 2.1)
Model	Suniva OPT245-60-4-100	Lenmar PTD9094	Lenmar LBZ378D	averaged values from multiple products	Fujitsu-Siemens UBP07677B	generic electric vehicle battery	Panasonic FPCBP64
Size [cm²]	165.4 X 98.1	-	-	162 X 98.6	-	-	-
Weight [g]	18819	799.9	310.3	24174	591	-	190
Peak power [W]	245	-	-	224	-	-	-
Voltage [V]	-	14.4	11.1	-	-	48	-
Capacity [mAh]	-	3000	4400	-	4500	-	4000
Energy [kWh]	-	-	-	-	-	2.1	
Number of battery cells	-	12	6	-	1	14	4

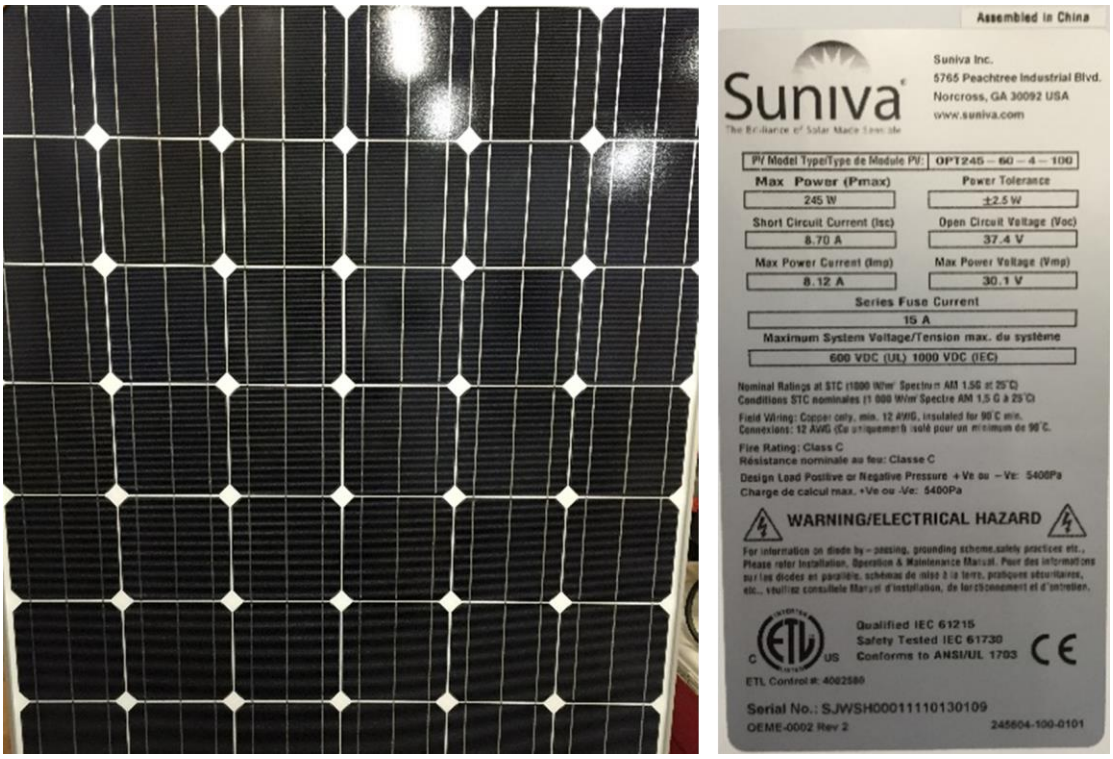

Figure 8.1: Images of the c-Si module with product description.

Table 8.2: Masses and mass ratios of components of the c-Si module with ecoinvent product data for reference.

c-Si Module Component	Mass [g]	Mass Ratio [g/g]	Mass/area (kg/m2)	ecoinvent 3 Reference Mass [g]	ecoinvent 3 Reference Mass Ratio [g/g]	ecoinvent 3 Reference Mass/area (kg/m2)
Aluminum frame	3439	0.1827	2.119	4200	0.1737	2.629
Junction box (polyamide)	154.7	0.0082	0.0953	300.0	0.0124	0.1878
Silicone	56.06	0.0030	0.0346	194.8	0.0081	0.1219
Solar glass	14054	0.7468	8.662	15939	0.6593	10.08
Active layer and backing	1116	0.0593	0.6878	3541	0.1465	2.217
Photovoltaic cells	*415.8*	*2.209×10^{-2}*	*2.563×10^{-1}*	*1025*	*4.239×10^{-2}*	*6.416×10^{-1}*
Solder	*14.22*	*7.556×10^{-4}*	*8.764×10^{-3}*	*14.00*	*5.791×10^{-4}*	*8.764×10^{-3}*
Ethylvinylacetate	*103.0*	*5.474×10^{-3}*	*6.349×10^{-2}*	*1600*	*6.618×10^{-2}*	*1.002*
Polyvinylfluoride film	*180.5*	*9.590×10^{-3}*	*1.112×10^{-1}*	*164.8*	*6.817×10^{-3}*	*1.032×10^{-1}*
Polyethylene terephthalate	*161.8*	*8.598×10^{-3}*	*9.972×10^{-2}*	*556.7*	*2.303×10^{-2}*	*3.486×10^{-1}*
Copper ribbons	*240.7*	*1.279×10^{-2}*	*1.483×10^{-1}*	*180.0*	*7.446×10^{-3}*	*1.127×10^{-1}*
Nickel plating	-	-	-	*0.260*	*1.075×10^{-5}*	*1.628×10^{-4}*
Measured via digestion (or from components for reference product)						
Ag	*16.30*	*8.663×10^{-4}*	*1.005×10^{-2}*	*14.20*	*5.875×10^{-4}*	*8.892×10^{-3}*
Al	*61.61*	*3.274×10^{-3}*	*3.797×10^{-2}*	*86.53*	*3.579×10^{-3}*	*5.417×10^{-2}*
Ba	*0.0119*	*6.338×10^{-7}*	*7.351×10^{-6}*			
Co	*0.0046*	*2.447×10^{-7}*	*2.839×10^{-6}*			
Cu	*240.7*	*1.279×10^{-2}*	*1.483×10^{-1}*	*188.5*	*7.797×10^{-3}*	*1.180×10^{-1}*
Fe	*0.705*	*3.748×10^{-5}*	*4.348×10^{-4}*			
Mn	*0.0340*	*1.809×10^{-6}*	*2.099×10^{-5}*			
Ni	-	-	-	*0.260*	*1.075×10^{-5}*	*1.628×10^{-4}*
Pb	*46.53*	*2.472×10^{-3}*	*2.868×10^{-2}*	*1.150*	*4.755×10^{-5}*	*7.197×10^{-4}*
Zn	*0.683*	*3.631×10^{-5}*	*4.211×10^{-4}*	*5.656*	*2.340×10^{-4}*	*3.541×10^{-3}*
Total module	***18819***			***24174***		

for by the metallization paste in the ecoinvent database were added using an additional metallization paste record. For the NiMH power tool battery (Figure 8.2, Table 8.3) and Li-ion laptop battery (Figure 8.3, Table 8.4), each component was disassembled and weighed, and the anode and cathode materials were digested to determine metal composition. For the NiMH battery, the negative electrode record was updated to include the additional metals measured via digestion not included in the ecoinvent record, in addition to adjusting the mass ratios of Co, Ni, and Zn. For the Li-ion battery, two records exist in the ecoinvent database: an older record for version 2.1 and an updated record for version 3. The record from version 2.1 was created based on a laptop battery, with a material composition more closely resembling the battery in this study; whereas the record from version 3 more closely resembles an electric vehicle battery with steel housing. However, because the version 2.1 record was replaced in version 3, and the updated version 3 record is used in this study (the ecoinvent version 2.1 data is presented in Table 8.4 for reference). For the Li-ion battery in ecoivent version 3, the mass ratios in the record do not sum to one; however, the mass ratios of the active materials of the reference product and the battery in this study are similar, so comparing the results from changing the cathode materials can be justified. The Li-ion battery cell record was updated to include components not accounted for in the ecoinvent version 3 record, and the $LiMn_2O_4$ cathode record was replaced with a new

Figure 8.2: Images of the NiMH power tool battery, including disassembled components.

Table 8.3: Masses and mass ratios of components of the NiMH power tool battery with ecoinvent product data for reference.

NiMH Battery Component	Mass [g]	Mass Ratio [g/g]	ecoinvent Reference Mass [g]	ecoinvent Reference Mass Ratio [g/g]
Battery housing	**106.13**	**0.1327**	**47.99**	**0.0812**
Plastic components (polycarbonate)	98.14	0.1227	47.99	0.0812
Top piece	*29.49*	*3.687×10^{-2}*		
Bottom piece	*65.34*	*8.168×10^{-2}*		
Connector piece	*3.31*	*4.138×10^{-3}*		
Metal components	7.99	0.0100		
Screws	*4.35*	*5.438×10^{-3}*		
Latches	*2.40*	*3.000×10^{-3}*		
Copper connector	*1.24*	*1.550×10^{-3}*		
Battery interior (excluding cells)	**14.55**	**0.0182**		
Packaging and separators	12.92	0.0162		
Paper adhesive pieces	*3.22*	*4.025×10^{-3}*		
Black foam pieces (EVA)	*1.59*	*1.988×10^{-3}*		
Paper covers on cylinders	*7.97*	*9.963×10^{-3}*		
Tape	*0.14*	*1.750×10^{-4}*		
Cable (16 AWG, 9.1 cm length)	1.63	2.038×10^{-3}		
Battery cells	**679.25**	**0.8491**	**543.01**	**0.9188**
Battery jackets (steel)	163.92	0.2049	27.34	0.0463
Terminals	5.52	6.901×10^{-3}	2.162×10^{-3}	3.659×10^{-6}
Cu	*5.465*	*6.832×10^{-3}*	*2.141×10^{-3}*	*3.622×10^{-6}*
Zn coating	*5.465×10^{-2}*	*6.832×10^{-5}*	*2.141×10^{-5}*	*3.622×10^{-8}*
Plastic rings	0.24	3.000×10^{-4}		
Metallic disks (steel)	2.64	3.300×10^{-3}		
Rolled anode/cathodes	506.93	0.6337	515.7	0.8725
Positive	*92.91*	*1.162×10^{-1}*	*197.89*	*3.348×10^{-1}*
Negative	*310.17*	*3.877×10^{-1}*	*212.14*	*3.590×10^{-1}*
Substrate	*33.89*	*4.237×10^{-2}*	*34.47*	*5.833×10^{-2}*
Separator	*22.20*	*2.775×10^{-2}*	*22.58*	*3.821×10^{-2}*
Polypropylene	10.77	1.346×10^{-2}	10.95	1.854×10^{-2}
Polyethylene	10.65	1.332×10^{-2}	10.84	1.833×10^{-2}
Acrylic acid	0.78	9.719×10^{-4}	0.79	1.338×10^{-3}
Electrolyte	*47.76*	*5.970×10^{-2}*	*48.58*	*8.220×10^{-2}*
Measured via digestion (or from components for reference product)				
Al	*2.731*	*3.414×10^{-3}*		
As	*7.073×10^{-1}*	*8.842×10^{-4}*		
Ba	*2.510×10^{-2}*	*3.138×10^{-5}*		
Co	*2.303×10^{1}*	*2.878×10^{-2}*	*1.773×10^{1}*	*3.000×10^{-2}*
Cu	*5.089×10^{1}*	*6.362×10^{-2}*		
Hg	*1.863×10^{-1}*	*2.329×10^{-4}*		
Mn	*9.799*	*1.225×10^{-2}*		
Ni	*2.665×10^{2}*	*3.332×10^{-1}*	*2.537×10^{2}*	*4.292×10^{-1}*
Pb	*9.600×10^{-2}*	*1.200×10^{-4}*		
Zn	*9.504*	*1.188×10^{-2}*	*1.773×10^{1}*	*3.000×10^{-2}*
Total battery	***799.93***		***591.00***	

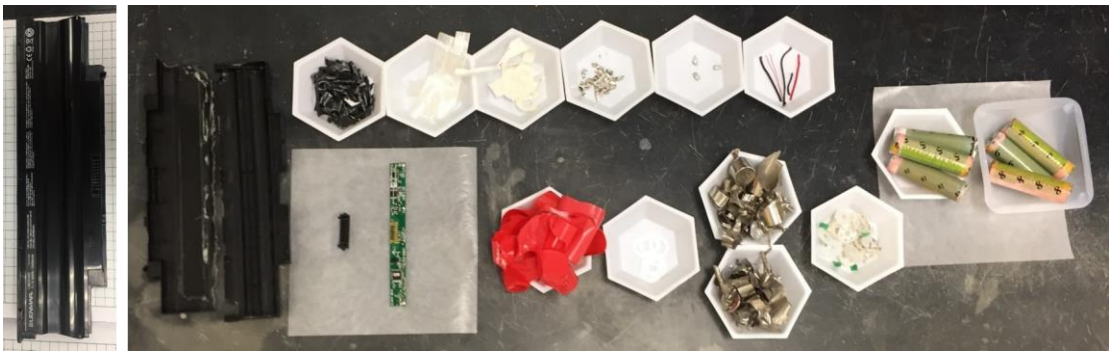

Figure 8.3: Images of the Li-ion laptop battery, including disassembled components.

$LiNiMnCoO_2$ cathode record to account for the metals measured via digestion. The material inventories for the products disassembled and digested are compared to the original ecoinvent datasets for each product type (Tables 8.2-4).

8.3.2 Software, data sources, and characterization methods

The use of LCA software facilitates the compilation and analysis of the inventory data, and for this project SimaPro was used (PRé, 2018). Inventory from databases, including ecoinvent (Ecoinvent Centre), and literature were used for the production of common raw materials in this study. During the assessment stage, the LCA software was used to translate the cumulative material inventory into meaningful environmental and health impacts by utilizing characterization factors. The USETox characterization method, which is the recommended modeling method for human and environmental toxicity has been used (Rosenbaum et al., 2011; Fantke et al., 2017). The USETox characterization results are reported as human toxicity cases (both cancer and non-cancer) and for freshwater ecotoxicity, potentially affected fraction (PAF) of species integrated over time and volume. The results are calculated by combining data on environmental fate, exposure routes, and effects (Fantke et al., 2017). The TRACI characterization method has been used for greenhouse gases and non-toxic effects for the product assemblies (Bare, 2002; USEPA, 2015).

Table 8.4: Masses and mass ratios of components of the Li-ion laptop battery with ecoinvent product data for reference.

Li-ion Battery Component	Mass [g]	Mass Ratio [g/g]	ecoinvent 3 Reference Mass Ratio [g/g]	ecoinvent 2.1 Reference Mass [g]	ecoinvent 2.1 Reference Mass Ratio [g/g]
Battery housing	**46.63**	**0.1503**	**0.1082**	**42.94**	**0.2260**
Plastic components (polyethylene)	46.63	0.1503		42.94	0.2260
Exterior	*45.73*	*0.1474*			
Connector piece	*0.90*	*2.901 x 10^{-3}*			
Steel			0.1082		
Battery interior (excluding cells)	**10.29**	**0.0332**	**0.0438**		
Packaging	4.48	0.0144			
Paper disks	*0.20*	*6.446 x 10^{-4}*			
Plastic covers (polyethylene)	*2.67*	*8.606 x 10^{-3}*			
Tape	*1.61*	*5.189 x 10^{-3}*			
Cables	0.78	0.0025	0.0412		
Black wires (4.1, 5.6, & 1.8 cm)	*0.50*	*1.612 x 10^{-3}*			
Uncoated wire (4.6 cm)	*0.06*	*1.934 x 10^{-4}*			
Red wire (3.8 cm)	*0.22*	*7.091 x 10^{-4}*			
Solder	0.44	1.418 x 10^{-3}			
Circuit board (11.6 cm by 1.25 cm)	4.59	1.479 x 10^{-2}	2.519 x 10^{-3}		
Battery cells	**253.34**	**0.8165**	**0.5949**	**147.3**	**0.7753**
Battery jackets (Al)	43.30	0.1396		23.56	0.1240
Terminals (Al for ecoinvent 3)	0.83	2.675 x 10^{-3}	9.282 x 10^{-3}	5.054 x 10^{-3}	2.660 x 10^{-5}
Cu	*8.218 x 10^{-1}*	*2.649 x 10^{-3}*		*5.004 x 10^{-3}*	*2.634 x 10^{-5}*
Sn coating	*8.218 x 10^{-3}*	*2.649 x 10^{-5}*		*5.004 x 10^{-5}*	*2.634 x 10^{-7}*
Plastic rings	1.78	0.0057	0.0413		
Rolled anode/cathodes	207.43	0.6686	0.5406	123.7	0.6512
Cathode	*70.61*	*0.2276*	*0.1840*	*61.88*	*0.3257*
Anode	*86.65*	*0.2793*	*0.2258*	*31.62*	*0.1664*
Separator	*11.59*	*0.0374*	*0.0302*	*11.95*	*0.0629*
Electrolyte	*38.58*	*0.1244*	*0.1006*	*18.28*	*0.0962*
Ethylene carbonate	34.47	0.1111	0.0898		
Lithium hexafluorophosphate	4.112	0.0133	0.0107		
Measured via digestion (or from components for reference product)					
Ag	*3.100 x 10^{-3}*	*9.992 x 10^{-6}*			
Al	*7.968*	*2.568 x 10^{-2}*	*7.222 x 10^{-2}*	*1.656 x 10^{1}*	*8.716 x 10^{-2}*
Ba	*3.234 x 10^{-3}*	*1.042 x 10^{-5}*			
Co	*1.269 x 10^{1}*	*4.090 x 10^{-2}*			
Cr	*3.571 x 10^{-3}*	*1.151 x 10^{-5}*			
Cu	*1.911 x 10^{1}*	*6.159 x 10^{-2}*	*1.184 x 10^{-1}*	*1.046*	*5.504 x 10^{-3}*
Hg	*1.656 x 10^{-1}*	*5.336 x 10^{-4}*			
Mn	*1.542 x 10^{1}*	*4.971 x 10^{-2}*	*1.041 x 10^{-1}*	*5.087 x 10^{1}*	*2.677 x 10^{-1}*
Ni	*2.902 x 10^{1}*	*9.354 x 10^{-2}*			
Pb	*4.726 x 10^{-2}*	*1.523 x 10^{-4}*			
Tl	*5.718 x 10^{-2}*	*1.843 x 10^{-4}*			
Zn	*3.202 x 10^{-3}*	*1.032 x 10^{-5}*			
Total battery	***310.26***			***190.00***	

8.4 Results and Discussion

8.4.1 Material inventory comparison with ecoinvent database products

By creating new records via updating the ecoinvent records based on the disassembly and digestion data for each product, the change in the environmental impacts based on the change in

the material assemblies can be compared. The USETox (Rosenbaum et al., 2011; Fantke et al., 2017) and TRACI (Bare, 2002; USEPA, 2015) characterization methods have been used to compare the updated product assemblies to the original database products. The results have been calculated per 1 m2 for the c-Si PV modules and per 1 kg for each of the batteries. Updating the inventories for these products is useful for comparing the results for the assembly phase to the EOL phase, in addition to comparing data from disassembling and digesting products to the ecoinvent data.

For the c-Si PV module, reducing the mass of the crystalline silicon cells accounted for the most change in the results, likely due to the reduction in energy requirements tied to the mass of the silicon within the database, but the actual change in energy should be further studied (Table 8.5, Figure 8.4). In the scenario without altering the crystalline silicon mass, the addition of the metals in the metallization paste originally unaccounted for along with the reduction in the

Table 8.5: Results from USEtox and TRACI for 1 m^2 of c-Si PV module assemblies for ecoinvent 3, the Suniva module with the updated cell mass, and the Suniva module with the original cell mass from ecoinvent.

			c-Si PV module		
	Impact category	**Unit**	**ecoinvent 3**	**Suniva; original cell mass**	**Suniva; cell mass reduced**
USEtox 2	Human toxicity, cancer	cases	2.0×10^{-5}	1.9×10^{-5}	1.5×10^{-5}
	Human toxicity, non-cancer	cases	1.0×10^{-4}	1.0×10^{-4}	9.1×10^{-5}
	Freshwater ecotoxicity	PAF.m3.day	1.2×10^{6}	1.2×10^{6}	9.8×10^{5}
TRACI 2.1	Ozone depletion	kg CFC-11 eq	5.4×10^{-5}	5.3×10^{-5}	4.5×10^{-5}
	Global warming	kg CO2 eq	2.7×10^{2}	2.6×10^{2}	1.7×10^{2}
	Smog	kg O3 eq	1.4×10^{1}	1.4×10^{1}	9.5
	Acidification	kg SO2 eq	1.4	1.4	9.4×10^{-1}
	Eutrophication	kg N eq	1.3	1.3	9.1×10^{-1}
	Carcinogenics	CTUh	2.1×10^{-5}	2.0×10^{-5}	1.6×10^{-5}
	Non carcinogenics	CTUh	1.2×10^{-4}	1.3×10^{-4}	1.1×10^{-4}
	Respiratory effects	kg PM2.5 eq	4.5×10^{-1}	4.3×10^{-1}	2.8×10^{-1}
	Ecotoxicity	CTUe	2.8×10^{3}	2.9×10^{3}	2.4×10^{3}
	Fossil fuel depletion	MJ surplus	2.5×10^{2}	2.3×10^{2}	1.6×10^{2}

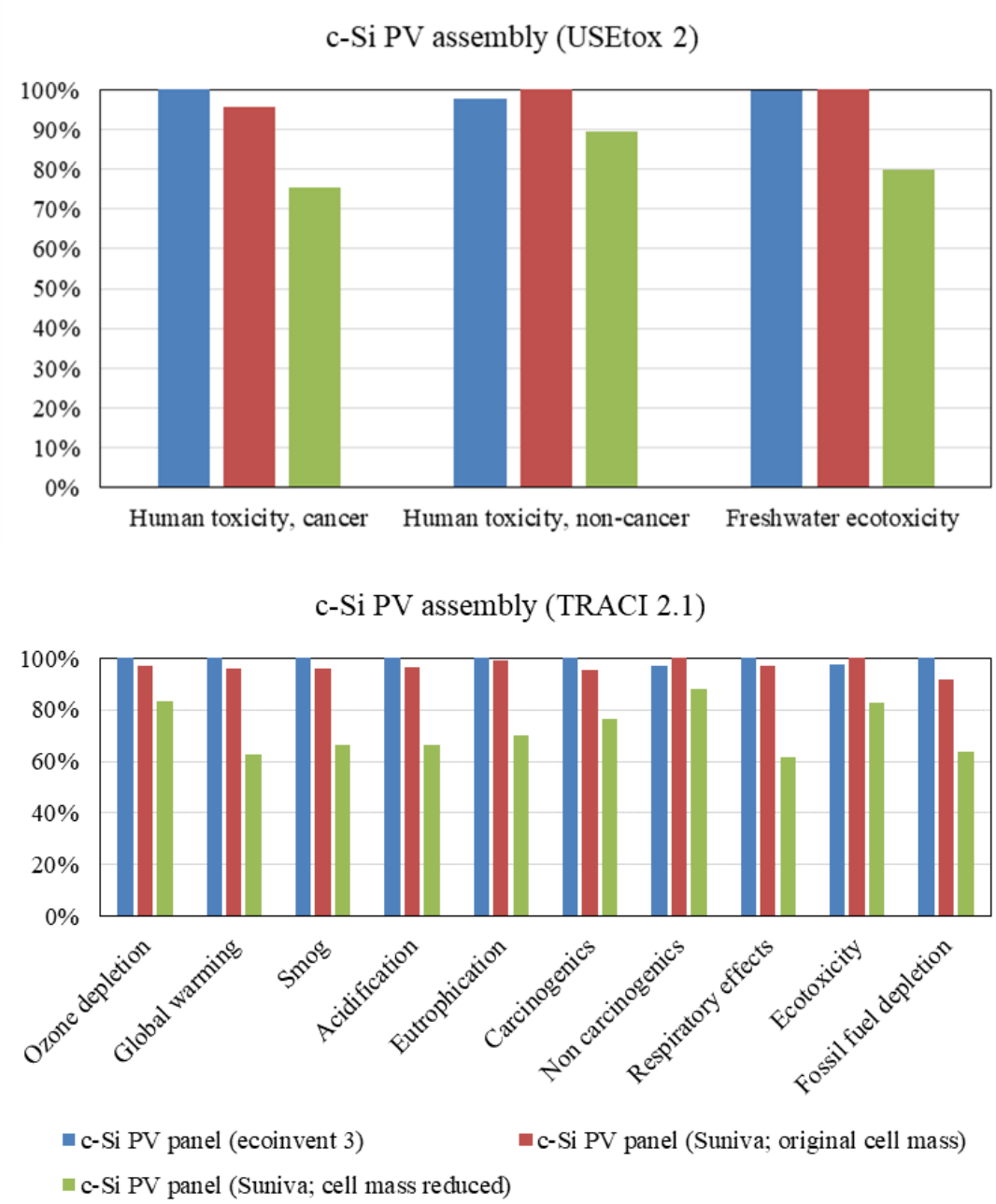

Figure 8.4: Comparison of normalized results from USEtox and TRACI for the c-Si PV module assemblies for ecoinvent 3, the Suniva module with the updated cell mass, and the Suniva module with the original cell mass from ecoinvent.

masses of the aluminum frame, glass, laminates, and plastics, resulted in a slight increase in human toxicity, non-cancer cases.

For the NiMH battery comparison, the updated assembly resulted in higher human toxicity (cancer and non-cancer) cases and freshwater ecotoxicity than the original ecoinvent NiMH battery (Table 8.6, Figure 8.5). Although the toxicity effects were greater, the updated assembly resulted in lower ozone depletion, global warming, smog, acidification, respiratory effects, and fossil fuel depletion. This decrease might be attributed to the decrease in the mass ratio of active materials, which require more energy and processing, to the masses of the other components of the battery.

The updated Li-ion battery assembly resulted in greater impacts for all categories (Table 8.7, Figure 8.6). The cathode in the reference ecoinvent battery was composed of $LiMn_2O_4$, but based on the metals digested in the Lenmar battery, the cathode composition was updated to

Table 8.6: Results from USEtox and TRACI for 1 kg of the NiMH battery assemblies for ecoinvent 3 and the Lenmar power tool battery.

			NiMH battery	
	Impact category	**Unit**	**ecoinvent 3**	**Lenmar**
USEtox 2	Human toxicity, cancer	cases	2.1×10^{-6}	3.2×10^{-6}
	Human toxicity, non-cancer	cases	1.4×10^{-5}	5.4×10^{-5}
	Freshwater ecotoxicity	PAF.m3.day	2.0×10^{5}	2.3×10^{5}
TRACI 2.1	Ozone depletion	kg CFC-11 eq	9.7×10^{-5}	3.5×10^{-5}
	Global warming	kg CO2 eq	2.0×10^{1}	1.4×10^{1}
	Smog	kg O3 eq	1.2	9.7×10^{-1}
	Acidification	kg SO2 eq	1.1	9.0×10^{-1}
	Eutrophication	kg N eq	1.4×10^{-1}	1.4×10^{-1}
	Carcinogenics	CTUh	2.2×10^{-6}	3.2×10^{-6}
	Non carcinogenics	CTUh	2.5×10^{-5}	5.3×10^{-5}
	Respiratory effects	kg PM2.5 eq	9.3×10^{-2}	7.1×10^{-2}
	Ecotoxicity	CTUe	6.6×10^{2}	7.2×10^{2}
	Fossil fuel depletion	MJ surplus	2.1×10^{1}	1.4×10^{1}

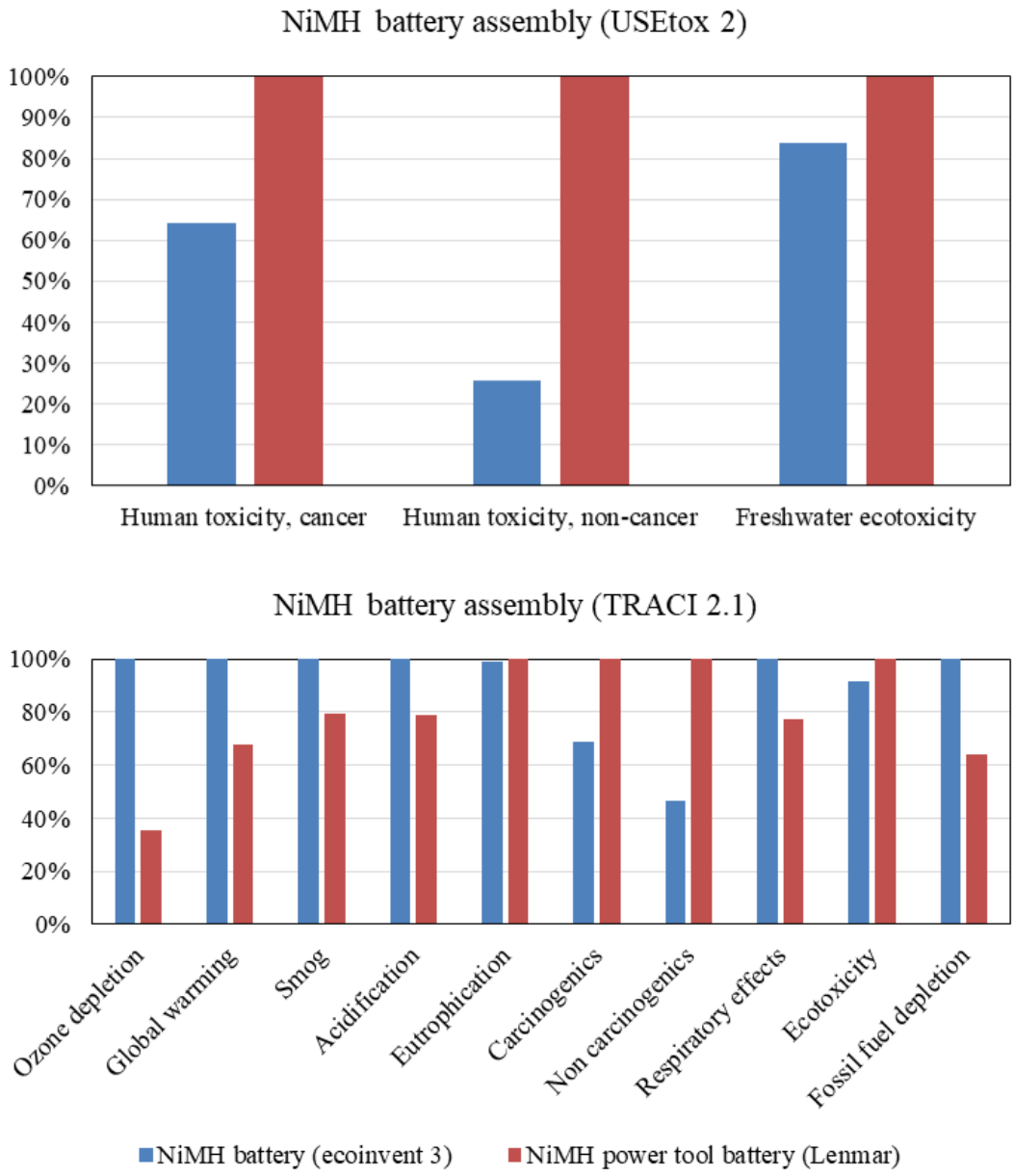

Figure 8.5: Comparison of normalized results from USEtox and TRACI for the NiMH battery assemblies for ecoinvent 3 and the Lenmar power tool battery.

$LiNiMnCoO_2$ which contributes to the increase in the toxicity effects. The mass ratio of the active materials for the updated Li-ion assembly was slightly greater than the original mass ratio of the active materials, which could also contribute to the increase. The housing for the original battery was steel, whereas the updated battery assembly contains aluminum for the individual battery

cells housing and polyethylene for housing the cells. The substitution of aluminum for steel could increase the production energy requirements, which would increase the environmental impacts.

8.4.2 Waste scenarios

Using metal leaching data collected in Chapters 5 and 7, different scenarios of metal emissions to groundwater were analyzed for toxicity effects using USEtox. The data have been normalized per 1 m2 for the c-Si PV module and per 1 kg for each of the batteries. A very unlikely (due to physical and chemical constraints) worst-case scenario was defined as the e-waste buried below the water table and complete dissolution of the metals measured via digestion into the groundwater occurs, which resulted in the greatest toxicity effects. The second scenario was built with the percentages of metals leaching from conducting the TCLP regulatory method on each e-waste, which can be used as an indicator for potential groundwater contamination of metals from waste materials (USEPA, 1992). For the third and fourth scenarios, the maximum percentages of

Table 8.7: Results from USEtox and TRACI for 1 kg of the Li-ion battery assemblies for ecoinvent 3 and the Lenmar laptop battery.

			Li-ion battery	
	Impact category	**Unit**	**ecoinvent 3**	**Lenmar**
USEtox 2	Human toxicity, cancer	cases	1.4×10^{-6}	3.6×10^{-6}
	Human toxicity, non-cancer	cases	1.5×10^{-5}	1.2×10^{-4}
	Freshwater ecotoxicity	PAF.m3.day	2.3×10^{5}	4.7×10^{5}
TRACI 2.1	Ozone depletion	kg CFC-11 eq	1.3×10^{-6}	2.0×10^{-6}
	Global warming	kg CO2 eq	6.1	1.3×10^{1}
	Smog	kg O3 eq	4.7×10^{-1}	1.1
	Acidification	kg SO2 eq	7.3×10^{-2}	3.5×10^{-1}
	Eutrophication	kg N eq	1.1×10^{-1}	2.6×10^{-1}
	Carcinogenics	CTUh	1.5×10^{-6}	3.4×10^{-6}
	Non carcinogenics	CTUh	2.4×10^{-5}	1.1×10^{-4}
	Respiratory effects	kg PM2.5 eq	1.3×10^{-2}	4.0×10^{-2}
	Ecotoxicity	CTUe	6.0×10^{2}	1.4×10^{3}
	Fossil fuel depletion	MJ surplus	6.4	1.3×10^{1}

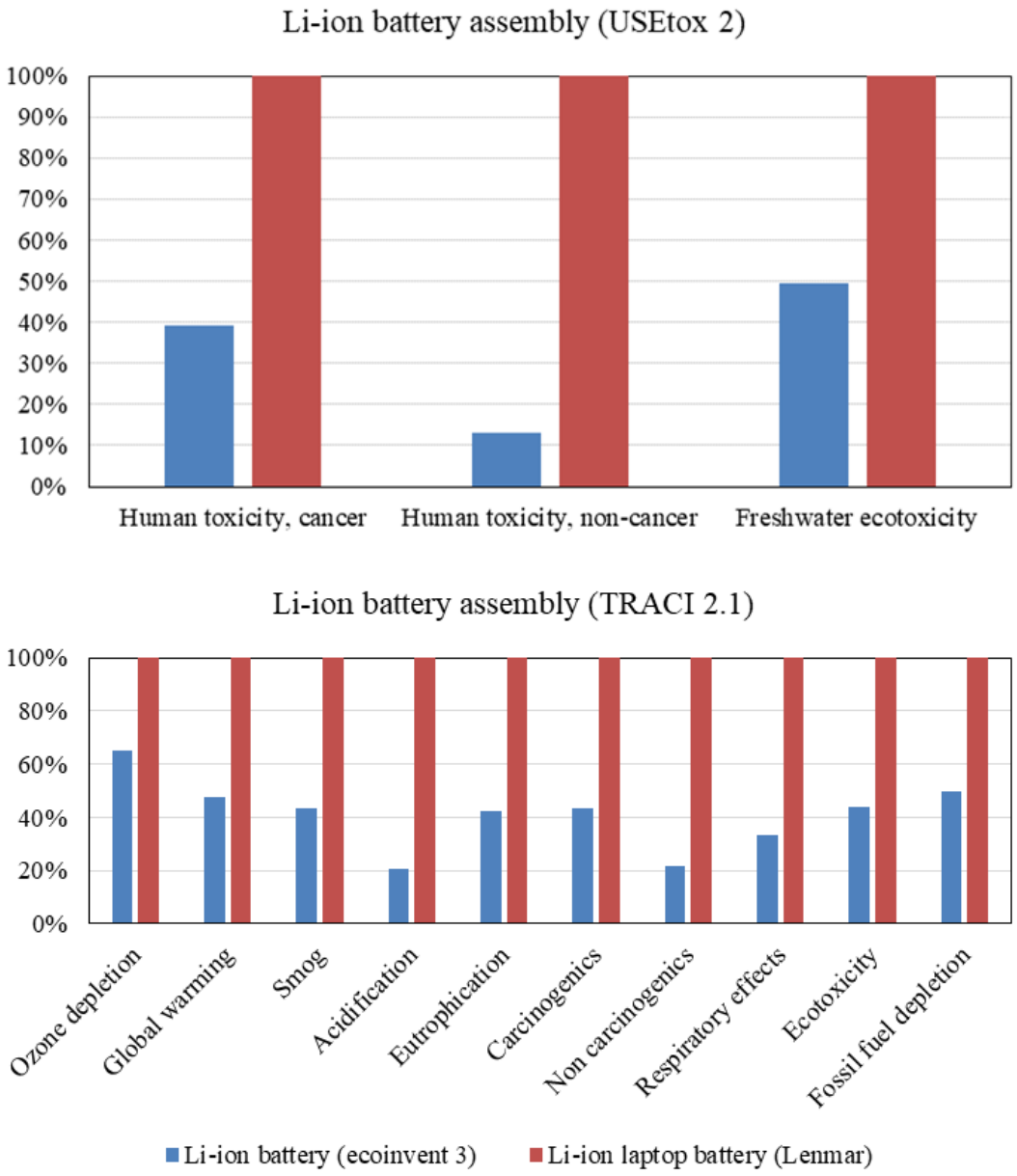

Figure 8.6: Comparison of normalized results from USEtox and TRACI for the Li-ion battery assemblies for ecoinvent 3 and the Lenmar laptop battery.

metals leaching observed during the batch tests and the batch test mixed with MSW, respectively, were used. For the fifth scenario, the maximum percentages of metals leaching observed in the leachate in the outdoor columns were used. For both the batch tests with MSW and the outdoor columns, which contained MSW, the metals observed in the MSW control (Al, Ba, Fe, Mn, and

Zn) were excluded from the datasets. The metal leaching in the MSW control was considered in a separate scenario. Recycling scenarios for the batteries were included, as these processes have been modeled in the ecoinvent database; however, no database process could be found for the c-Si PV panel. Additionally, the data for the disposal of 1 kg of generic MSW to a sanitary landfill was included (Table 8.8). The database record for the disposal of MSW to a sanitary landfill includes emissions to air and water in addition to the energy and equipment requirements to operate a landfill allocated to the 1 kg of MSW. If considering the results from the generic MSW as a baseline, the effects from metal leaching from the e-waste could be considered in addition to the calculated values. However, a more in-depth model combining e-waste metal leaching with the impacts from operating landfills, including leachate treatment processes, should be considered in future work. The USEtox results for each of these scenarios are presented in Tables 8.9-10.

Normalizing the calculated effects for each scenario and product to an equivalent mass of generic MSW disposal allows for comparison amongst the scenarios. Although the disposal of generic MSW includes more processes than metal emissions to groundwater, it is useful to determine if the effects from metals leaching from e-waste disposal are greater or less than the disposal of

Table 8.8: Composition of the MSW control and the generic MSW ecoinvent data.

Batch MSW Control Composition	Mass (%)
Paper	34.13
Plastics	12.30
Metal	8.18
Glass	7.20
Food	13.20
Soil	25.00

Generic MSW Composition	Mass (%)
Paper	21.00
Mixed cardboard	8.00
Plastics	15.00
Laminated materials	3.00
Laminated packaging	2.00
Combined goods	3.00
Glass	3.00
Textiles	2.00
Minerals	8.00
Natural products	9.00
Compostable material	22.00
Inert materials	2.65
Volatile materials	1.00
Batteries	0.0065
Electronic goods	0.34

Table 8.9: Results from USEtox for 1 m^2 of the Suniva c-Si PV module, 1 kg of the Lenmar NiMH power tool battery, and 1 kg of the Lenmar laptop battery at EOL for metals leaching into groundwater.

Impact category	**Unit**	**Worst case (digestion)**	**TCLP reg. method**	**Batch tests**	**Batch with MSW**	**Outdoor column**	**Recycling**
c-Si PV module							
Human toxicity, cancer	cases	4.1×10^{-9}	5.4×10^{-10}	8.4×10^{-10}	-	-	-
Human toxicity, non-cancer	cases	6.3×10^{-6}	2.1×10^{-7}	3.2×10^{-7}	-	-	-
Freshwater ecotoxicity	PAF.m3.day	1.6×10^{6}	4.5×10^{2}	1.2×10^{5}	-	-	-
NiMH battery							
Human toxicity, cancer	cases	4.0×10^{-5}	2.2×10^{-6}	6.9×10^{-7}	2.3×10^{-7}	3.2×10^{-8}	3.3×10^{-8}
Human toxicity, non-cancer	cases	3.2×10^{-5}	9.4×10^{-6}	5.5×10^{-6}	1.3×10^{-8}	1.8×10^{-9}	7.2×10^{-7}
Freshwater ecotoxicity	PAF.m3.day	7.5×10^{5}	5.4×10^{3}	1.1×10^{4}	7.7×10^{2}	1.5×10^{2}	1.8×10^{3}
Li-ion battery							
Human toxicity, cancer	cases	1.1×10^{-5}	2.7×10^{-8}	6.4×10^{-7}	1.1×10^{-6}	7.3×10^{-7}	5.8×10^{-8}
Human toxicity, non-cancer	cases	1.1×10^{-5}	3.1×10^{-9}	3.7×10^{-8}	6.0×10^{-8}	4.1×10^{-8}	3.1×10^{-7}
Freshwater ecotoxicity	PAF.m3.day	7.4×10^{5}	9.6×10^{4}	9.0×10^{4}	1.7×10^{4}	2.2×10^{3}	5.4×10^{3}

Table 8.10: Results from metals leaching from the batch MSW control and for the disposal of 1 kg of generic MSW.

Impact category	**Unit**	**Batch MSW control**	**Generic MSW**
Human toxicity, cancer	cases	0	3.0×10^{-8}
Human toxicity, non-cancer	cases	5.5×10^{-9}	4.3×10^{-7}
Freshwater ecotoxicity	PAF.m3.day	1.8×10^{3}	6.4×10^{4}

generic MSW. For the c-Si PV module worst-case disposal scenario, the human toxicity (non-cancer) and freshwater ecotoxicity effects exceeded the calculated effects for the landfill disposal of an equivalent mass of generic MSW (Figure 8.7). For the TCLP regulatory method and the batch tests, the calculated effects were much less than the generic MSW disposal. In the batch tests with MSW and outdoor column, the metals observed in the leachate were also observed in the MSW control, and therefore these scenarios were not included in the results. For the NiMH power tool battery worst-case disposal scenario, the calculated effects for human toxicity (both cancer and non-cancer) and freshwater ecotoxicity exceeded the effects for landfill disposal of an equivalent mass of generic MSW by more than ten times, with the effects for human toxicity (cancer) greater than 1000 times (Figure 8.8). The calculated effects for human toxicity (both

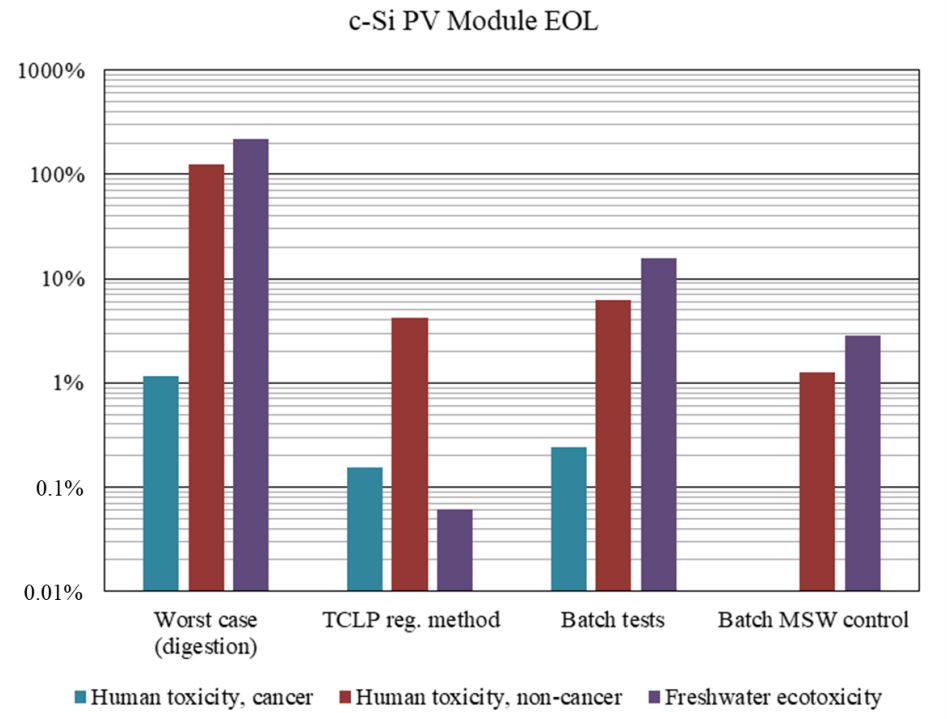

Figure 8.7: Comparison of results from USEtox for the c-Si PV module EOL scenarios normalized to the effects of an equivalent mass of generic MSW disposal. Note: Batch MSW control results are for an equivalent mass of 1 m^2 of module.

cancer and non-cancer) for the TCLP regulatory method and batch test scenarios also exceeded the effects for landfill disposal of generic MSW by ten times. The calculated effects for human toxicity (cancer) for the batch tests with MSW, outdoor column, and recycling scenarios exceeded the effects for landfill disposal of generic MSW. For the Li-ion laptop battery worst-case disposal scenario, the calculated effects for human toxicity (both cancer and non-cancer) and freshwater ecotoxicity exceeded the effects for landfill disposal of an equivalent mass of generic MSW by more than ten times, with the effects for human toxicity (cancer) greater than 100 times (Figure 8.9). For the batch tests, batch tests with MSW, and outdoor columns, the human toxicity (cancer) cases were greater than ten times the cases for generic MSW.

To determine if the calculated effects for EOL should be included in LCAs, the results for

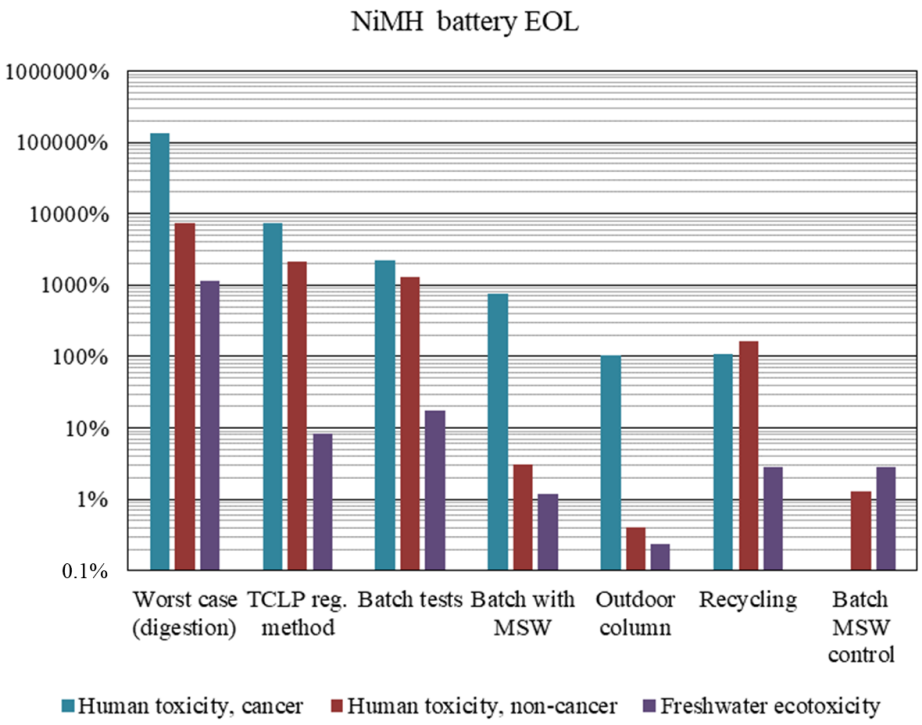

Figure 8.8: Comparison of results from USEtox for the NiMH power tool battery EOL scenarios normalized to the results of 1 kg of generic MSW disposal. Note: Batch MSW control results are for 1 kg.

the EOL scenarios have been normalized to the assembly results for each product (Table 8.11). For the c-Si PV module, the freshwater ecotoxicity effects for the worst-case scenario exceeded the effects for the assembly of the c-Si PV module, with copper leaching to groundwater accounting for most of the results. For the batch test scenario, the freshwater ecotoxicity result was equal to approximately 12 percent of the freshwater ecotoxicity result for the assembly. For the NiMH power tool battery, human toxicity (cancer) cases and freshwater ecotoxicity results for the worst-case scenario were much greater than the NiMH battery assembly results, with nickel leaching to groundwater accounting for most of the human toxicity cases and copper and nickel accounting for most of the freshwater ecotoxicity results. For the Li-ion laptop battery, human toxicity (cancer) cases and freshwater ecotoxicity results for the worst-case scenario were much

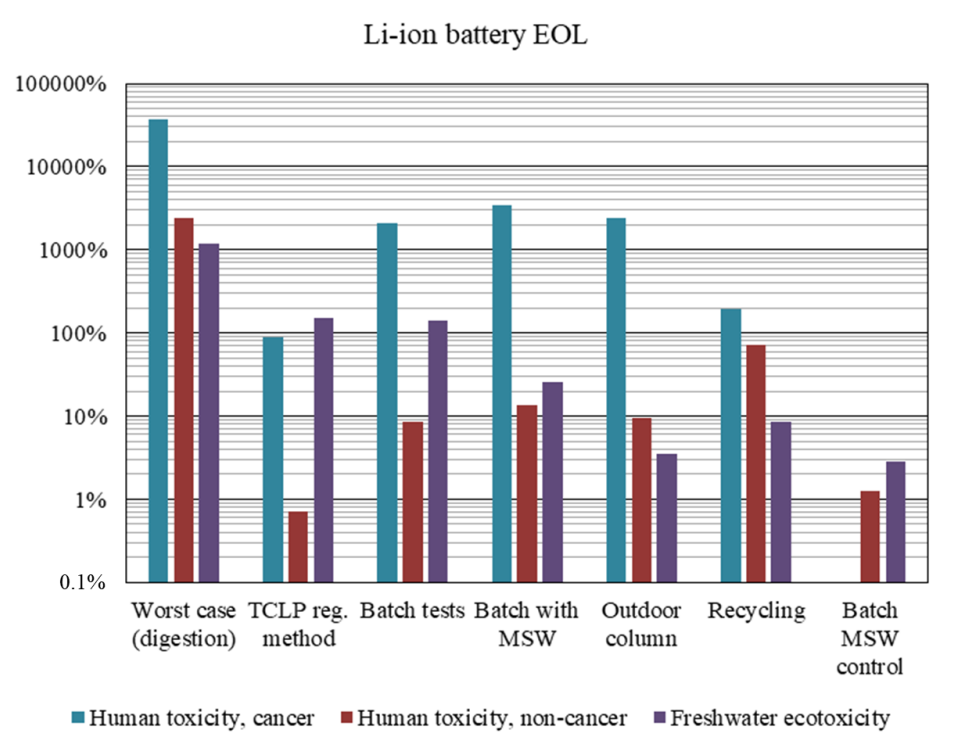

Figure 8.9: Comparison of results from USEtox for the Li-ion laptop battery EOL scenarios normalized to the results of 1 kg of generic MSW disposal. Note: Batch MSW control results are for 1 kg.

Table 8.11: EOL scenario results normalized to the assembly results for each product. Note: values greater than one percent of the calculated effects for the assembly of each product have been bolded.

Impact category	Worst case (digestion)	TCLP reg. method	Batch tests	Batch with MSW	Outdoor column	Recycling
c-Si PV module						
Human toxicity, cancer	0.028%	0.004%	0.006%	-	-	-
Human toxicity, non-cancer	**6.90%**	0.229%	0.345%	-	-	-
Freshwater ecotoxicity	**166%**	0.046%	**12.0%**	-	-	-
NiMH battery						
Human toxicity, cancer	**1243%**	**69.7%**	**21.3%**	**7.25%**	0.989%	**1.01%**
Human toxicity, non-cancer	**58.7%**	**17.2%**	**10.2%**	0.024%	0.003%	**1.33%**
Freshwater ecotoxicity	**318%**	**2.29%**	**4.76%**	0.329%	0.063%	0.760%
Li-ion battery						
Human toxicity, cancer	**313%**	0.766%	**17.9%**	**29.5%**	**20.4%**	**1.62%**
Human toxicity, non-cancer	**8.85%**	0.003%	0.031%	0.050%	0.035%	0.261%
Freshwater ecotoxicity	**158%**	**20.4%**	**19.0%**	**3.52%**	0.469%	**1.15%**

greater than the Li-ion battery assembly results, with nickel leaching to groundwater accounting for most of the human toxicity cases and copper and aluminum accounting for most of the freshwater ecotoxicity results. For the batch tests, batch tests with MSW, and outdoor column scenarios, the human toxicity (cancer) cases were approximately 18, 30, and 20 percent, respectively, of the assembly human toxicity (cancer) cases. With the worst-case scenario effects exceeding those of the assemblies and with notable effects for the other scenarios, the inclusion of EOL metal leaching is merited in LCAs of these products.

8.5 Conclusions and Future Work

Including landfill disposal with the potential for metal emissions to groundwater in LCAs of Li-ion and NiMH batteries and PV modules is useful to understand how this potential EOL scenario compares to the other life cycle phases of these products. Before comparing the potential EOL scenarios, the assemblies for each product were updated with disassembly and digestion data. Comparing the results from the EOL scenarios to the updated assembly results for each product demonstrated that although the effects for the EOL scenarios (not including the worst-case) were less than the assembly results, the effects were not insignificant and merit inclusion and further

study. Additionally, the abundance of these products used worldwide will lead to a large waste stream, and although the effects from the disposal of one product may be small, the effects from many will not.

Although the product assembly materials were updated in this study, the auxiliary manufacturing materials, energy, and transport values were not updated and should be evaluated in future work. This study focused on comparing the ecoinvent database products to disassembled and digested products, but future work could consider how changing, for example, the LiMnO4 cathode for the LiNiMnCoO2 cathode or the aluminum for steel housing, affects the entire life cycle environmental impacts by considering the possible changes in the use phase from altering the energy density or useful lifetime of the batteries when substituting materials. For this study, the functional unit used to compare the assemblies of the c-Si PV modules was 1 m^2 with a smaller mass per area for the Suniva module, but the efficiencies of modules have improved since the ecoinvent record was created. Therefore, per area, the Suniva module would generate more electricity, and the effect on the entire life cycle results should be investigated further. While this study focused on characterizing toxicity impacts from metal leaching from the active materials of e-waste at EOL, further investigation is needed for the other components of the products and their fate at EOL. Although narrowly focused on one life cycle aspect, the results from this study show that if EOL metal leaching is included in the disposal phase in the LCAs of these products, the potential toxicity effects are not as insignificant as previously thought in the literature.

8.6 References

Alsema, E. A.; de Wild-Scholten, M. J.; Fthenakis, V. M. Environmental Impacts of PV Electricity Generation-a Critical Comparison of Energy Supply Options. In *21st European Photovoltaic Solar Energy Conference, Dresden, Germany*; **2006**; Vol. 3201.

Bare, J. C. Traci. *J. Ind. Ecol.* **2002**, *6* (3–4), 49–78.

Battisti, R.; Corrado, A. Evaluation of Technical Improvements of Photovoltaic Systems through Life Cycle Assessment Methodology. *Energy* **2005**, *30* (7), 952–967.

Bayod-Rújula, Á. A.; Lorente-Lafuente, A. M.; Cirez-Oto, F. Environmental Assessment of Grid Connected Photovoltaic Plants with 2-Axis Tracking versus Fixed Modules Systems. *Energy* **2011**, *36* (5), 3148–3158.

Desideri, U.; Proietti, S.; Zepparelli, F.; Sdringola, P.; Bini, S. Life Cycle Assessment of a Ground-Mounted 1778kW P Photovoltaic Plant and Comparison with Traditional Energy Production Systems. *Appl. Energy* **2012**, *97*, 930–943.

DuPont. DuPont Tedlar Polyvinyl Fluoride (PVF) Films http://www.dupont.com/content/dam/dupont/products-and-services/membranes-and-films/pvf-films/documents/DEC_Tedlar_GeneralProperties.pdf (accessed Mar 29, 2018).

Ecoinvent Centre. Ecoinvent http://www.ecoinvent.org/ (accessed Sep 13, 2016).

Fantke, P.; Bijster, M.; Guignard, C.; Hauschild, M.; Huijbregts, M.; Jolliet, O.; Kounina, A.; Magaud, V.; Margni, M.; McKone, T.; et al. *USEtox 2.0 Documentation*; **2017**.

Fthenakis, V.; Kim, H. C.; Frischknecht, R.; Raugei, M.; Sinha, P.; Stucki, M. *Life Cycle Inventories and Life Cycle Assessment of Photovoltaic Systems*; International Energy Agency, **2011**; Vol. T12–02:201.

Fthenakis, V. M.; Kim, H. C.; Alsema, E. Emissions from Photovoltaic Life Cycles. *Environ. Sci. Technol.* **2008**, *42* (6), 2168–2174.

Gaustad, G.; Ganter, M.; Wang, X.; Bailey, C.; Babbitt, C.; Landi, B. Economic and Environmental Trade Offs for Li-Based Battery Recycling. In *Energy Technology 2012: Carbon Dioxide Management and Other Technologies*; **2012**; pp 219–226.

Gerbinet, S.; Belboom, S.; Léonard, A. Life Cycle Analysis (LCA) of Photovoltaic Panels: A Review. *Renew. Sustain. Energy Rev.* **2014**, *38*, 747–753.

Hawkins, T.; Gausen, O.; Stromman, A. Environmental Impacts of Hybrid and Electric vehicles—A Review. *Int. J. Life Cycle Assess.* **2012**, *17* (8), 997–1014.

Hawkins, T.; Singh, B.; Majeau-Bettez, G.; Strømman, A. Comparative Environmental Life Cycle Assessment of Conventional and Electric Vehicles. *J. Ind. Ecol.* **2013**, *17* (1), 53–64.

Hischier, R.; Classen, M.; Lehmann, M.; Scharnhorst, W. *Life Cycle Inventories of Electric and Electronic Equipment: Production, Use and Disposal; Ecoinvent Report No. 18*; **2007**.

Jungbluth, N.; Stucki, M.; Frischknecht, R. *Photovoltaics; Ecoinvent Report No. 6-XII*; **2009**.

Kang, D.; Chen, M.; Ogunseitan, O. Potential Environmental and Human Health Impacts of Rechargeable Lithium Batteries in Electronic Waste. *Environ. Sci. Technol.* **2013**, *47* (10), 5495–5503.

Larcher, D.; Tarascon, J.-M. Towards Greener and More Sustainable Batteries for Electrical Energy Storage. *Nat. Chem.* **2015**, *7* (1), 19–29.

Majeau-Bettez, G.; Hawkins, T. R.; Strømman, A. H. Life Cycle Environmental Assessment of Lithium-Ion and Nickel Metal Hydride Batteries for Plug-in Hybrid and Battery Electric Vehicles. *Environ. Sci. Technol.* **2011**, *45* (10), 4548–4554.

Mason, J. E.; Fthenakis, V. M.; Hansen, T.; Kim, H. C. Energy Payback and Life-Cycle CO2 Emissions of the BOS in an Optimized 3· 5 MW PV Installation. *Prog. Photovoltaics Res. Appl.* **2006**, *14* (2), 179–190.

Notter, D.; Gauch, M.; Widmer, R.; Wager, P.; Stamp, A.; Zah, R.; Althaus, H. Contribution of Li-Ion Batteries to the Environmental Impact of Electric Vehicles. *Environ. Sci. Technol.* **2010**, *44* (17), 6550–6556.

Olofsson, Y.; Romare, M. Life Cycle Assessment of Lithium-Ion Batteries from Plug-in Hybrid Buses, Chalmers University of Technology, **2013**.

Polman, A.; Knight, M.; Garnett, E. C.; Ehrler, B.; Sinke, W. C. Photovoltaic Materials: Present Efficiencies and Future Challenges. *Science (80-.).* **2016**, *352* (6283).

PRé. SimaPro 8. **2018**.

Richa, K.; Babbitt, C.; Gaustad, G.; Wang, X. A Future Perspective on Lithium-Ion Battery Waste Flows from Electric Vehicles. *Resour. Conserv. Recycl.* **2014**, *83*, 63–76.

Rosenbaum, R. K.; Huijbregts, M. a. J.; Henderson, A. D.; Margni, M.; McKone, T. E.; Meent, D.; Hauschild, M. Z.; Shaked, S.; Li, D. S.; Gold, L. S.; et al. USEtox Human Exposure and Toxicity Factors for Comparative Assessment of Toxic Emissions in Life Cycle Analysis: Sensitivity to Key Chemical Properties. *Int. J. Life Cycle Assess.* **2011**, *16* (8), 710–727.

SEIA National PV Recycling Program http://www.seia.org/seia-national-pv-recycling-program (accessed Aug 20, 2017).

USEPA. Method 1311 Toxicity Characteristic Leaching Procedure.

USEPA. *Application of Life-Cycle Assessment to Nanoscale Technology: Lithium-Ion Batteries from Electric Vehicles EPA 744-R-12-001*; **2013**.

USEPA. Tool for Reduction and Assessment of Chemicals and Other Environmental Impacts (TRACI) http://www.epa.gov/chemical-research/tool-reduction-and-assessment-chemicals-and-other-environmental-impacts-traci (accessed Feb 3, 2016).

Wang, Y.; Yu, Y.; Huang, K.; Chen, B.; Deng, W.; Yao, Y. Quantifying the Environmental Impact of a Li-Rich High-Capacity Cathode Material in Electric Vehicles via Life Cycle Assessment. *Environ. Sci. Pollut. Res.* **2017**, *24* (2), 1251–1260.

Yu, Y.; Chen, B.; Huang, K.; Wang, X.; Wang, D. Environmental Impact Assessment and End-of-Life Treatment Policy Analysis for Li-Ion Batteries and Ni-MH Batteries. *Int. J. Environ. Res. Public Health* **2014**, *11* (3), 3185–3198.

Zhong, Z. W.; Song, B.; Loh, P. E. LCAs of a Polycrystalline Photovoltaic Module and a Wind Turbine. *Renew. Energy* **2011**, *36* (8), 2227–2237.

Chapter 9: Conclusions and Future Work

As the use of photovoltaic (PV) modules and batteries rapidly increases to meet the growing worldwide energy demand, so does the waste stream of these products. At end-of-life (EOL), these products could be disposed of with municipal solid waste (MSW), which is likely to occur in locations without sufficient recycling laws or take-back programs. In this work, metal leaching from PV modules and two types of batteries (Li-ion and nickel metal hydride (NiMH)) was studied using the regulatory Toxicity Characteristic Leaching Procedure (TCLP) as well as batch leaching and outdoor column testing. The data from the leaching tests were used to build waste scenarios utilizing life cycle assessment (LCA) software.

The experimental data collected from the batch leaching tests and outdoor columns in Chapters 4, 5, and 7 demonstrate the complexity of characterizing PV and battery e-waste and developing EOL regulations and procedures that are applicable to each type of e-waste. Although for some of the e-wastes tested that would not be classified as hazardous waste based on TCLP results, metal concentrations observed in the batch leaching tests using a simulated landfill leachate and over a longer time period were much greater than observed for the TCLP. These observed differences signal that the TCLP might not be adequate for predicting metal concentrations leached from some types of e-wastes in landfill conditions. For the batch tests with e-waste mixed with MSW, both lower (Pb and Hg) and higher (Co and Ni) metal leachate concentrations were observed than for the batch tests without MSW, demonstrating the complexity of developing laboratory tests to predict or describe metal leaching in landfill conditions. In the outdoor column experiments, As, Hg, and Pb were not detected in column leachate samples, even though they were present in the batch leaching tests. Co, Cu, and Ni were detected in leachate samples, which could be of concern in an improperly managed landfill.

Taking the data gathered from the leaching tests, EOL scenarios for metal emissions to groundwater were modeled using LCA software to characterize toxicity effects. The results showed that the worst-case EOL scenario effects exceeded those of the assembly of each product. Notable effects of greater than one percent of the assembly effects where observed for the other EOL scenarios, demonstrating that the inclusion of EOL metal leaching is merited in LCAs of these products and should be studied further. Appropriate characterization tools and techniques to ensure adequate protection of the environment are necessary to avoid a growing e-waste problem while simultaneously promoting renewable energy sources.

Moving forward, more work is needed to fully understand the EOL phase of the complex e-waste stream for PV and battery technologies. Although the batch and column leaching tests and LCA modeling in this work contribute to understanding some aspects of landfill disposal of these products, many questions still remain. As discussed below, additional testing under different conditions with different products as well as exploring long-term trends in sorption behavior under changing landfill conditions are needed. This work focused on silicon PV modules, which have the largest market share for PV types, but future work should consider other types of PV including thin films and emerging technologies such as organic and perovskite cells. Because the changing conditions within a solid waste landfill are not well represented by leaching tests in a laboratory setting, i.e., an aerobic atmosphere at room temperature, additional factors and conditions affecting leaching behavior should be studied. Changes in temperature could affect leaching kinetics and extent, and redox cycling from aerobic to anaerobic conditions will affect metal speciation which will in turn affect leachate concentrations. The leachates used in the batch tests represented the acidic phase in the lifetime of landfills, but e-waste degradation in leachates representing other phases in the lifetime of landfills, especially when less organic matter is present, should be studied.

In the batch tests mixed with MSW, the microbial community and structure, especially for the biofilm, should be examined because metal ion partitioning to the biofilm affected the metal ion concentrations in the leachate. Future work should also examine the behavior of the sulfide minerals formed during the leaching tests and their interactions with the metals leached from the e-wastes. Will the sulfide minerals remain insoluble over a longer time period than the sampling period for this study or can conditions within the waste matrix change sufficiently over time for the metals to become soluble again? Similarly, as the composition of landfill waste changes as current efforts to divert organic wastes to composting or incineration become more prevalent, the capacity for MSW landfills to keep metals immobile could diminish, and such a scenario should be considered in future work.

After the outdoor columns have aged longer in the test bed, the waste columns should be dissected to examine the physical degradation of the e-wastes. Samples of the e-wastes could be examined using optical microscopy and electron microscopy to determine physical and chemical changes compared to samples of the e-wastes not aged in the columns. Additionally, samples of the MSW and soil mixture removed from the columns could be digested using a sequential extraction method to determine metal partitioning to the different components of the waste matrix, especially Pb partitioning. Dissecting the columns could provide additional insight into the rate and extent of metal leaching from e-wastes and the potential mobility of metals in landfill conditions. During this work, it was determined that a multi-year exposure of the e-waste to leachate in the columns would be beneficial. Thus, the outdoor columns were in left in place for future destructive testing.

Utilizing LCA software, the product assemblies in the ecoinvent database were updated for the PV module and Li-ion and NiMH batteries, but the auxiliary manufacturing materials, energy, and transport values were not. The auxiliary processes could have changed since the

database was last updated and the sensitivity of the results to changes should be investigated further. Future work could consider how changing materials, such as the cathode, electrolyte, or housing, in batteries affects the entire life cycle environmental impacts, including possible changes in the use phase from altering the energy density or useful lifetime of the batteries. For different product applications, the components could be optimized by product designers and manufacturers to have the least environmental impacts over their life cycles. In addition to characterizing toxicity impacts from metal leaching from the active materials of e-waste at EOL, further investigation is needed for the other components of the products and their fate at EOL. A more in-depth model combining e-waste metal leaching with the impacts from operating landfills, including leachate treatment processes, should be developed.

Appendices

Appendix A: Supplementary Data from Chapter 5

Table A.1: Extractable masses for the PV module pieces without module frame and battery electrodes without battery housing. Waste labels and numbers correspond to Table 5.1.

	1 c-Si module	2 mc-Si module	3 laptop battery (per cell)	3 laptop battery (per battery)	4 NiMH power tool battery (per cell)	4 NiMH power tool battery (per battery)	5 Li-ion power tool battery (per cell)	5 Li-ion power tool battery (per battery)	6 phone replacement battery	7 flashlight battery	8 solar light battery	9 camera battery	10 watch battery
	[mg]	[mg]	[mg]	[mg]	[mg]	[mg]	[mg]	[mg]	[mg]	[mg]	[mg]	[mg]	[mg]
Ag	16303	8636	0.517	3.10	ND	ND	0.966	5.80	0.073	0.249	0.011	0.596	0.271
Al	61609	65569	1328	7968	227.6	2731	1986	11918	1085	1843	521	4.70	2.12
As	ND	ND	ND	ND	58.94	707	ND	ND	0.127	ND	ND	ND	ND
Ba	11.9	54.7	0.539	3.23	2.09	25.10	0.321	1.93	0.077	0.057	0.081	ND	ND
Bi	ND	ND	ND	ND	ND	ND	ND	ND	ND	ND	ND	0.277	0.122
Co	4.6	172	2115	12691	1919	23026	1079	6471	7694	9985	1.05	0.154	0.076
Cr	ND	ND	0.595	3.57	ND	ND	0.873	5.24	ND	0.215	0.290	7.15	0.397
Cu	240690	274730	3185	19109	4241	50891	7596	45577	3122	4065	1304	1.31	0.453
Fe	705	748	ND	ND	ND	ND	ND	ND	ND	ND	896	33.19	0.433
Ga	ND	ND	ND	ND	ND	ND	ND	ND	0.964	ND	0.053	ND	ND
Hg	ND	ND	27.59	166	15.53	186	8.39	50.32	157.0	201.7	ND	ND	ND
In	ND	ND	ND	ND	ND	ND	ND	ND	14.06	17.56	ND	0.097	0.070
Mn	34.0	256	2570	15422	817	9799	3217	19304	0.332	959	0.348	3282	1436
Ni	ND	310	4837	29022	22212	266546	2634	15803	993	2078	0.851	0.179	0.129
Pb	46528	18291	7.88	47.26	8.00	96.00	14.15	84.9	12.96	16.35	2.45	0.187	0.100
Se	ND	ND	ND	ND	ND	ND	ND	ND	ND	ND	ND	1.01	0.447
Tl	ND	ND	9.53	57.18	ND	ND	4.66	28.0	38.00	49.02	ND	0.580	0.300
Zn	683	511	0.534	3.20	792	9504	0.414	2.48	1.18	0.703	1.06	0.038	0.098
Percent:	2.4%	2.5%	43.3%	-	74.9%	-	61.3%	-	61.2%	55.7%	31.2%	35.0%	41.2%
Electrode (no plastics) mass [g]:	-	-	32.56	-	40.44	-	26.98	-	21.44	34.47	8.73	9.51	3.50
Total mass [g]:	15170	14910	42.5	310.26	56.20	799.93	40.70	351.89	25.40	45.90	14.85	16.35	6.65

Appendix B: Dielectric Permittivity and Water Content Calibration of Decagon 5TE Sensors for EPSCoR Soil, Soil and Sand, and Landfill Materials

Decagon 5TE sensors measure apparent dielectric permittivity (unitless range from 1 to 80) using an oscillator running at 70 MHz, which can be converted to volumetric water content. For a typical soil, the Topp Equation (Topp et al., 1980) can be used for the conversion. However, if higher accuracy is desired or the media is not a typical soil, then a calibration needs to be performed. Decagon has developed a calibration method (Cobos and Chambers, 2010), which has been used to determine the calibration curves for the media (soil) used in the EPSCoR lysimeters and (simulated landfill material) used in the landfill columns.

To perform the calibration, air dry media is packed into a container large enough to accommodate the 5TE sensor range at approximately the bulk density of the lysimeters or simulated landfill columns. The 5TE sensor is inserted vertically and a dielectric permittivity reading is recorded. The sensor is removed and re-inserted in a slightly different area, and another reading is recorded, which is repeated once more. A volumetric sample is taken from the media, mass recorded, and placed in an oven at 75 degrees Celsius to dry for 48 hours. These steps are repeated to obtain a second set of readings and volumetric sample at each water content. Approximately one milliliter of DDI water for SRS soil or simulated landfill leachate for bioreactor columns per ten milliliters of media volume is mixed into the media and the sensor reading and volumetric sample steps are repeated until the media reaches saturation, which is approximately five repetitions. After the media samples are dry, their masses are recorded, and the volumetric water content of each sample is calculated and plotted against the dielectric permittivity readings (Figures B.1–B.3). For the SRS soil, a linear fit described the data with a R^2 value of 0.9832 (Eq. B.1).

$$VWC_{SRS\ Soil} = 100(0.0245(dp) - 0.0533) \qquad \text{(Eq. B.1)}$$

$VWC_{SRS\ Soil}$ is the volumetric water content of the SRS soil expressed as a percentage and dp is the dielectric permittivity.). For the SRS soil (50%) and sand (50%) mixture, a linear fit described the data with a R^2 value of 0.9807 (Eq. B.2).

$$VWC_{SRS\ Soil/Sand} = 100(0.0237(dp) - 0.029) \qquad \text{(Eq. B.2)}$$

Where $VWC_{SRS\ Soil/Sand}$ is the volumetric water content of the SRS soil/sand mixture expressed as a percentage and dp is the dielectric permittivity. For the simulated landfill materials, a quadratic fit described the data with a R^2 value of 0.9038 (Eq. B.3). For media with a high organic matter content, the best fit is sometimes found using a quadratic equation (Cobos and Chambers, 2010).

$$VWC_{Landfill} = 100(-0.0001(dp)^2 + 0.0135(dp) + 0.0064) \qquad \text{(Eq. B.3)}$$

Where $VWC_{Landfill}$ is the volumetric water content of the simulated landfill materials expressed as a percentage and dp is the dielectric permittivity.

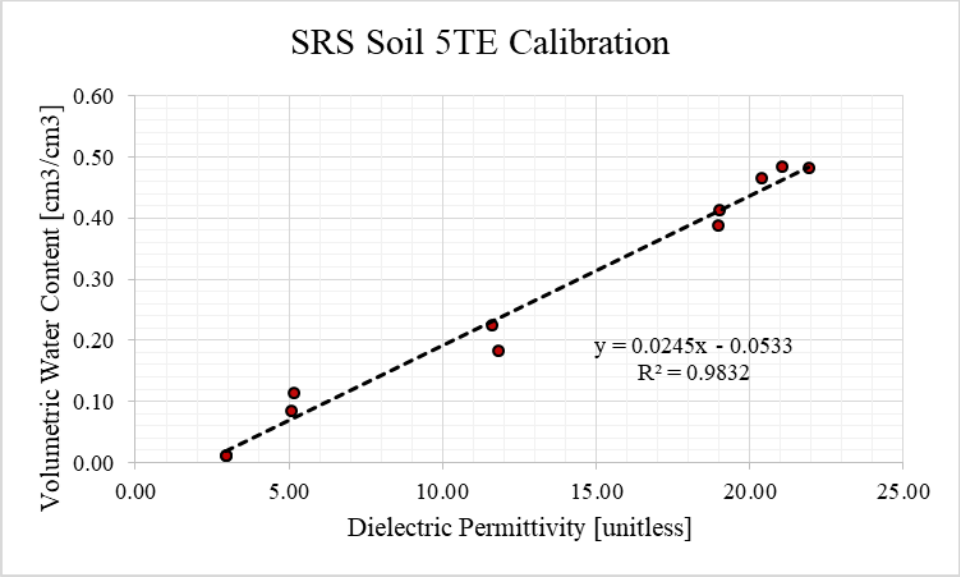

Figure B.1: Volumetric water content 5TE calibration for SRS soil.

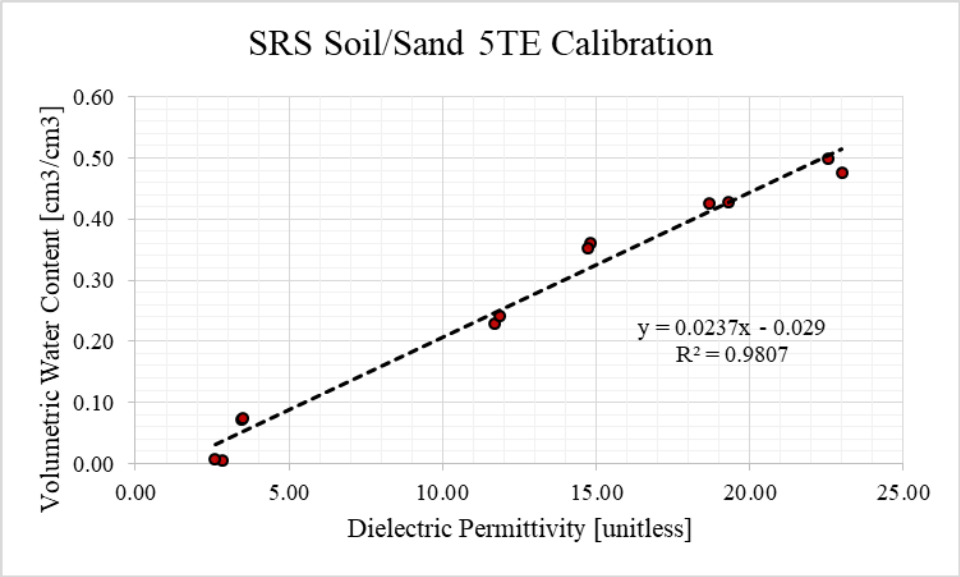

Figure B.2: Volumetric water content 5TE calibration for SRS soil/sand.

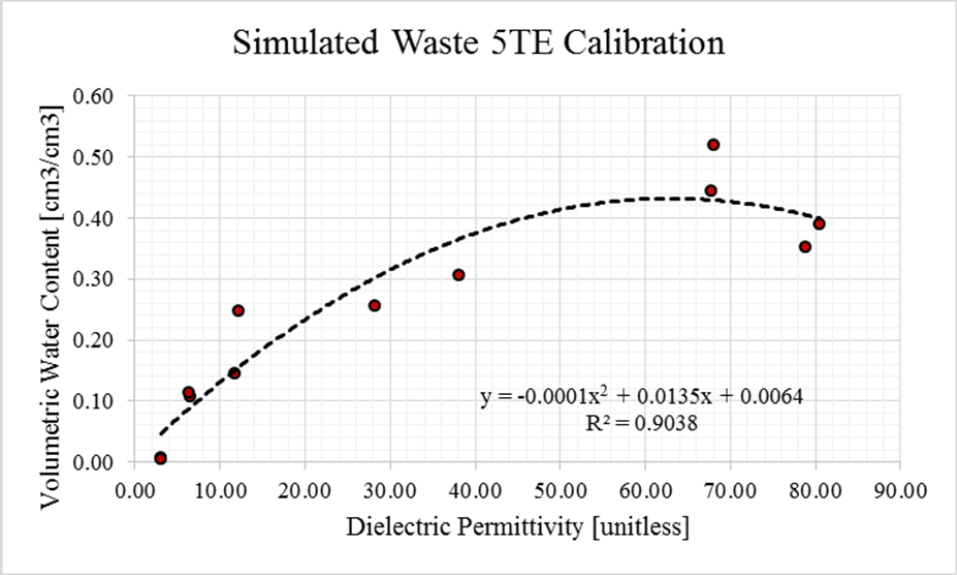

Figure B.3: Volumetric water content 5TE calibration for waste materials.

Appendix C: Wiring Guide and CRBasic Programs for Dataloggers

Table C.1: Wiring guide for CR6 dataloggers and AM16/32B multiplexers.

CR6 #1	**AM16/32 #1 (2X32)**
SW1	COM Odd H
U3	COM Odd H
U1	COM Odd L
U4	COM Odd L
G	COM G
C4	RES
C1	CLK
12V	12V
G	G

CR6 #2	**AM16/32 #1 (4X16)**
U1	COM Odd H
U2	COM Odd L
G	COM G
C4	RES
C1	CLK
12V	12V
G	G
U3	COM Even H
G	G

CR6 #1	**AM16/32 #2 (2X32)**
SW1	COM Odd H
U7	COM Odd H
U5	COM Odd L
U8	COM Odd L
G	COM G
C4	RES
C2	CLK
12V	12V
G	G

CR6 #2	**AM16/32 #2 (4X16)**
U5	COM Odd H
U6	COM Odd L
G	COM G
C4	RES
C2	CLK
12V	12V
G	G
U7	COM Even H
G	G

CR6 #1	**AM16/32 #3 (2X32)**
SW1	COM Odd H
U11	COM Odd H
U9	COM Odd L
U12	COM Odd L
G	COM G
C4	RES
C3	CLK
12V	12V
G	G

CRBasic code for CR6 #1 which can have three multiplexers connected in 2X32 mode.

```
' This program works for CR6 #1 which has two multiplexers in 2X32 mode. (Can be updated to
' accommodate a third multiplexer)
' This program is configured for deploying 7 lysimeters with Decagon sensors on the first multiplexer,
' and 5 lysimeters with Decagon sensors on the second multiplexer.
' The 1st four lysimeters (#'s: 1, 11, 12, and 13) only have 5TE sensors.
' Note: the order of deployment does not follow numerical order

' Lysimeter Descriptions (Multiplexer #1)
   ' Lysimeter 1: "Baraka" Kathryn NpO2 (3 5TEs)
   ' Lysimeter 11: Kayla Waste PV (3 5TEs)
   ' Lysimeter 12: Kayla Waste Battery1 (3 5TEs)
   ' Lysimeter 13: Kayla Waste Battery2 (3 5TEs)
   ' Lysimeter 3: "Kylo" only plant (3 5TEs and 2 MPS-6s)
   ' Lysimeter 4: "Luke" U-P and Na-22 (3 5TEs and 2 MPS-6s)
   ' Lysimeter 5: "Leia" U-P and Na-22 (3 5TEs and 2 MPS-6s)

' Lysimeter Descriptions (Multiplexer #2)
   ' Lysimeter 8: "Gareth" Manchester UO2 (3 5TEs and 2 MPS-6s)
   ' Lysimeter 9: "Connaugh" Manchester U-Mag (3 5TEs and 2 MPS-6s)
   ' Lysimeter 10: "Will" Manchester UO3 (3 5TEs and 2 MPS-6s)
   ' Lysimeter 6: "Han" U-P and Na-22 no plant (3 5TEs and 2 MPS-6s)
   ' Lysimeter 7: "Chewie" U-P (3 5TEs and 2 MPS-6s)

' Set up scanning intervals for data collection (2 hours = 7200 sec)
Const DATA_INTERVAL_SECONDS = 7200
Const SCAN_INTERVAL_SECONDS = 7200

' Number of lysimeters with only 5TE sensors on the first multiplexer
Const LYSIMETER_COUNT_SPECIAL = 4

' Number of lysimeters with 5TE and MPS6 to measure on each of the three multiplexers
' LYSIMETER_COUNT_1 for the fully instrumented lysimeters on the 1st multiplexer
Const LYSIMETER_COUNT_1 = 3
' LYSIMETER_COUNT_2 for lysimeters connected to the 2nd multiplexer
Const LYSIMETER_COUNT_2 = 5
' LYSIMETER_COUNT_3 for lysimeters connected to the 3rd multiplexer (commented out because there
' isn't a third multiplexer right now)
'Const LYSIMETER_COUNT_3 = 0

' Each lysimeter has three 5TE sensors and two MPS6 sensors (the special lysimeters still have 3 5TEs)
Const LYSIMETER_5TE_COUNT = 3
Const LYSIMETER_MPS6_COUNT = 2

' The total number of 5TE sensors and MPS6 sensors
Const TOTAL_5TE = (LYSIMETER_COUNT_1 + LYSIMETER_COUNT_2 +
LYSIMETER_COUNT_SPECIAL) * LYSIMETER_5TE_COUNT
Const TOTAL_MPS6 = (LYSIMETER_COUNT_1 + LYSIMETER_COUNT_2) *
LYSIMETER_MPS6_COUNT

' Data for each sensor set
Public Data_5TE(TOTAL_5TE, 3)
```

```
Public Data_MPS6(TOTAL_MPS6, 2)

Dim Current_5TE, Current_MPS6

' Labels for the 5TE sensor data. These labels appear in the actual data file
' which is output by LoggerNet. If less than ten lysimeters are deployed, apostrophes
' need to be added in front of each unused label.

' Lysimeter 1: "Baraka" Kathryn NpO2
Alias Data_5TE(1, 1) = VWC_1_1
Alias Data_5TE(1, 2) = BEC_1_1
Alias Data_5TE(1, 3) = TMP_1_1
Alias Data_5TE(2, 1) = VWC_1_2
Alias Data_5TE(2, 2) = BEC_1_2
Alias Data_5TE(2, 3) = TMP_1_2
Alias Data_5TE(3, 1) = VWC_1_3
Alias Data_5TE(3, 2) = BEC_1_3
Alias Data_5TE(3, 3) = TMP_1_3

' Lysimeter 11: Kayla Waste PV
Alias Data_5TE(4, 1) = VWC_11_1
Alias Data_5TE(4, 2) = BEC_11_1
Alias Data_5TE(4, 3) = TMP_11_1
Alias Data_5TE(5, 1) = VWC_11_2
Alias Data_5TE(5, 2) = BEC_11_2
Alias Data_5TE(5, 3) = TMP_11_2
Alias Data_5TE(6, 1) = VWC_11_3
Alias Data_5TE(6, 2) = BEC_11_3
Alias Data_5TE(6, 3) = TMP_11_3

' Lysimeter 12: Kayla Waste Battery1
Alias Data_5TE(7, 1) = VWC_12_1
Alias Data_5TE(7, 2) = BEC_12_1
Alias Data_5TE(7, 3) = TMP_12_1
Alias Data_5TE(8, 1) = VWC_12_2
Alias Data_5TE(8, 2) = BEC_12_2
Alias Data_5TE(8, 3) = TMP_12_2
Alias Data_5TE(9, 1) = VWC_12_3
Alias Data_5TE(9, 2) = BEC_12_3
Alias Data_5TE(9, 3) = TMP_12_3

' Lysimeter 13: Kayla Waste Battery2
Alias Data_5TE(10, 1) = VWC_13_1
Alias Data_5TE(10, 2) = BEC_13_1
Alias Data_5TE(10, 3) = TMP_13_1
Alias Data_5TE(11, 1) = VWC_13_2
Alias Data_5TE(11, 2) = BEC_13_2
Alias Data_5TE(11, 3) = TMP_13_2
Alias Data_5TE(12, 1) = VWC_13_3
Alias Data_5TE(12, 2) = BEC_13_3
Alias Data_5TE(12, 3) = TMP_13_3

' Lysimeter 3: "Kylo" only plant
```

```
Alias Data_5TE(13, 1) = VWC_3_1
Alias Data_5TE(13, 2) = BEC_3_1
Alias Data_5TE(13, 3) = TMP_3_1
Alias Data_5TE(14, 1) = VWC_3_2
Alias Data_5TE(14, 2) = BEC_3_2
Alias Data_5TE(14, 3) = TMP_3_2
Alias Data_5TE(15, 1) = VWC_3_3
Alias Data_5TE(15, 2) = BEC_3_3
Alias Data_5TE(15, 3) = TMP_3_3

' Lysimeter 4: "Luke" U-P and Na-22
Alias Data_5TE(16, 1) = VWC_4_1
Alias Data_5TE(16, 2) = BEC_4_1
Alias Data_5TE(16, 3) = TMP_4_1
Alias Data_5TE(17, 1) = VWC_4_2
Alias Data_5TE(17, 2) = BEC_4_2
Alias Data_5TE(17, 3) = TMP_4_2
Alias Data_5TE(18, 1) = VWC_4_3
Alias Data_5TE(18, 2) = BEC_4_3
Alias Data_5TE(18, 3) = TMP_4_3

' Lysimeter 5: "Leia" U-P and Na-22
Alias Data_5TE(19, 1) = VWC_5_1
Alias Data_5TE(19, 2) = BEC_5_1
Alias Data_5TE(19, 3) = TMP_5_1
Alias Data_5TE(20, 1) = VWC_5_2
Alias Data_5TE(20, 2) = BEC_5_2
Alias Data_5TE(20, 3) = TMP_5_2
Alias Data_5TE(21, 1) = VWC_5_3
Alias Data_5TE(21, 2) = BEC_5_3
Alias Data_5TE(21, 3) = TMP_5_3

' Lysimeter 8: "Gareth" Manchester UO2
Alias Data_5TE(22, 1) = VWC_8_1
Alias Data_5TE(22, 2) = BEC_8_1
Alias Data_5TE(22, 3) = TMP_8_1
Alias Data_5TE(23, 1) = VWC_8_2
Alias Data_5TE(23, 2) = BEC_8_2
Alias Data_5TE(23, 3) = TMP_8_2
Alias Data_5TE(24, 1) = VWC_8_3
Alias Data_5TE(24, 2) = BEC_8_3
Alias Data_5TE(24, 3) = TMP_8_3

' Lysimeter 9: "Connaugh" Manchester U-Mag
Alias Data_5TE(25, 1) = VWC_9_1
Alias Data_5TE(25, 2) = BEC_9_1
Alias Data_5TE(25, 3) = TMP_9_1
Alias Data_5TE(26, 1) = VWC_9_2
Alias Data_5TE(26, 2) = BEC_9_2
Alias Data_5TE(26, 3) = TMP_9_2
Alias Data_5TE(27, 1) = VWC_9_3
Alias Data_5TE(27, 2) = BEC_9_3
Alias Data_5TE(27, 3) = TMP_9_3
```

```
' Lysimeter 10: "Will" Manchester UO3
Alias Data_5TE(28, 1) = VWC_10_1
Alias Data_5TE(28, 2) = BEC_10_1
Alias Data_5TE(28, 3) = TMP_10_1
Alias Data_5TE(29, 1) = VWC_10_2
Alias Data_5TE(29, 2) = BEC_10_2
Alias Data_5TE(29, 3) = TMP_10_2
Alias Data_5TE(30, 1) = VWC_10_3
Alias Data_5TE(30, 2) = BEC_10_3
Alias Data_5TE(30, 3) = TMP_10_3

' Lysimeter 6: "Han" U-P and Na-22 no plant
Alias Data_5TE(31, 1) = VWC_6_1
Alias Data_5TE(31, 2) = BEC_6_1
Alias Data_5TE(31, 3) = TMP_6_1
Alias Data_5TE(32, 1) = VWC_6_2
Alias Data_5TE(32, 2) = BEC_6_2
Alias Data_5TE(32, 3) = TMP_6_2
Alias Data_5TE(33, 1) = VWC_6_3
Alias Data_5TE(33, 2) = BEC_6_3
Alias Data_5TE(33, 3) = TMP_6_3

' Lysimeter 7: "Chewie" U-P
Alias Data_5TE(34, 1) = VWC_7_1
Alias Data_5TE(34, 2) = BEC_7_1
Alias Data_5TE(34, 3) = TMP_7_1
Alias Data_5TE(35, 1) = VWC_7_2
Alias Data_5TE(35, 2) = BEC_7_2
Alias Data_5TE(35, 3) = TMP_7_2
Alias Data_5TE(36, 1) = VWC_7_3
Alias Data_5TE(36, 2) = BEC_7_3
Alias Data_5TE(36, 3) = TMP_7_3

' Labels for the MPS6 sensor data.

' Lysimeter 1 (doesn't have MPS6 sensors)
' Lysimeter 11 (doesn't have MPS6 sensors)
' Lysimeter 12 (doesn't have MPS6 sensors)
' Lysimeter 13 (doesn't have MPS6 sensors)

' Lysimeter 3: "Kylo" only plant
Alias Data_MPS6(1, 1) = POTENTIAL_3_1
Alias Data_MPS6(1, 2) = MPS6_TEMP_3_1
Alias Data_MPS6(2, 1) = POTENTIAL_3_2
Alias Data_MPS6(2, 2) = MPS6_TEMP_3_2

' Lysimeter 4: "Luke" U-P and Na-22
Alias Data_MPS6(3, 1) = POTENTIAL_4_1
Alias Data_MPS6(3, 2) = MPS6_TEMP_4_1
Alias Data_MPS6(4, 1) = POTENTIAL_4_2
Alias Data_MPS6(4, 2) = MPS6_TEMP_4_2
```

```
' Lysimeter 5: "Leia" U-P and Na-22
Alias Data_MPS6(5, 1) = POTENTIAL_5_1
Alias Data_MPS6(5, 2) = MPS6_TEMP_5_1
Alias Data_MPS6(6, 1) = POTENTIAL_5_2
Alias Data_MPS6(6, 2) = MPS6_TEMP_5_2

' Lysimeter 8: "Gareth" Manchester UO2
Alias Data_MPS6(7, 1) = POTENTIAL_8_1
Alias Data_MPS6(7, 2) = MPS6_TEMP_8_1
Alias Data_MPS6(8, 1) = POTENTIAL_8_2
Alias Data_MPS6(8, 2) = MPS6_TEMP_8_2

' Lysimeter 9: "Connaugh" Manchester U-Mag
Alias Data_MPS6(9, 1) = POTENTIAL_9_1
Alias Data_MPS6(9, 2) = MPS6_TEMP_9_1
Alias Data_MPS6(10, 1) = POTENTIAL_9_2
Alias Data_MPS6(10, 2) = MPS6_TEMP_9_2

' Lysimeter 10: "Will" Manchester UO3
Alias Data_MPS6(11, 1) = POTENTIAL_10_1
Alias Data_MPS6(11, 2) = MPS6_TEMP_10_1
Alias Data_MPS6(12, 1) = POTENTIAL_10_2
Alias Data_MPS6(12, 2) = MPS6_TEMP_10_2

' Lysimeter 6: "Han" U-P and Na-22 no plant
Alias Data_MPS6(13, 1) = POTENTIAL_6_1
Alias Data_MPS6(13, 2) = MPS6_TEMP_6_1
Alias Data_MPS6(14, 1) = POTENTIAL_6_2
Alias Data_MPS6(14, 2) = MPS6_TEMP_6_2

' Lysimeter 7: "Chewie" U-P
Alias Data_MPS6(15, 1) = POTENTIAL_7_1
Alias Data_MPS6(15, 2) = MPS6_TEMP_7_1
Alias Data_MPS6(16, 1) = POTENTIAL_7_2
Alias Data_MPS6(16, 2) = MPS6_TEMP_7_2

' Construct a DataTable out of the 5TE Public arrays above
DataTable(Output5TE, True, -1)
  DataInterval(0, DATA_INTERVAL_SECONDS, Sec, 0)
  Sample(TOTAL_5TE * 3, Data_5TE(), FP2)
EndTable

' Construct a DataTable out of the MPS6 Public arrays above
DataTable(OutputMPS6, True, -1)
  DataInterval(0, DATA_INTERVAL_SECONDS, Sec, 0)
  Sample(TOTAL_MPS6 * 2, Data_MPS6(), FP2)
EndTable

Sub ResetCounters()
  Current_5TE = 0
  Current_MPS6 = 0
EndSub
```

```
' Go to the next input on the mux connected to port C1.
Sub MuxNext_1()
  ' Pulse the CLK port of the multiplexer for 10ms and allow for settling with
  ' a delay.
  PulsePort(C1, 10000)
  Delay(0, 15, mSec)
EndSub

' Go to the next input on the mux connected to port C2.
Sub MuxNext_2()
  ' Pulse the CLK port of the multiplexer for 10ms and allow for settling with
  ' a delay.
  PulsePort(C2, 10000)
  Delay(0, 15, mSec)
EndSub

' Commented out because the third multiplexer isn't being used
' Go to the next input on the mux connected to port C3.
'Sub MuxNext_3()
  ' Pulse the CLK port of the multiplexer for 10ms and allow for settling with
  ' a delay.
'  PulsePort(C3, 10000)
'  Delay(0, 15, mSec)
'EndSub

Sub SensorOn()
  SW12(1, 1)
  Delay(0, 1, Sec)
EndSub

Sub SensorOff()
  SW12(1, 0)
EndSub

Sub MuxOn()
  PortSet(C4, 1)
EndSub

Sub MuxOff()
  PortSet(C4, 0)
EndSub

' Measure 5TE sensors on the first multiplexer
Sub Measure5TE_1()
  Current_5TE += 1
  SDI12Recorder(Data_5TE(Current_5TE, 1), U1, 1, "?!", 1.0, 0)
  SDI12Recorder(Data_5TE(Current_5TE, 1), U1, 1, "M!", 1.0, 0)
EndSub

' Measure 5TE sensors on the second multiplexer
Sub Measure5TE_2()
  Current_5TE += 1
  SDI12Recorder(Data_5TE(Current_5TE, 1), U5, 1, "?!", 1.0, 0)
```

```
  SDI12Recorder(Data_5TE(Current_5TE, 1), U5, 1, "M!", 1.0, 0)
EndSub

' Measure MPS6 sensors on the first multiplexer.
Sub MeasureMPS6_1()
  Current_MPS6 += 1
  SDI12Recorder(Data_MPS6(Current_MPS6, 1), U1, 1, "?!", 1.0, 0)
  SDI12Recorder(Data_MPS6(Current_MPS6, 1), U1, 1, "M!", 1.0, 0)
EndSub

' Measure MPS6 sensors on the second multiplexer.
Sub MeasureMPS6_2()
  Current_MPS6 += 1
  SDI12Recorder(Data_MPS6(Current_MPS6, 1), U5, 1, "?!", 1.0, 0)
  SDI12Recorder(Data_MPS6(Current_MPS6, 1), U5, 1, "M!", 1.0, 0)
EndSub

' Measure all the sensors connected to one lysimeter on the first multiplexer.
Sub MeasureLysimeter_1()
  Dim i

  For i = 1 To LYSIMETER_5TE_COUNT
    MuxNext_1()
    SensorOn()
    Measure5TE_1()
    SensorOff()
  Next i

  For i = 1 To LYSIMETER_MPS6_COUNT
    MuxNext_1()
    SensorOn()
    MeasureMPS6_1()
    SensorOff()
  Next i
EndSub

' Measure the lysimeters with only 5TE sensors connected to the first multiplexer
Sub MeasureSpecialLysimeter()
  Dim i

  For i = 1 To LYSIMETER_5TE_COUNT
    MuxNext_1()
    SensorOn()
    Measure5TE_1()
    SensorOff()
  Next i
EndSub

' Measure all the sensors connected to one lysimeter on the second multiplexer.
Sub MeasureLysimeter_2()
  Dim i

  For i = 1 To LYSIMETER_5TE_COUNT
```

```
    MuxNext_2()
    SensorOn()
    Measure5TE_2()
    SensorOff()
  Next i

  For i = 1 To LYSIMETER_MPS6_COUNT
    MuxNext_2()
    SensorOn()
    MeasureMPS6_2()
    SensorOff()
  Next i
EndSub

SequentialMode
BeginProg
  Scan(SCAN_INTERVAL_SECONDS, Sec, 0, 0)
    ResetCounters()
    MuxOn()

    Dim i

    ' Lysimeters with only 5TES are the first ones on the first mux!
       For i = 1 To LYSIMETER_COUNT_SPECIAL
            MeasureSpecialLysimeter()
       Next i

       For i = 1 To LYSIMETER_COUNT_1
         MeasureLysimeter_1()
       Next i

       For i = 1 To LYSIMETER_COUNT_2
         MeasureLysimeter_2()
       Next i

    MuxOff()

    CallTable(Output5TE)
    CallTable(OutputMPS6)
  NextScan
EndProg
```

CRBasic code for CR6 #2 which can have two multiplexers connected in 4X16 mode.

```
' This program works for CR6 #2 which has one multiplexer in 4X16 mode.
' This program is configured for deploying 5 lysimeters with load cells on one multiplexer.
' An additional multiplexer in 4X16 mode can be added later.

' Set up scanning intervals for data collection (300 seconds = 5 minutes)
Const DATA_INTERVAL_SECONDS = 300
Const SCAN_INTERVAL_SECONDS = 300
```

```
' Number of lysimeters with loadcells to measure on each of the two multiplexers
' LYSIMETER_COUNT_1 for lysimeters connected to first multiplexer
Const LYSIMETER_COUNT_1 = 5
' LYSIMETER_COUNT_2 for lysimeters connected to second multiplexer
'Const LYSIMETER_COUNT_2 = 0

' Each lysimeter has three load cells
Const LYSIMETER_LOADCELL_COUNT = 3

' The total number of load cells for the datalogger
Const TOTAL_LOADCELL = (LYSIMETER_COUNT_1) * LYSIMETER_LOADCELL_COUNT

' Data for each load cell and battery voltage reading
Public Data_LOADCELL(TOTAL_LOADCELL,1)
Public BattV

Dim Current_LOADCELL

' Labels for loadcell data. Lysimeters 6 and 7 deployed first, then 3,4,5

'Lysimeter 6: "Han" U-P and Na-22 no plant
Alias Data_LOADCELL(1) = LOADCELLOUTPUT_6_1
Alias Data_LOADCELL(2) = LOADCELLOUTPUT_6_2
Alias Data_LOADCELL(3) = LOADCELLOUTPUT_6_3

' Lysimeter 7: "Chewie" U-P
Alias Data_LOADCELL(4) = LOADCELLOUTPUT_7_1
Alias Data_LOADCELL(5) = LOADCELLOUTPUT_7_2
Alias Data_LOADCELL(6) = LOADCELLOUTPUT_7_3

' Lysimeter 3: "Kylo" only plant
Alias Data_LOADCELL(7) = LOADCELLOUTPUT_3_1
Alias Data_LOADCELL(8) = LOADCELLOUTPUT_3_2
Alias Data_LOADCELL(9) = LOADCELLOUTPUT_3_3

' Lysimeter 4: "Luke" U-P and Na-22
Alias Data_LOADCELL(10) = LOADCELLOUTPUT_4_1
Alias Data_LOADCELL(11) = LOADCELLOUTPUT_4_2
Alias Data_LOADCELL(12) = LOADCELLOUTPUT_4_3

' Lysimeter 5: "Leia" U-P and Na-22
Alias Data_LOADCELL(13) = LOADCELLOUTPUT_5_1
Alias Data_LOADCELL(14) = LOADCELLOUTPUT_5_2
Alias Data_LOADCELL(15) = LOADCELLOUTPUT_5_3

' Construct a DataTable out of load cell Public arrays above and the battery voltage data
DataTable(LoadCell, True, -1)
  DataInterval(0, DATA_INTERVAL_SECONDS, Sec, 0)
  Minimum(1,BattV,FP2,False,True)
  Sample(TOTAL_LOADCELL, Data_LOADCELL, FP2)
EndTable
```

```
Sub ResetCounters()
  Current_LOADCELL = 0
EndSub

' Go to the next input on the mux connected to port C1.
Sub MuxNext_1()
  ' Pulse the CLK port of the multiplexer for 10ms and allow for settling with
  ' a delay.
  PulsePort(C1, 10000)
  Delay(0, 15, mSec)
EndSub

' Commented out because second multiplexer is not used.
' Go to the next input on the mux connected to port C2.
'Sub MuxNext_2()
  ' Pulse the CLK port of the multiplexer for 10ms and allow for settling with
  ' a delay.
'  PulsePort(C2, 10000)
'  Delay(0, 15, mSec)
'EndSub

Sub SensorOn()
  SW12(1, 1)
  Delay(0, 1, Sec)
EndSub

Sub SensorOff()
  SW12(1, 0)
EndSub

Sub MuxOn()
  PortSet(C4, 1)
EndSub

Sub MuxOff()
  PortSet(C4, 0)
EndSub

' Measure load cells on the first multiplexer.
Sub MeasureLOADCELL_1()
  Current_LOADCELL += 1
  Battery(BattV)
  BrFull(Data_LOADCELL(Current_LOADCELL, 1), 1, mV5000, U1, U3, 1, 2500, True, True, 500, 60, 1,
0)
EndSub

' Commented out because second multiplexer is not used.
'Sub MeasureLOADCELL_2()
'  Current_LOADCELL += 1
'  Battery(BattV)
'  BrFull(Data_LOADCELL(Current_LOADCELL, 1), 1, mV5000, U5, U7, 1, 2500, True, True, 500, 60,
1, 0)
'EndSub
```

```
' Measure the load cells connected to one lysimeter on the first multiplexer.
Sub MeasureLysimeter_1()
  Dim i
  For i = 1 To LYSIMETER_LOADCELL_COUNT
    MuxNext_1()
    SensorOn()
    MeasureLOADCELL_1()
    SensorOff()
  Next i
EndSub

' Measure the load cells connected to one lysimeter on the second multiplexer.
' Commented out because not using second multiplexer.
'Sub MeasureLysimeter_2()
'  Dim i
'  For i = 1 To LYSIMETER_LOADCELL_COUNT
'    MuxNext_2()
'    SensorOn()
'    MeasureLOADCELL_2()
'    SensorOff()
'  Next i
'EndSub

SequentialMode
BeginProg
  Scan(SCAN_INTERVAL_SECONDS, Sec, 0, 0)
    ResetCounters()
    MuxOn()

    Dim i

    For i = 1 To LYSIMETER_COUNT_1
      MeasureLysimeter_1()
    Next i

    'For i = 1 To LYSIMETER_COUNT_2
    '  MeasureLysimeter_2()
    'Next i

    MuxOff()

    CallTable(LoadCell)
  NextScan
EndProg
```

Appendix D: Ground, Air, and Lysimeter Temperature Comparison

Because the columns and lysimeters are placed in the outer housing with air surrounding them, the temperature gradient within them could differ from the ground temperature gradient. To compare the temperature gradient with depth in the lysimeters to the ground temperature gradient, two Decagon 5TE sensors were buried in holes near the test bed. Two holes were dug and backfilled with SRS soil. The sensors were placed into the SRS soil so that the prongs and the plastic casing were surrounded by SRS soil (Figure D.1). For both holes, the SRS soil was covered with the original topsoil. The 5TE sensor connected to datalogger EM34048 is buried at approximately 30 centimeters below the ground surface, which is similar to the depth of the "_2" labeled sensors. The 5TE sensor connected to datalogger EM33536 is buried in a hole that is approximately 15 centimeters deep, which is similar to the depth of the "_1" labeled sensors. The air temperature data is collected by the Decagon VP-4 sensors which are part of the weather stations at the test bed.

Temperature data collected from August 20 to 28, 2017, for the three simulated landfill columns, two buried 5TE sensors, and the air temperature are shown in Figure D.2. For the simulated landfill columns, the "_1" labels are the sensors inserted near the top of the columns, "_2" labels are sensors inserted near the middle of the columns, and the "_3" labels are the sensors inserted near the bottom of the columns. Ambient air temperature exhibits the largest daily fluctuations, and the 5TE sensors inserted near the bottom of the columns exhibit the smallest daily fluctuations. The temperature data for deeper buried 5TE ground probe and the "_2" labeled sensors data are well aligned, however the shallower buried 5TE ground probe exhibits lower minimun and maximum temperatures than the "_1" labeled sensors.

Figure D.1: Placement of Decagon 5TE sensors in the ground near the test bed.

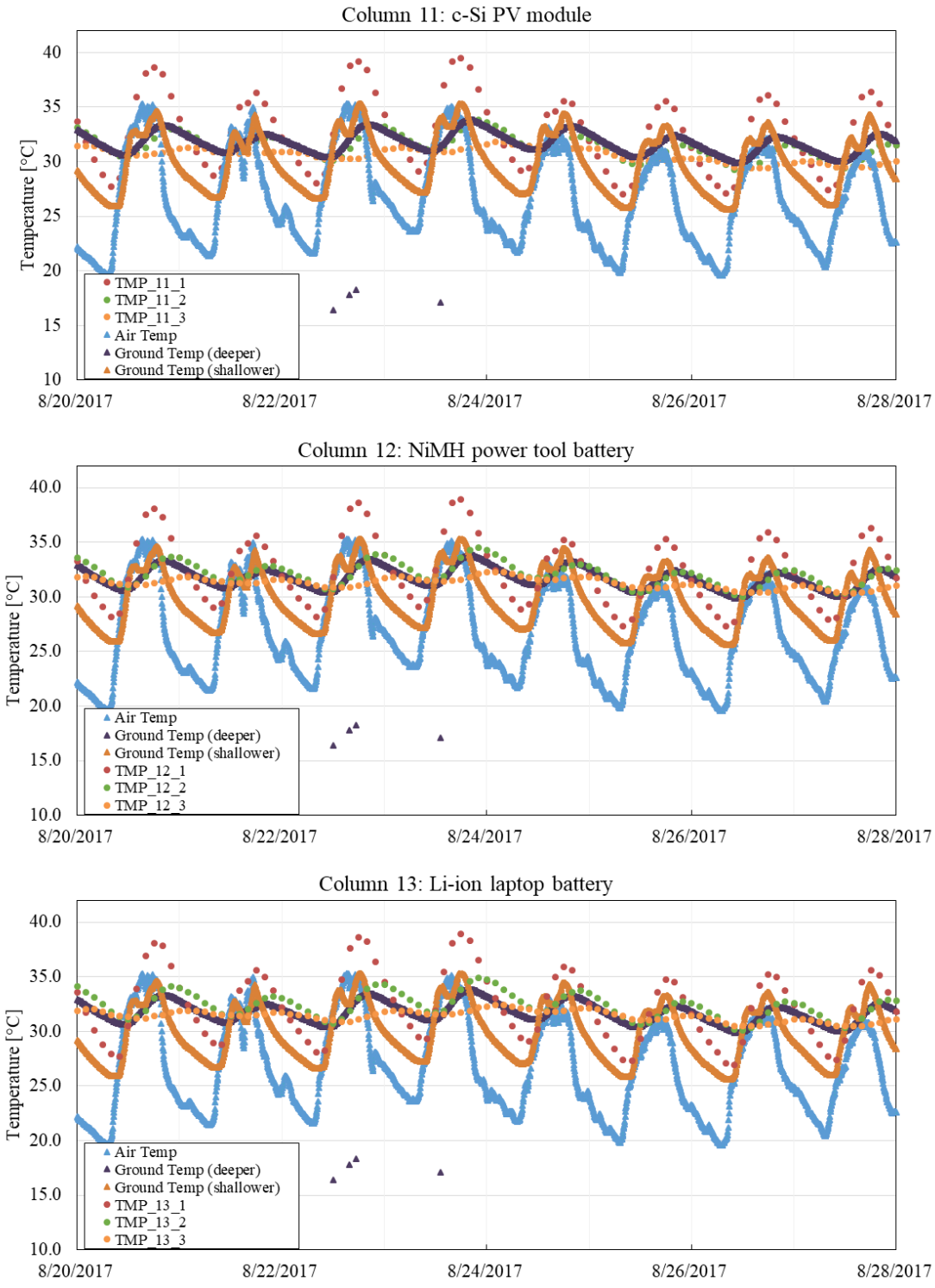

Figure D.2: Temperature comparison of the lysimeters to the ground at different depths.

Appendix E: Calculation of the FAO Penman-Monteith Equation and Corresponding Python Script

The daily evapotranspiration rate is calculated using the FAO Penman-Monteith equation (Eq. E.1) using weather data collected at the site every five minutes for temperature, relative humidity, wind speed, and solar radiation (Allen et al., 1998).

$$ET_O = \frac{0.408\Delta(R_n - \mathrm{G}) + \gamma\frac{900}{T+273}u_2(e_s - e_a)}{\Delta + \gamma(1 + 0.34u_2)} \qquad \text{(Eq. E.1)}$$

Where ET_O is the reference evapotranspiration [mm/day], R_n is the net radiation at the crop surface [MJ/m^2/day], G is the soil heat flux density [MJ/m^2/day], T is the mean daily air temperature at 2 m height [degrees Celsius], u_2 is the wind speed at 2 m height [m/s], e_s is the saturation vapor pressure [kPa], e_a is the actual vapor pressure [kPa], Δ is the slope of the vapor pressure and temperature curve [kPa/degree Celsius], and γ is the psychrometric constant [kPa/degree Celsius].

The mean daily air temperature, T, is defined as the mean of the maximum and minimum temperatures and not an average of the measurements. The slope of the vapor pressure curve and temperature curve, Δ (Eq. E.2), is calculated using the mean air temperature, T.

$$\Delta = \frac{4098\left(0.6108\exp\left(\frac{17.27T}{T+237.3}\right)\right)}{(\mathrm{T}+237.3)^2} \qquad \text{(Eq. E.2)}$$

The psychrometric constant, γ, is calculated by multiplying the barometric pressure, P (Eq. E.3), by 0.000665, where P is calculated using the elevation, z [m], of Clemson.

$$P = 101.3\left(\frac{293 - 0.0065\mathrm{z}}{293}\right)^{5.26} \qquad \text{(Eq. E.3)}$$

The saturation vapor pressure, e_s, is the average of the saturation vapor pressure, e^o (Eq. E.4), at the minimum and maximum daily temperatures.

$$e^o(\mathrm{T}) = 0.6108\exp\left(\frac{17.27\mathrm{T}}{T+237.3}\right) \qquad \text{(Eq. E.4)}$$

The actual vapor pressure, e_a (Eq. E.5), is calculated using the daily minimum (RHmin) and maximum (RHmax) relative humidity data [%] and the saturation vapor pressure at the minimum (Tmin) and maximum (Tmax) daily temperatures.

$$e_a = \frac{e^o(Tmin)\frac{\text{RHmax}}{100} + e^o(Tmax)\frac{\text{RHmin}}{100}}{2} \qquad \text{(Eq. E.5)}$$

If the wind speed, u_2, is not measured at a height of 2 m but at a different height (h), then the measured wind speed value (u_z) needs to be adjusted (Eq. E.6).

$$u_2 = u_z \frac{4.87}{\ln(67.8\text{h} - 5.42)} \qquad \text{(Eq. E.6)}$$

The net radiation at the crop surface, R_n, is the difference between the incoming net short-wave radiation, R_{ns} (Eq. E.7), and the net outgoing long-wave radiation R_{nl} (Eq. E.13a and E.13b).

$$R_{ns} = 0.0864(1 - 0.23)R_s \qquad \text{(Eq. E.7)}$$

Where R_s is the average incoming solar radiation measured at the site [W/m^2].

The clear sky radiation, R_{so} (Eq. E.12), is needed to calculate the net outgoing long-wave radiation, and the extraterrestrial radiation, R_a (Eq. E.8) is needed to calculate the clear sky radiation.

$$R_a = \frac{24(60)}{\pi} G_{sc} d_r [\omega_s sin(\varphi) \sin(\delta) + \cos(\varphi)\cos(\delta)\sin(\omega_s)] \qquad \text{(Eq. E.8)}$$

Where G_{sc} is the solar constant (0.0820 MJ/m^2/min), d_r is the inverse relative distance between the Earth and Sun (Eq. E.9), ω_s is the sunset hour angle (Eq. E.10), φ is the latitude [rad], and δ is the solar decimation (Eq. E.11).

$$d_r = 1 + 0.33cos\left(\frac{2\pi}{365}J\right) \qquad \text{(Eq. E.9)}$$

Where J is the number of the day of the year, with January 1 corresponding to day 1.

$$\omega_s = arcos(-\tan(\varphi)\tan(\delta)) \qquad \text{(Eq. E.10)}$$

$$\delta = 0.409sin\left(\frac{2\pi}{365}J - 1.39\right) \qquad \text{(Eq. E.11)}$$

$$R_{so} = (0.75 + 2E - 5z)R_a \qquad \text{(Eq. E.12)}$$

If the ratio of Rs/Rso is less than or equal to 1,

$$R_{nl} = \sigma\left(\frac{(Tmax+273.16)^4+((Tmin+273.16)^4}{2}\right)(0.34 - 0.14\sqrt{e_a})\left(1.35\frac{R_s}{R_{so}} - 0.35\right) \quad \text{(Eq. E.13a)}$$

If the ratio of Rs/Rso is greater than 1,

$$R_{nl} = \sigma\left(\frac{(Tmax+273.16)^4+((Tmin+273.16)^4}{2}\right)(0.34 - 0.14\sqrt{e_a}) \quad \text{(Eq. E.13b)}$$

The soil heat flux density, G, is assumed to be zero for daily ET_O estimates. Compared to the net radiation, the soil heat flux density is much smaller.

To automate the calculation of the FAO Penman-Monteith equation, a Python script has been written based on a Matlab script (Thrash, 2016). The script requires an input file in the comma separated variables (CSV) format with the following columns, which are the data gathered from each weather station datalogger: measurement date, measurement time, precipitation, relative humidity, temperature, vapor pressure, solar radiance, wind speed, wind gusts, and wind direction. The script calculates the daily ET_O values and creates a CSV file with the dates and ET_O values.

```
"""
This function calculates daily evapotranspiration using the FAO Penman-Monteith method.
Reference evapotranspiration (ETo) = (0.408 * Del * (Rn - G) + y * (900 / (Tmean + 273) * u2)
   * (es - ea)) / (Del + y * (1 + 0.34 *u2))
"""
import numpy as np
import collections

#Define a function with input for weather_data file name and output_file name.
def Weather_data_analysis(weather_data, output_file):
   #Columns in csv data: Measurement Date (in Excel days since Jan 1, 1900 format),
   #Measurement Time, mm Precip, RH, degrees C Temp, kPa Pressure, Solar W/m2,
   #m/s Wind Speed, m/s Wind Gusts, Wind Direction
   #Open data file and split into strings using "," as delimiter.
   samples = np.loadtxt(weather_data, dtype="str", delimiter=",", skiprows=3)

   #Create a dictionary (data structure) to save data from the file.
   by_date = {}
   by_date = collections.OrderedDict()

   #Add the weather data to its respective key in the dictionary.
   for row in samples:
```

```
        date = row[0]
        value = by_date.setdefault(date, {})
        sample_data = value.setdefault("samples", [])
        sample_data.append(row)

    #Header for output file
    header = [("Date",  "Evapotranspiration value")]
    #Calculate the different parameters for each date and return the values.
    for date in by_date:
        value = by_date[date]
        sample_data = np.array(value["samples"])

        #Temperature [°C]
        Tmax = np.amax([float(Tmax) for Tmax in sample_data[:,4]])
        Tmin = np.amin([float(Tmin) for Tmin in sample_data[:,4]])
        Tmean = (Tmax + Tmin)/2

        #Saturation vapor pressure/temperature curve (Del [kPa °C^-1])
        Del = ((4098 * 0.6108 * np.exp((17.27 * Tmean)/(Tmean + 237.3))) /
        (Tmean + 237.3) ** 2)

        #Psychrometric constant (y [kPa °C^-1])
        z = 221 #Elevation of Clemson, SC [m]
        P = 101.3 * ((293 - 0.0065 * z) / 293) ** 5.26 #General barametric pressure at Clemson
        y = 0.000665 * P

        #Vapor pressure (es = saturated; ea = actual [kPa])
        RHmax = np.amax([float(RHmax) for RHmax in sample_data[:,3]])
        RHmin = np.amin([float(RHmin) for RHmin in sample_data[:,3]])
        es = ((0.6108 * np.exp((17.27*Tmax)/(Tmax + 237.3)) +
        (0.6108 * np.exp((17.27*Tmin)/(Tmin + 237.3)))) / 2)
        ea = (((0.6108 * np.exp((17.27*Tmin)/(Tmin + 237.3))) * RHmax +
        (0.6108 * np.exp((17.27*Tmax)/(Tmax + 237.3))) * RHmin) / 2)

        #Wind speed [m/s]
        z1 = 4.7 #height of wind measurements [m]
        vmean = np.mean([float(vmean) for vmean in sample_data[:,7]])
        u2 = vmean * (4.87/np.log(67.8 * z1 - 5.42))

        #Solar radiation [MJ/m^2/day]
        a = 0.23 #a = albedo coefficient (0.23 for hypothetical grass reference)
        Rs = np.mean([float(Rs) for Rs in sample_data[:,6]]) * 0.0864 #converts from [W/m^2] to
[MJ/m^2*day]
        Rns = (1 - a)* Rs #net solar radiation

        theta = 4.903E-9 #[MJ/K^4/m^2*day] Stefan-Boltzmann constant
```

```
        Gsc = 0.0820 # [MJ/m^2/min] Solar Constant
        #In Excel's 1900 date format (number of days since Jan 1, 1900),
        #January 1, 2017 is 42736. To calculate the day of the year in 2017,
        #subtract 42735 from the date in Excel's format, therefore Jan 1, 2017
        # is day 1. For 2018 dates, subtract 43100 from the date in Excel.
        sample_date = np.amax([float(date) for date in sample_data[:,0]])
        J = sample_date - 42735 #number of the day of the year
        num = (2 * np.pi / 365) * J - 1.39
        d = 0.409 * np.sin(num) #solar decimation [rad]
        j = (np.pi / 180) * 34.67 #latitude of Clemson [rad]
        dr = 1 + 0.033 * np.cos((2 * np.pi / 365) * J) #inverse relative distance Earth-Sun
        ws = np.arccos(-1 * np.tan(j) * np.tan(d)) #sunset hour angle [rad]
        Ra = (24 * 60 / np.pi * Gsc * dr * (ws * np.sin(j) * np.sin(d) + np.cos(j)
        * np.cos(d) * np.sin(ws))) # extraterrestrial radiation [MJ/m^2/day]
        Rso = (0.75 + 2E-5*z) * Ra #clear sky radiation [MJ/m^2/day]

        #Alternative Rs calculation when actual data is not available
        #n =  #actual duration of sunshine [hr]
        #N =  24 / np.pi * ws
        #Rs = (0.25 + 0.5 * n / N) * Ra
        #Rns = (1 - a)* Rs #net solar radiation

        #The ratio of Rs/Rso is not allowed to be greater than one.
        if Rs/Rso <= 1:
           k = 1.35 * (Rs/Rso) - 0.35
           Rnl = (theta * (((Tmax + 273.16) ** 4 + (Tmin + 273.16) ** 4) / 2) *
           (0.34 - 0.14 * np.sqrt(ea)) * k) #net outgoing longwave radiation [MJ/m^2/day]
        else:
           Rnl = (theta * (((Tmax + 273.16) ** 4 + (Tmin + 273.16) ** 4) / 2) *
           (0.34 - 0.14 * np.sqrt(ea)))
        Rn = Rns - Rnl #net radiation [MJ/m^2/day]

        #Soil heat flux (assumed to be zero for daily ETo estimates; really small compared to net radiation)
        G = 0

        #FAO Penman-Monteith Equation
        ETo = ((0.408 * Del * (Rn - G) + y * 900 / (Tmean + 273) * u2 * (es - ea)) /
        (Del + y * (1 + 0.34 * u2)))

        header.extend([(sample_date, ETo)])

    #Create an output file containing Date and Evapotranspiration value
    np.savetxt(output_file, header, delimiter=",", fmt="%s")

Weather_data_analysis("weather data.csv","Evapotranspiration values.csv")
```

References

Allen, R. G.; Pereira, L. S.; Raes, D.; Smith, M. *Crop Evapotranspiration - Guidelines for Computing Crop Water Requirements - FAO Irrigation and Drainage Paper 56*; 1998.

Cobos, D.; Chambers, C. *Calibrating ECH2O Soil Moisture Sensors*; 2010.

Thrash, C. Measuring and Interpreting Vertical Displacements Related to Shallow Hydrologic Processes, Clemson University, 2016.

Topp, G. C.; Davis, J. L.; Annan, A. P. Electromagnetic Determination of Soil Water Content: Measurements in Coaxial Transmission Lines. *Water Resour. Res.* **1980**, *16* (3), 574–582.